ELECTROLYTE- GATED THIN FILM TRANSISTORS WITH SOLUTION- PROCESSED SEMICONDUCTORS

by

Abdullah Faisal M. Al Naim

A thesis submitted in partial fulfillment of the requirements for the degree of

Doctor of Philosophy in Physics

UNIVERSITY OF SHEFFIELD

Hicks Building

May, 2014

Contents

List of figures

List of Tables

To all my loved family

(Mum, Dad, Nuha, Faisal, Mohamad and Abdulaziz)

Acknowledgements

University of Bari (Italy), for providing XPS data for ZnO and **Dr. Mary Deasy**, Institute of Technology Tallaght (Dublin, Ireland), for providing calixarenes.

My grateful thanks are given to my parents who always send me their unconditional love, support and supplication to be better and unique person. I hope I can give back at least a little of their favor.

At last but not the least, I would like to thank my wife, **Nuha**, and my children (**Faisal, Mohamad and Abdulaziz**). I know you all have suffered and sacrificed a lot, and you deserve to share this success with me, and I will try my best to compensate you by my care, love and more in coming days.

Abstract

The work in this thesis is concentrated on studies of improving the functionality of electrolyte- gated thin film transistors with solution- processed semiconductors in order to provide a promising platform in particular for sensor as transducers and introduce sensitizer layer on the top of the devices to improve their response to specific analytes. Calixarenes, a family of organic macrocycles, were used to bind selectively to waterborne cations, making them an attractive sensitizer option for such species. Here, it is found that calixarenes deposited over the surface of semiconductors using the Langmuir trough also show a positive impact on the performance of *TFTs* in terms of reducing unwanted electrochemical doping, which often competes with field effect. Also, electron- transporting and electrolyte- gated thin film transistors were demonstrated using precursor- route zinc- oxide (ZnO) semiconductors with hydrophobic surface modifications. This avoids the well- known problem of electron trapping in organic semiconductors. ZnO also shows ambipolar behavior when gated by an ionic liquid (*IL*) at high applied voltages. Moreover, it is found some organic solvents may act as *EDL* gate media for *TFTs*, thus establishing a new family of gate media, in addition to the previously known options (water, *ILs*, solid electrolytes). This ability is a property of the solvent, not the semiconductor, and a criterion is identified to qualify an organic solvent to act as *EDL* gate medium. The organic nano- wire (*NW*) morphology is attractive for sensor applications, due to the high surface area of *NWs*. Here, both *p-* type and *n-* type organic *NW* films were gated by water. *NW TFTs* of the hole- transporting polymer P3HT, grown via different solution- based routes, showed lower drain currents, but also lower thresholds, compared to conventional P3HT film *TFTs*. Water- gated electron- transporting organic *TFTs* were demonstrated using nano- belts of the *n-* type organic semiconductor *BBL*. Performance was improved significantly when using an aprotic organic solvent as *EDL* gate medium for *BBL* nano- belt films.

CHAPTER 1

Introduction

Electronic devices have been and are still affecting positively on every aspect of our life, starting from small and simple devices such as an electronic timer and reaching more sophisticated and advanced devices such as computers and medical instrumentations. Demands on novel generation of electronics holding new functionalities that are not achievable using the traditional silicon technology are increasing. Examples for such demands are cheap, flexible, stable sensors; electronic artificial skins; smart fabrics; radio- frequency identification and e- heath monitors (measuring heart rate, level of blood pressure, for example) implanted under skin. Thus, the thin film transistors (*TFTs*) using organic semiconductors and metal oxides as active channels have attracted a remarkable attention in recent years. For large devices' production of thin film transistors with different proposes (light- emitting diode *LEDs* display and solar cell, for example), solution- processable materials are a suitable choice. In recent years, an alternative has emerged to the gate dielectrics conventionally used in solution- processed thin film transistors (*TFTs*), in the form of (liquid or solid) electrolytes. These display exceptionally high capacitance due to the formation of an ultrathin *EDL* at the electrolyte/semiconductor interface, leading to low operating voltages (typically$\leq 1\,V$) compatible with battery- powered devices. Such *TFTs* have been proved to show adequate long- term stability.

In this work, many ideas will be introduced to highlight the issues related to the use of electrolytes as gate media for thin film transistors. These include the control of parasitic electrochemical doping identifying a new family of EDL gate media, establishing n- type water gated TFTs, and introducing electrolyte- gating of unconventional (but practically attractive) organic semiconductor morphologies.

Chapter 1 gives the introduction and an overview of all relevant topics to this work. Chapter 2 reports, in more details, on devices fabrication and techniques used in this work. Chapter 3 shows the experimental methodology for the transistor characterization. Chapters 4, 5, 6 and 7 give a detailed account of my own work on electrolyte- gated TFTs. Finally, chapter 8 is a brief summary and outlook with suggestions for future work.

1.1 Basic concepts of atomic orbitals and energy levels in molecules and crystals

Quantum mechanics is used to describe the behavior of a microscopic system such as atoms. The Hamiltonian operator is used to be applied to Schrödinger equation in order to find the energy of electron and nuclei constituting a molecule. Being Used to solve the Schrödinger equation, the wave function $\Psi(r,t)$, a dimensionless quantity, represents the probability to find a particle at location r at time t, once it is squared $|\Psi(r,t)|^2$. In an atom, Schrödinger's equation leads to a discrete set of solutions for permitted electronic wave functions $\Psi_{n,l,m}(r,t)$, called orbitals, with discrete quantum numbers n,l,m. These numbers would determine the orbital's shape and energy which are principle Quantum Number (QN) (n), orbital angular momentum QN (l) and magnetic QN (mi). Electrons occupy these orbitals according to Pauli's principle, which prevents any two electrons sharing the same set of quantum numbers (n,l,m). The energy level, also called electron shell, correspond with the principle Quantum Number QN (n). The nearest shell to the nucleus is the first shell, also called "K shell", the second shell is called "L shell", and so on, as used in the X-ray notation. The valence shell represents the outermost shell of an atom. The atoms with complete valence shells, for example noble gas, are considered chemically non- reactive. The complete valence shells means that all possible orbitals for a given principle QN are filled, and all shells of the next principle QN are empty. In contrary, the atoms with incomplete shells tend to engage in chemical bonds, since the valence shell is partly completed. Each shell may include one or more sub- shells which may include one or more atomic orbitals, such as the second (L) shell having two sub- shells which are called 2s and 2p.

The s and p orbitals especially in carbon are interesting atomic orbitals in understanding clearly the electrical conduction behavior of organic and inorganic semiconductors and any other physical and chemical phenomena.

Once two atoms come closer, the electrons of incomplete atomic shell (valence electrons) start overlapping and forming molecular orbitals. This results in splitting original energy level. This so- called a linear combination of atomic orbitals is either constructive or destructive molecular orbital which form bonding orbitals and anti- bonding orbitals, respectively. The former possesses lower energy than original combined atoms with stable energy and help molecular to bond, but the latter is destabilized with higher energy, do not form chemical bonds and forces the molecule

to break apart. Anti- bonding refers to an excited state of π- orbitals in conjugated molecules (i.e. carbon based molecules).

On organic semiconductors side, after attaching closely more and more organic molecules, this presents two different orbital levels which are the Highest Occupied Molecular Orbital (*HOMO*) by which is highest energy level occupied electrons, and the Lowest Occupied Molecular Orbital (*LUMO*) which is the lowest energy not occupied by electrons. Organic semiconductors are molecules where the *HOMO-LUMO* energy gap is relatively small, approximately 3.5 eV or less. The only molecules with gaps even smaller are conjugated organic molecules, i.e. organic molecules with alternating carbon-carbon single- and double bonds along the molecular backbone. More details will be provided in section 1.2.

In inorganic semiconductor crystals, the periodical arrangement of atoms in solid causes the energy level's separation into bands (conduction C_B and valence V_B bands), as described from Kronig- Penney model in 1930. Electrons are described as waves, with a wave vector k. Electrons become delocalised, once Electrons are not associated with any single atom or one covalent bond, and its orbital extends over several adjacent atoms. The band structure of a solid is the discrete set of Eigenvalues of the Schrödinger- equation solutions as a function of k, $E_n(k)$. In a semiconductor, there is the highest energy fully occupied band (the valence band) V_B, and the highest energy level in the valence band is E_v. Similar concept is applied also to C_B (completely empty band) and E_c. No net movement of electrons can take place, If all the states in the conduction band (valence band) are unoccupied (fully occupied). Thus, the band cannot contribute to conduct current (charge carriers), i.e. insulators and ceramics. The energy difference between (E_c-E_v) defines band- gap E_g concept. If the highest occupied/lowest unoccupied state take place at the same quasimomentum (often=0), a momentum- like vector is related to the movement of electrons in a crystal lattice, the bandgap is called direct bandgap. If it is not the same value of momentum, it is called indirect bandgap. The Fermi level E_F is, thus, located between occupied and empty states. By definition, in a semiconductor, the Fermi level must fall in between E_v and E_c, and is near enough to the bands to be thermally populated with either holes or/and electron. *F(E)* represents the Fermi-Dirac distribution which describes, at certain temperature, the distribution of electrons in energy levels. For example, at *T*=0 **K**, *F(E)* equal 1 which means all the energy level below Fermi level become fully occupied, and above Fermi level the energy level are completely empty [*F(E)*=0].

The electrical properties of materials are determined as semiconducting or insulating by verifying the size of band-gap E_g and the position of Fermi level E_F related to the conduction band, once the materials are attached to metal contacts. Moreover, introducing impurities or/and defects in the crystalline structure leads to breakdown the symmetry which, therefore, produces more diverse band structure and more different electrical and optical properties. This breaking up of symmetry can also break up bonds which, in turn, induce more free electrons in a system. These free electrons contribute to the electrical conduction as well as holes which is the electron shortage in the atoms. Both are referred as charge carriers. More details will be provided in section 1.3.

The *HOMO* and *LUMO* descriptions of the organic conjugated molecule are analogous to the V_B and C_B descriptions of inorganic semiconducting crystals. Consequently, the energy difference between *LUMO* and *HOMO* in a conjugated molecule is called the 'bandgap'. There are different characteristics between conjugated molecules and inorganic semiconductors, as well as similarities.

1.2   Organic semiconductors

Even though, both semiconductors, organic and inorganic materials, have relatively similar features in terms of band- gap and energy bands, the charge carriers transport differently because the charge carriers in organic semiconductors are more localized in their original molecule than the counterpart, inorganic materials. Thus, this section and section 1.3 give a detailed description of the generation, and transport, of charge carriers in organic and inorganic semiconductors, respectively.

Carbon element (C-H bond, strictly) is the major backbone in many organic materials. However, there are some exceptions for this definition, such as Fullerene and Carbonates. Despite containing Carbon, they are, therefore, not organic. In first glance, carbon binds to just two elements, since carbon atom possess only two unpaired valence electrons, as seen in the electron configuration of a carbon atom ($1s^2$ $2s^2$ $2p^2$ $\equiv$ $1s^2$ $2s^2$ $2p_x^1$ $2p_y^1$ $2p_z^0$). However, the situation is not as simple as it can be imagined, because the simplest alkane which is methane shows that carbon binds with four hydrogen (CH_4). Therefore, the model of bonding of carbon is only clarified by vital concept that is so- called hybridization. One electron from the *2s* orbital is transferred to the empty orbital of *$2p_z$*. This offers four unpaired valence electrons rather than two which are ($2s^1$ $2p_x^1$ $2p_y^1$ $2p_z^1$). Thus, three possible combinations of hybrid orbitals can be introduced.

Firstly, the sp^3 hybrid can form four bonds with the outer orbitals of its neighbouring atoms (CH_4 example). Two Carbon with sp^3 hybrids are coupled together by a strong bond (C-C), called sigma (σ) bond. The angle between four bonds is roughly 109.5° which forms tetrahedron shape, as seen in Table 1.

Secondly, the three sp^2 hybrid orbitals have only two of three p-orbitals mixing with s-orbital forming 120° angles between them. This hybridisation leaves the remaining p orbital to be perpendicular to the common plane of sp^2 hybrid orbitals. For forming double- bond, two sp^2 hybrid orbitals must be brought together. The two hybrids bind together by a strong σ bond, and a weaker bond because of the overlap of their remaining perpendicular p orbitals forming double- bond (C=C), as encountered in alkenes. This weaker bond is called π bond, and their shared electron is labelled as π electron. The orbitals of π bonds are more far away from their original nuclei comparing to the orbitals of σ bonds. This important phenomenon is called delocalisation, since π electrons are loosely bound to their original nuclei.
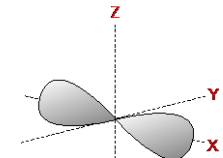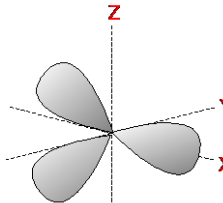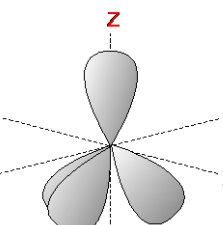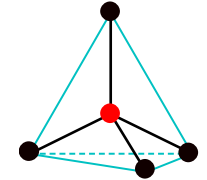
Atomic Orbitals	Hybrid Orbitals	Bonding Electrons around Central Atom	Geometry
1 s Orbital & 1 p Orbital	sp hybrid (2 orbitals)	2	Linear
1 s Orbital & 2 p Orbital	sp^2 hybrid (3 orbitals)	3	Trigonal planar
1 s Orbital & 3 p Orbital	sp^3 hybrid (4 orbitals)	4	Tetrahedral

Table 1, the possible shapes of carbon in hybrid orbitals.

Lastly, *sp* hybrid orbitals have only one of three *p*-orbitals mixing with *s*-orbital forming 180° angle between them as linear shape. Also, this hybridisation leaves the remaining *p* orbitals, but this time two of *p* orbitals are perpendicular to the linear bound of *sp* hybrid orbital. The triple-bound containing one σ bond from *sp* hybrid orbital of two linked Carbons and two π bonds coming from two perpendicular *p*-orbitals of same linked Carbons. This formation of bonds is recognized as triple-bond (C≡C), as found alkynes. Also, the orbitals of π bonds are delocalised, as well, over their original nuclei, but this delocalisation does not describe the delocalised of π electrons over the whole molecule, yet. This phenomenon leads to an important topic which is a benzene ring in order to understand how π electrons are delocalised over the whole molecule.

1.2.1   Benzene ring

This aromatic ring is formed as a regular hexagon with alternative Carbon-Carbon single- and double- bonds containing six sp^2 hybridised Carbon atoms. Thus, the double-bond offers π electrons to be delocalized all over the ring (Figure 1, left). Therefore, the cloud of electron will cover the molecule containing benzene rings to some extent. Delocalised π electrons lead to molecules with smaller band- gaps E_g. The Benzene ring is an important example of a conjugated molecule, and it is, also, an important building block in many organic semiconductors (*OSC*). However, a single benzene ring is not yet large enough to bring the band- gaps E_g into the semiconductor regime. Nevertheless, when, for example, many benzene rings are fused at their edges (e.g. 5 rings fused into pentacene, Figure 1, right), π electrons can delocalise over a larger area. Since, the band-gap's size depends on the delocalisation of π electrons and, in turn, on the conjugation of the molecule, the band -gap's size decreases in few eV which is about (2.5 eV). By this band- gap's size, Pentacene is considered an organic semiconductor.
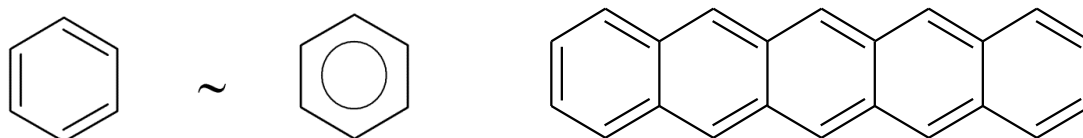
Figure 1, left: the structure of Benzene ring, right: chemical structure of pentacene

1.2.2   Thiophene ring

Forming a regular pentagon shape, Thiophene is an example of what is called 'heterocycles'; conjugated rings with atoms other than just Carbon in them. But in this

case, the electron pairs of Sulphur atom induces π electron in the ring. Thus, there are six π electrons which are four from the double- bonds of Carbons and two from electron pairs on Sulphur, as seen in Figure 2. In the presence of Sulphur, the π electrons delocalised over the thiophene ring. This ring can be found as building blocks in many organic semiconductors materials, such as P3HT and PBTTT (containing also two fused rings in its repeatable units).
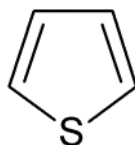
Figure 2, the structure of Thiophene ring.

1.2.3   Charge injection into organic semiconductors

Charge injection is one of essential factors for *OSC* device performance (even more important in organic light emitting diodes (*LEDs*)), since it determines how efficient the organic semiconductor devices perform especially in thin film transistors (*TFT*). Charge carriers need, therefore, to be injected by electrode into an organic semiconductor to mobilise and pass through channel until reaching another electrode. For achieving injection in case of *n-* type and *p-* type organic semiconductors, electrons and holes must be injected in *LUMO* and *HOMO* level of a molecule, respectively. In organic semiconductors, the charge carriers are called electron and hole polarons. Adding an electron into the *LUMO* level of molecule generates an electron polarons. Hole polarons are created, when an electron (hole) is removed (added) in *HOMO* level. In general, this action of injecting electrons and holes leads to change in nucleus positions and the molecular orbitals conformations which, in turn, respond by a relaxation to a new position of minimum energy.

Because of the strong coupling between the charge carrier and the local lattice relaxation, removing an electron from its energy level requires slightly less in energy than the *HOMO* suggests, and adding an electron give the molecule slightly additional energy than the *LUMO* suggests. Instead, the required energies are called Ionisation potential (I_p) and electron affinity (E_a). They are required energies to take away the electron from *HOMO* level into vacuum level, which means injecting hole, and to inject the electron from a vacuum level into *LUMO* level, respectively.

In order to inject hole/electron efficiently in organic semiconductor materials, the injection barriers between the ionisation potential/electron affinity and the work

function of electrode; moving an electron from a metal, should be overcome, an example seen in Figure 3.
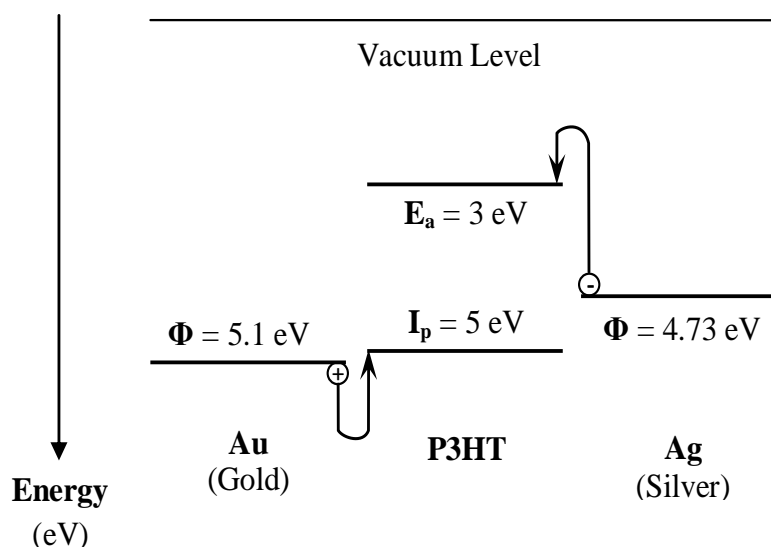
Figure 3, This shows electron injection into P3HT, and the energy levels diagram of electron and hole injection barriers from metal electrodes into P3HT before applying bias. Also this shows how hole injection from Au works better than hole injection from Ag, since the Au contact is closer to ionisation potentials.

The simple way of reducing the injection barriers is to use a deep *LUMO* of *OSC* which have such a high electron affinity or by choosing low work function values for electron injection and high work function metals for hole injection, as Marcus Ahles *et al* used Calcium contact (2.8 eV) for injecting electrons in order to have the *n-* channel operation of pentacene transistors (*LUMO*=2.5 eV)[1]. Once the voltage (potential) is applied at the sides of the organic semiconductor, the energy level of material becomes tilted that means the carriers are more preferable energetically at side than another side, seen in Figure 4. The gradient of tilted energy level is determined by the amount of applied voltage.
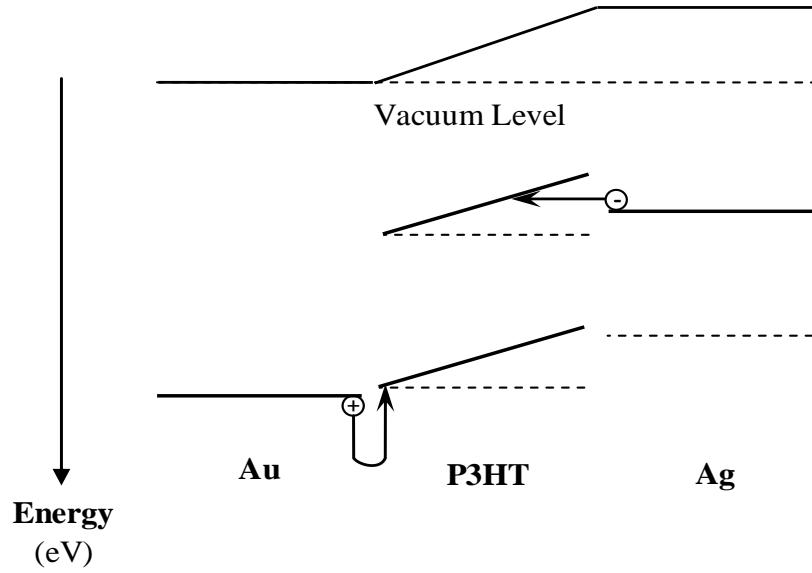
Figure 4, the energy level of organic semiconductor during applying bias potential.

The injection from a metal into an organic semiconductor is described into two mechanisms. The idea of overcoming the injection barrier by gaining adequate energy of the potential barrier is described by the thermionic (Schottky) emission. Also, Fowler-Nordheim tunnelling describes the injection mechanism using the concept of quantum mechanical tunnelling in order to pass through the barrier. As seen in Richardson-Schottky equation (1-1), Schottky emission demonstrates that the rate of injection (J_{RS}) depends highly on temperature and weakly on E-field.

$$(1\text{-}1) \qquad J_{RS} \propto T^2 \exp\left(\frac{\Phi_B}{kT}\right) . \exp\left(\frac{\beta_{RS} \sqrt{E}}{kT}\right)$$

Where Φ_B is the height of potential barrier and β_{RS} is a constant.

Conversely, Fowler-Nordheim tunnelling equation depends heavily on E-field and not in temperature. So, the probability of tunnelling can be increased by reducing the width, not the height of a potential barrier.

$$(1\text{-}2) \qquad J_{FN} \propto \frac{E^2}{\Phi_B} \exp\left(-\frac{\gamma\, \Phi_B^{\frac{3}{2}}}{E}\right)$$

Where γ is a constant.

Another way of reducing potential barrier is to dope the semiconductor between electrodes and semiconductor itself which produces Schottky junction. This action would bend the tilted band after applying voltage. This is because the E-field

concentrates on the doped areas beside the contact in which, in turn, result an effectively shorter tunnelling distance, as seen in Figure 5.
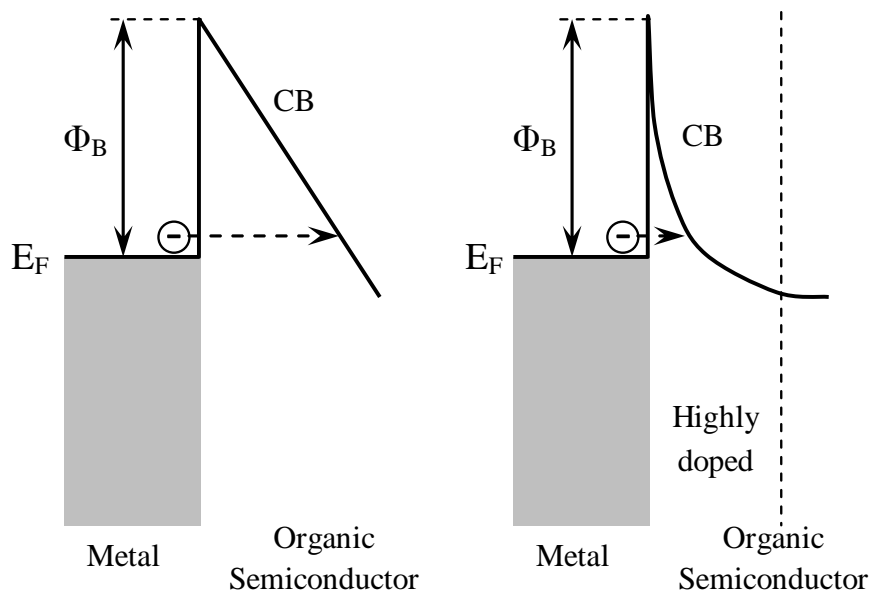
Figure 5, Energy diagrams showing band tilting as voltage applied (left) and band bending as voltage applied in present of highly doped area next to contact (right).

1.2.4 Charge carrier transport, Mobility

For practical applications, carriers need to be mobile not only to across the size of conjugated molecule but also to travel over a longer distance to reach another contact. This is why the charge transport is fundamental to be determined in order to know how carriers pass through the neighbouring conjugated molecules.

It is better to begin with the comparison between mobility in inorganic crystalline semiconductors, and organic semiconductors, which can be understood by explaining the concepts of the delocalisation *vs.* localisation.

Delocalised carriers (band- like) are described by wave number k and are in motion, by default. The mobility is limited only by scattering by lattice defects or vibrations (phonons); as a result, the mobility is high, but decreases with increasing temperature (more phonons), more details in section 1.3.3.

On another side, organic carriers are localised on a particular molecule and are not moving, by default. Motion is by 'thermally assisted tunnelling' between molecular sites (colloquially known as 'hopping'); therefore, mobility is low but increases with increasing temperature.

The consequences of the localisation of carriers (in organic semiconductors) lead to a strong coupling between charges and the local lattice, which deforms bond lengths and angles, and leads to a redistribution of electron density *LUMO* and *HOMO*, as mentioned before.

In terms of trap sites, localised carriers are susceptible to being caught in trap sites (described in section 1.2.5); however, it is not an issue for delocalised (wave- like) carriers. A lattice defect may act as scattering site for wavelike carriers, which somewhat reduces mobility, but waves cannot be caught in a specific, localised site. For localised carriers, a localised defect can act as a trap and stop the carrier from moving permanently (or at least for a long time).

Clearly distinguish between conventional crystalline semiconductors (i.e. Si and GaAs), with delocalised carriers, and molecular (organic) semiconductors. Even when, an organic semiconductor has crystallised into a molecular crystal; carriers are still localised on a single molecule because the overlap between neighbouring molecules is too weak to form bands, at least not at ambient T. This is because of many reasons including disorder and the weakness interaction of van der Waals inter-molecular.

The magnitude of organic semiconductors' mobilities varies widely from 10^{-6}–10^{-3} ($cm^2V^{-1}s^{-1}$) in amorphous polymers to 10–10^2 ($cm^2V^{-1}s^{-1}$) in single crystal[2]. This is an obvious indication of how the chemical structure and purity of organic semiconductors strongly affects mobility.

The mobility is defined as a quantity of the average velocity $\langle v \rangle$ of carriers generated per unit of electric field (E). The common unit of mobility is ($cm^2V^{-1}s^{-1}$)

(1-3) $$\langle v \rangle = \mu E$$

Various and developed models for the carriers transports' concept either organic or inorganic semiconductors have been proposed to describe how parameters interact with each other in order to be fitted well with the experimental results.

In organic semiconductors with well- ordered construction, for example, small molecules in polycrystalline films, the multiple trapping and release (*MTR*) model considers that the transport of charge carrier takes place in extended states as bands, and most of the charge carriers get trapped because of impurities or defects[3]. As described in equation (1-4), the model assumes that localised trap states are situated near the transport band edge, as holes and electrons trap states locates near *HOMO*

and *LUMO* levels, respectively. The charge carriers get seized in trap states, and the releasing process is only thermally controlled, as assumed by the model.

$$(1-4) \qquad\qquad \mu_{eff} = \mu_0 \alpha e^{-(E_c - E_t)/kT}$$

Since μ_0 is the mobility, E_c and E_t are the energy of the transport band edge and the trap states, respectively. α is the ratio of trap density of states (*DoS*) to effective *DoS* at the transport band edge. Also, the effective mobility equal $\mu_{eff} = \Theta \mu_0$, and Θ is the ratio of trapped carriers to total carriers including trapped and free carriers. This more or less applies crystalline *OSCs*, as long as crystal boundaries are ignored. In reality, crystal boundaries often come with deep traps, and a few deep traps can dominate behaviour of charge carriers transporting.

In more disordered organic semiconductors, the charge carrier transport is considered as thermally activated hopping from localised states of a molecule to another. Poole-Frenkel model describes this activated hopping by the following equation,

$$(1-5) \qquad\qquad \mu = \mu_0 e^{-(\Delta_0 - \beta\sqrt{E})/kT_{eff}}$$

Where $\frac{1}{T_{eff}} = \frac{1}{T} - \frac{1}{T^*}$, $\mu_0 = \mu(T=T^*)$, Δ_0 is the energy barrier required to be overcomed and β is the *PF* factor.

There are two problem with this model in terms of the *PF* factor which does not fulfil the requirement predicted by *PF* theory[3] and T_{eff} which has no physical meaning.

Bässler suggested that the localized density of states[4], in the transport manifold, follow a Gaussian distribution. As described by equation (1-6), the applied field controls the direction of the random movement of carriers hopping from site *i* to site *j*.

$$(1-6) \qquad\qquad \nu = \nu_0 e^{-2\gamma\Delta R_{ij}} e^{-\Delta\varepsilon_{ij}/kT}$$

Where ν is the frequency of hopping, ν_0 is the attempt-to-hop-frequency, ΔR_{ij} is the distance between hopping sites, γ is the inverse localisation length and $\Delta\varepsilon_{ij}$ is the difference between energies of sites level.

Moreover, Bässler describes the disorder in the position of hopping sites using a second Gaussian distribution which is called the off-diagonal disorder as variance Σ^2.

Through Monte-Carlo simulation, Bässler created other equation in order to describe the behaviour of carrier mobility.

$$(1\text{-}7) \qquad \mu = \mu_0 \exp\left[-\left(\frac{2\sigma}{3kT}\right)^2\right] \exp\left[C\left\{\left(\frac{\sigma}{kT}\right)^2 - \Sigma^2\right\}\sqrt{E}\right]$$

where C is an empirical constant, μ_0 is the disordered free mobility at the limit of infinite temperature and field equalling zero[5] and Σ^2 is replaced by 2.25 for all $\Sigma \geq 1.5$.

The key results of this model are that μ scales as $\ln(\mu) \propto (T)^{-2}$ and $\ln(\mu) \propto E^{0.5}$. The $\ln(\mu) \propto E^{0.5}$ dependence of the Bässler model is supported by data that from Redecker et al[6]. At high E field, $\ln(\mu)$ may depend linearly on $E^{0.5}$, but the dependency may turn round at low field. Bässler's model suggests to plot $\ln(\mu)$ against a $E^{0.5}$ scale, and this is expected to have a straight line. This is often approximately observed[7]; the straight line may have either positive or negative slope, depending on the comparison between diagonal and off- diagonal disorder.

1.2.5 Traps

Trapped carriers are defined as charge carriers that are immobilised in localized states. In principle, but not in *TFT*, two scenarios that can take place for trapped carriers are subject to two factors which are a retention period until it becomes released and a recombination rate; combining carriers with opposite charge carriers. The latter not usually in *TFTs*, as there are only holes, or only electrons. Once the recombination rate is lower than the release rate, this scenario forms *Trap*; otherwise, when the recombination rate becomes a dominant factor, the localised states are described as *recombination centres*. The same localised states may have dual behaviours depending on temperature and the ratio of electrons and holes as charge carriers.

Traps and its columbic charge influence strongly charge transport and electric field distribution in the bulk of a device. The delay in the release of charge carriers from traps leads to hysteresis effects in devices, when applying voltage is altered in different direction[8]. The localised state catching hole above the valence band and catching electrons below the conduction band are called hole trap and electron trap, respectively, in case of inorganic semiconductors. In contrast, localised states in organic semiconductors is situated below the ionisation potential level (for hole trap) or over the electron affinity level (for electron trap). To clarify this point, these traps are not present only at the interface to an insulator, but also in the bulk of the *OSC*.

Since, the semiconductor-insulator interface contains high densities of traps that capture selectively one kind of charge carriers, organic semiconductors are likely to be unipolar (transporting one type of charge carriers) and rarely to be ambipolar. When semiconductors transport both kind of nearly equal concentrations of charge carriers, this semiconductors are known as ambipolar semiconductors. Chua *et al* reveals that once the interface is freed from common electron traps which is a hydroxyl group (*OH*), the polymers of hole charge carriers (*p*- type) can confirm the presence of electron charge carriers (*n*-type), as well[9]. Even though, the trapped charge carriers become immobilised in localised trap states, the charge fields weaken electric field within the bulk of a semiconductor. Another reason of unipolar behaviour is that most of the conjugated organic semiconductors have large gaps bigger than 1.5 eV, so the injection of one carrier from a contact metal matches just one energy level of organic semiconductors not both. Organic transistors that operate under ambipolar behaviour can be accomplished by either having materials with small gaps[10], blend of two different semiconductors[11] or hetero-structure (bilayers) of two materials[12]. However, for sensing applications transistors with ambipolar behaviour are not desirable because of large off-current that may interfere with sensing action and large power consumption.

The two reasons may explain the sources of traps including impurities and structural defects. Nicolai *et al* pointed out that, in different polymers tested, all share common Gaussian electron- trap distribution approximately around E_{trap} ~ 3.6 eV below the vacuum level[13]. Also, he proved that when the electron affinity is larger than 3.6 eV, the charge carriers transport in trap-free states, as indicated in Figure 6. The reason of the electron traps is because of bishydrated- oxygen, such as H_2O-O_2 complexes, as proposed by Quantum chemical calculations[13]. Once the conjugated semiconductors are exposed to different air- borne species, such as oxygen and water, the materials get oxidized. For example, the hydrogen atoms in central benzene rings of pentacene are replaced by oxygen forming double- bonds with carbons. This means that the conjugation of central benzene rings is destroyed which, in turn, reduces the overlapping of π system over molecules.
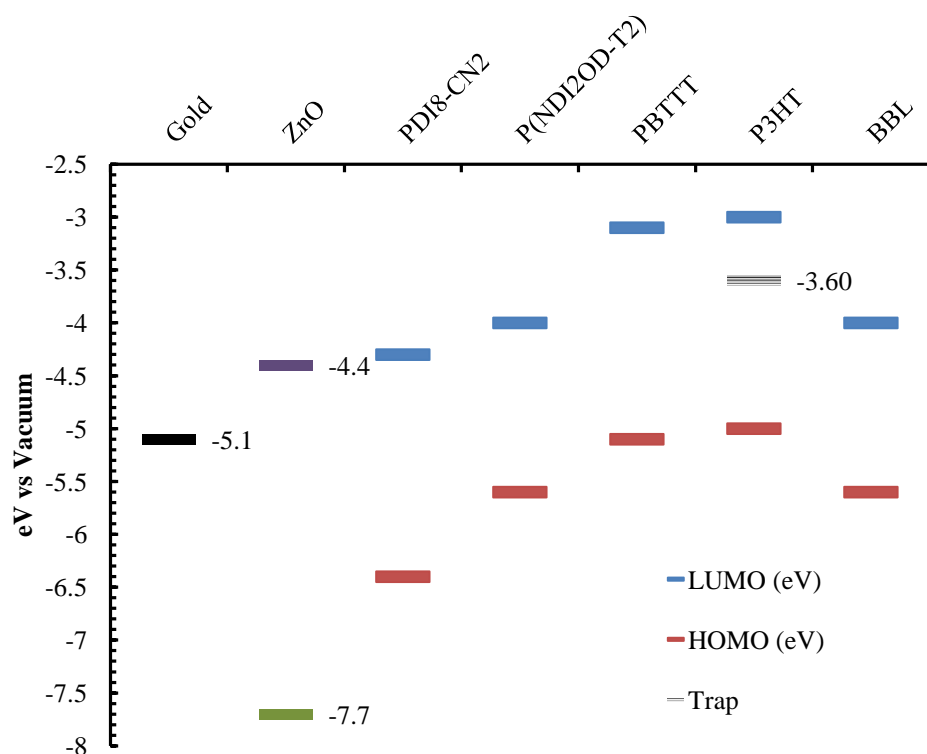
Figure 6, the LUMO and HOMO level of materials used in this thesis, also including conduction (**Violet line**) and valence (**Green line**) bands of ZnO with the work function of gold contact (**Black line**) and traps at 3.6 eV[13].

1.3 Inorganic semiconductors

Inorganic compounds are lack of carbon-hydrogen bonds. The inorganic semiconductor material that is commonly and heavily used is silicon. Silicon is the basis of the evolution of advanced transistor technology, such as CMOS integrated circuits. The heavily doped silicon can reach mobility of 1,450 $cm^2V^{-1}s^{-1}$ (for electrons) and 500 $cm^2V^{-1}s^{-1}$ (for hole) at 300 K[14].

The aim, in this section, is to present briefly the important concepts of an inorganic semiconductor starting with crystals arrangement ending to the charge carriers transporting.

1.3.1 Crystals and energy bands

In *3D* space, the crystals are built initially by smallest block unit called a *unit cell* which may contain one or more than one atom. The atoms, silicon atoms, for example, in this sort of lattice are bound together by covalent bonding which means they share electrons in their outer shell of orbital with their close neighbours. These electrons are subject to the *Bloch's theorem* which describes the propagation of waves, here

electrons, in a periodic structure. This overlapping of neighbouring atoms in a crystal would increase the number new allowed energy levels to be occupied by electrons following *Pauli principle*; no two electrons may share the same set of quantum numbers, otherwise the total wave function would not be anti- symmetric under exchange of these two electrons. Also, this overlapping would split the existing energy level into more closely spaced ones. The *density of states (DoS)* is defined as the number of allowed energy states of a given energy range per unit volume.

As seen in the electron configuration of silicon atom ($1s^2$ $2s^2$ $2p^6$ $3s^2$ $3p^2$ $\equiv$ $3s^2$ $3p_x^1$ $3p_y^1$ $3p_z^0$), the outer shell consists of two degenerated energy level. At absolute zero (*T*=0K), two of four valence electrons are located in $3s$ and other two electrons in $3p$. However, in crystal case, a new energy level generated in 3s sub-shell and $3p$, as well, (total of four quantum states each) because of overlapping of electrons; therefore, all four valence electrons occupy ground states in the valence band and leaving conduction band unoccupied. As described in section 1.1, the concept of band-gap and Fermi level are defined.

In the ground state, the crystal does not display electrical conductivity. Only when, electrons are excited into the conduction band by heat or light which also produces electron deficiencies in valence band called holes. Both electrons and holes participate in charge conduction.

1.3.2 Intrinsic and extrinsic semiconductors, and the transport of charge carrier

The thermal activation at a given non-zero temperature is a capable mechanism to induce the electron- hole pair generation. The semiconductor is considered as an *intrinsic*, once the amount of impurities in a semiconductor crystal are little comparing to the amount of thermally- generated carriers. Otherwise, the addition of dopants to the crystal produces new energy levels below the conduction band and above valence band. This semiconductor material is called as *extrinsic*. In Silicon case, the common *n-* type and *p-* type dopants are *acceptors* from Group III and *donors* from Group V in periodic table elements, respectively. In general, a doping agent being more electronegative than the main crystal element provides electrons to the crystal, so such dopants are called *donors*. The extra provided electrons are loosely bound to their original nuclei and can mo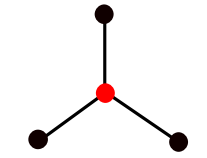re be excited easily to become free electrons and contribute to the overall charge carriers. The *ionisation energy* is the required energy for exciting electrons. In the contrary, electropositive dopants provide holes to the crystal by occupying neighbouring electrons, so dopants are called as *acceptors*. Pentavalent

impurities (i.e. Arsenic and Phosphorous) having 5 valence electrons contribute extra electrons and make *n-* type semiconductors. Trivalent impurities (i.e. Boron, Aluminium and Gallium) having the fourth valence electron missing results in *p-* type semiconductors, and holes move without restraint in Silicon lattice.

The total amount of electrons per unit volume in a semiconductor can be calculated using the following equation,

(1-8) $$\frac{N}{V} = \int_{-\infty}^{\infty} g(E)F(E)dE$$

where *g(E)* is the probability of an electron occupying each state of *F(E)* for a range which extends from the top of the conduction band to the bottom of the valence band, *F(E)* is known as *Fermi distribution function*.

In the case of intrinsic semiconductors at room temperature, the Fermi energy is located about in the middle of the bandgap E_g. The *electron density* at the bottom of the conduction band alone is denoted by *n*, whereas the *hole density* at the top of the valence band by *p*. For an intrinsic semiconductor, the *intrinsic carrier density* is calculated by,

(1-9) $$n = p = n_i$$

In lightly-doped semiconductors, called as *non-degenerate semiconductors*, the electron or hole density is very small compared to the effective density of states in the conduction or valence band, respectively. In the case of *donors*, it is believed that all donors can be activated thermally, at room temperature, and their density is denoted by N_D. This mechanism is well-known as *complete ionisation*[15]. The level of Fermi energy is changing because of this doping and moves towards the bottom of the conduction band and its value can be calculated by:

(1-10) $$E_C - E_F = k_B T \ln\left(\frac{N_C}{N_D}\right)$$

Where k_B is the Boltzmann's constant, and T is the absolute temperature.

Also, once *acceptors* of density N_A are available in the crystal, the level of Fermi energy moves nearer to the top of the valence band. Its value can be calculated by:

$$(1\text{-}11) \qquad\qquad E_F - E_V = k_B T \ln\left(\frac{N_V}{N_A}\right)$$

Since, the *intrinsic Fermi level* is referred to E_i, the charge carrier densities with respect to the intrinsic quantities is expressed as n_i and E_i;

$$(1\text{-}12) \qquad\qquad n = n_i \, exp\left(\frac{E_F - E_i}{kT}\right)$$

and

$$(1\text{-}13) \qquad\qquad p = n_i \, exp\left(\frac{E_i - E_F}{kT}\right)$$

As in the case of intrinsic semiconductors, the product of n and p constantly equals n_i^2 at thermal equilibrium. This relationship is known as *mass action law*:

$$(1\text{-}14) \qquad\qquad n \, p = n_i^2$$

When both donors and acceptors exist in the same crystal, the one of the highest concentration determines the kind of the conduction. The carriers that are present in higher/lower concentration are called majority/minority carriers, respectively. In an extrinsic semiconductor, once electrons are the majority carriers, the semiconductor is considered as *n-* type. Similarly, when holes are in the majority, it is called *p-* type.

In the case of inorganic semiconductors, many factors contribute to the conduction and transport of charge carriers, such as *carrier drift* and *diffusion*, as main factors. Also, other conduction mechanism can have a big contribution to semiconductors, such as *quantum tunnelling*, *electron hole pair generation* and *recombination* and many other. A brief description will be provided to just two main factors.

1.3.3 Carrier mobility in crystals

In the presence of impurities, crystal defects and the thermal vibration of the lattice, the moving of charge carriers described as waves with wave vector k may come across to collisions and scattering in their way. The thermal vibration is activated thermally at non-zero temperature, so the lattice vibrations supply kinetic energy to charge carriers. Thus, either impurities or scattering centres are effectively slow charge carriers down. The model employed to describe a band- like transport is called Drude model[16], as described in equation (1-16).

Once a bias voltage is applied to a semiconductor, the free electrons in partially occupied conduction bands get affected by electrostatic force and carriers drift along the applied field. The drift velocity that is induced by the electric field in x-axis is calculated by following,

$$(1\text{-}15) \qquad \frac{d}{dt}\langle v_x\rangle = \frac{q}{m_e^*}E_x - \frac{1}{\tau}\langle v_x\rangle$$

Where, q the charge carrier, m_e^* is the effective mass on the charge carrier (electron in this case), τ is the time between to collusion (mean free time) and E is the electric field produced by applied voltage. Steady state corresponds to $\frac{d}{dt}\langle v_x\rangle = 0$. Under such circumstances, the solution for the previews equation is written as,

$$(1\text{-}16) \qquad \langle v_x\rangle = \frac{q\tau}{m_e^*}E_x = \mu_e E_x$$

The value of $q\tau/m_e^*$ represents electron mobility μ_e. In same way, μ_h is correspond to hole mobility. This model is valid under one condition which is that λ is the mean distance between two collision (mean free path) is the distance between two atoms in crystals. The mean free path is taken from following equation,

$$(1\text{-}17) \qquad \lambda = v_{th}\tau$$

Where, $v_{th} = \sqrt{3kT/m_e^*}$ is electron thermal velocity (~105 m/s at room temperature. For both equations (1-16) and (1-17), the mobility is defined as,

$$(1\text{-}18) \qquad \mu = \frac{q\lambda}{m_e^* v_{th}}$$

The standard electron mass that used to be utilized in vacuum cannot be used in the crystal lattice, since the periodic forces affect the atoms[17], and charge carriers move in the distance beyond the size of the unit cell. This would imply to introduce the effective mass of electrons and holes, and both depend on energy-momentum relationship $E(k)$ as mention in,

$$(1\text{-}19) \qquad m_e^* = \frac{\hbar k^2}{2(E(k)-E_0)}$$

Since $E(k)$ is the energy of electon in band, E_0 is the edge energy of the band, $\hbar$ is the Planck constant (~6.582×10^{-10} eV.s) and k is the wave vactor.

Turing back to an important parameter in both organic and inorganic semiconductors which is mobility, it usually suffers from different scattering mechanisms, while charge carriers pass through a semiconductor. Coulomb scattering and phonon scattering are due to deflection of charge carriers because of ionised impurities and thermal lattice vibration, respectively. Both mechanisms are temperature dependent. It is found that the dependence follows the next equation,

(1-20) $$\mu(T) \propto T^{-n}$$

In most cases, n is positive. When temperature is declined, the mobility increases. At low temperatures, coulomb scattering is dominant especially in highly-doped semiconductors. However, at high temperature, the phonon scattering dominates the mobility degradation leading to a higher probability of collisions and shorten the mean free time τ. This effect is dissimilar to organic semiconductors, since temperature increase the mobility of materials because of different mechanisms involved (see section 1.2.3).

The summation of electron and hole drift current gives the conductivity σ because of the effect of electric field according to,

(1-21) $$\sigma = qn\mu_n + qp\mu_p$$

Where, n is the density of electrons and p is the density of holes.

So far, drift current, as a result of the potential gradient, is the only transport mechanism assuming that the semiconductor is uniformly doped. However, this assumption is not true, since the semiconductor always possesses impurities that are not distributed uniformly. This moving from high to low concentration regions results in concentration gradients. The diffusion current is calculated as,

(1-22) $$J_{diff} = \frac{I_{diff}}{A} = q \left(D_n \frac{dn}{dx} - D_p \frac{dp}{dx} \right)$$

Where D_n and D_p are the diffusion coefficients of electrons and holes, respectively, and dn/dx and dp/dx are the spatial derivatives of electron density for electrons and holes, as well. This sum up the components of current density for both electrons and holes including the drift current[18] as following,

$$J_e = q \left(n\mu_n E + D_n \frac{dn}{dx} \right)$$

$$(1\text{-}23) \qquad\qquad J_h = q\left(p\mu_h E + D_h \frac{dp}{dx} \right)$$

The diffusion constant and mobility are connected by the Einstein relation[17] describing the diffusion dependency on mobility,

$$(1\text{-}24) \qquad\qquad D_h = \frac{kT}{q}\mu_h \quad \text{and} \quad D_e = \frac{kT}{q}\mu_e$$

Where k is Boltzmann'a constant, $(1.38 \times 10^{-10}$ J $\mathbf{K}^{-1})$, and T is the temperature.

1.4   History of transistor

Although, the concept of metal-oxide-semiconductor field effect transistor (*MOSFET*) was filed as a patent credited to Lilienfeld in 1925, the bulky and electricity-consumed vacuum tube was used that time as a signal processing device. Since, the invention of first (bipolar) transistor in 1947 was attributed to John Bardeen, Walter Brattain and William Shockley, rewarded the 1956 Noble Prize later, the transistors have passed through other remarkable inventions in terms of building integrated circuit by Kilby and Noyce between 1958 and 1959, and constructed metal oxide semiconductor field effect transistor (*MOSFET*) by Atalla and Kahng in 1959[19]. Silicon based transistor technology was an excellent alternative to bulky, power-consuming vacuum tubes. Nowadays, the transistor is the cornerstone beyond of all sophisticated electronics devices such as mobile phones and computers. Moreover, in the last decade going back to 1970s for inorganic – *ISFET* = 'ion sensitive field effect transistor', the ambition to develop sufficient devices for detecting and quantifying chemical and biochemical materials has been increasingly attracting scientists. Sensor applications include odour sensors for airbone analytes[20] and environmental monitoring sensors for aqueous pollutants[21-22].

In spite of its flexibility, low cost and ease of fabrication, polymer materials were considered as insulating materials in the past. This sole application was, however, modified by the discovery of Alan J. Heeger, Alan G. MacDiarmid and Hideki Shirakawa, awarded the Noble Prize in 2000. By exposing to iodine vapour, polyacetylene became more conductive by several orders of magnitude[23]. This produced a new category of materials which are called as 'synthetic- metals'= highly doped semiconductors. These newly invented materials have attracted a great interested in its electronic application such as light-emitting diode, photovoltaic cell, sensors and thin- film semiconductors. Since, the physical and chemical properties of organic materials can be modified by manipulating the chemical structure; this field of

research can be located in the edge between physics and chemistry. Consequently, Organic semiconductors offer unique potential for selective and specific interactions with analytes, and thus selective and specific sensor response[24]. To be more specific, an electrolyte- gated organic field effect transistor (*EGOFET*) may have the ability to play this role for sensing these elements. In fact, water- gated transistor was proved by Kergoat *et al*[25-26] that it possesses a stable electrical characteristic with very low voltage operation range comparable to voltage provided by regular batteries.

1.5   Thin film transistors

The useful transistors configuration for organic semiconductors in practical applications is the thin-film transistors (*TFT*). In the 1960s, Paul Weimer initially developed and proposed this concept in polycrystalline inorganic transistors[27]. In the 1980s, an organic *TFT* was first reported[28-29].
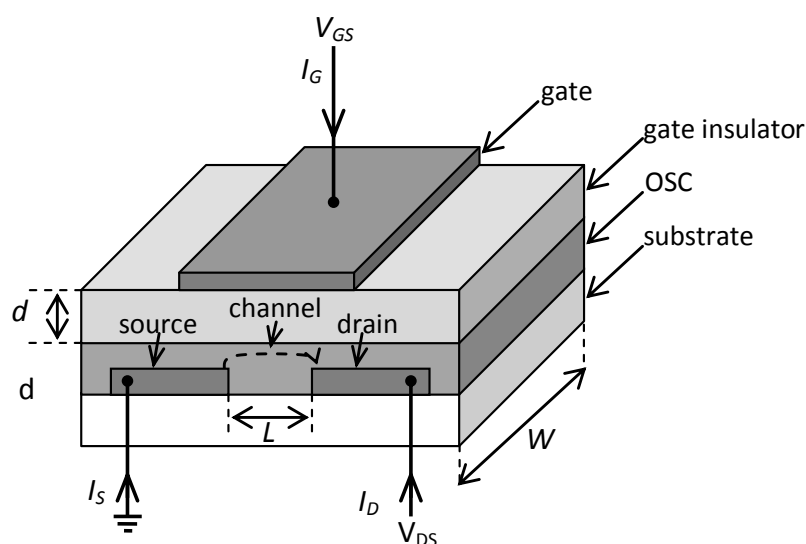
Figure 7, the illustration for the structure of a TFT with channel width *W*, channel length *L*. the flow of charges in the channel is signified by the dashed line.

From Figure 7, the organic semiconductor is deposited between two metal contacts (source, drain) and a gate insulator. The gate contact is deposited over a gate insulator. All layers are deposited at the surface of insulated substrates, such as glass and Silicon oxides. The first organic transistor containing an electrolyte rather than the metal gate contact was verified in 1984[30], but that transistor operated as electrochemical transistors (*ECT*) not field-effect transistor (*FET*) which is clearly demonstrated later by Tsumura *et al*[28]. The accumulation regime of the field-effect describes transistors that usually are 'normally off', but the transistors become conductive between 'Source' and 'Drain' only when the voltage of appropriate polarity is applied to a third contact (the gate contact). Consequently, passing current

in channel (*on-* current) is controlled by applying a voltage to the gate. On contrary, the depletion regime is normally on and requires a gate voltage to be switched off. The later regime is not related to field effect transistor. The way of using an electrical field to control the resistance of a semiconductor was described by Oskar Heil in 1935[31]. More descriptions about transistor's operation and configurations will be mentioned in next sections.

The field effect transistor is adopting an accumulation regime rather than depletion, since organic materials induces just one type of charge carrier either electrons or holes and utilizes an undoped property of semiconductors. As a result, the depletion regime will not be mentioned. The important parameters of *OFET*, which can be used for many applications including sensing, are charge carrier mobility (μ) and threshold voltage (V_{Th}) which means the required gate voltage to switch on the *OFET*.

1.5.1   Structure of Organic and Inorganic FET

The device's performance differs significantly with various device architectures in terms of the sequence of deposited contacts and organic/inorganic semiconductors, and each one of four architectures has its own advantages and disadvantages and specific applications. Four main and possible architectures can be employed for *FET*.

In any design, most importantly, the gate contact must be placed in front of the semiconductor's channel separated by gate insulator or attached directly to semiconductor in order for the channel to build electric double layer efficiently. Also, the energy barriers must be small between a semiconductor material and contacts' (source and drain) interfaces in order to reduce the hindrance of the charge carriers' movement between contacts.
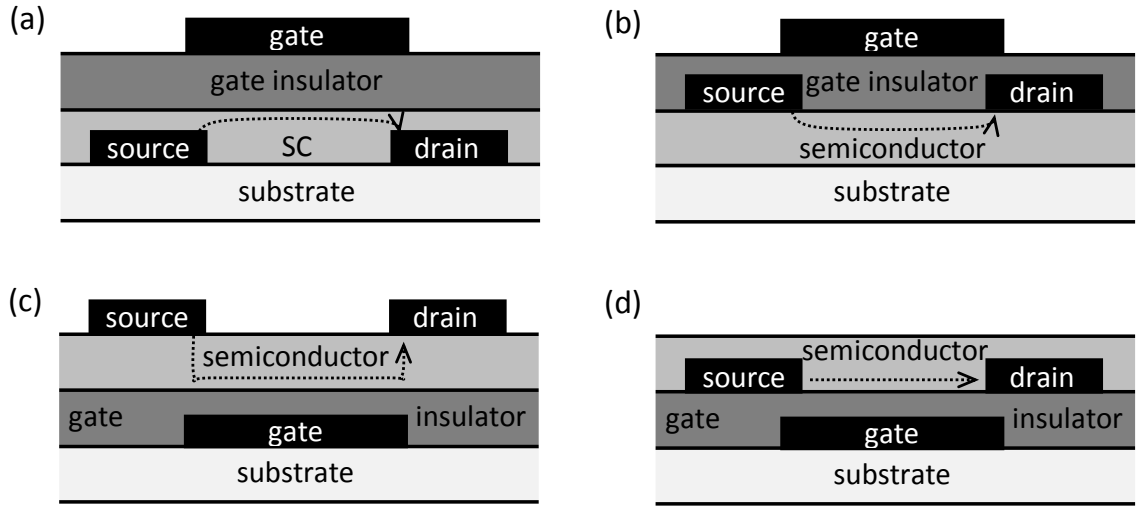
Figure 8, four different TFT configurations: the staggered structure consisting of (a) top-gate /bottom- contact structure and (c) bottom- gate/ top- contact structure, and other designs that are called coplanar that represented by (b) top-gate/top contact structure and (d) bottom-gate/bottom- contact. The flow of charge carriers is signified by dashed lines.

Experiments and simulations demonstrated that the staggered structures (Figure 8, a and c) are less influenced by energy barriers comparing to the coplanar structures (Figure 8, b and d), and this is considered as an advantage of using the staggered structures. Moreover, the modifying by proper treatment (such as, thin metal oxide[32]) of contacts' surface would reduce the energy barriers which, in turn, affects the contact resistance.

1.5.2 Operation principle and equations of FET

As seen in Figure 8, the stack of gate/insulator/semiconductor is capable of being considered as a capacitor. The capacitance of gate dielectric per unit area C_i is equal to:

(1-25) $$C_i = \frac{\varepsilon_0 \kappa}{d}$$

Where ε_0 is the vacuum permittivity, κ is relative permittivity of gate insulator and d is the thickness of gate insulator.

Once a sufficiently high voltage is applied to the gate contact, an accumulation layer builds up in the channel of transistors. A positive (negative) gate voltage introduces negative (positive) charge carriers in the channel. The built up charges are restrained in just few nano- layers of the semiconductors next to gate insulator. Usually, inorganic *FET* is depended on extrinsic (doped) semiconductors, for example *MOSFETs*; however, organic *FET* operates in the accumulation regime, since organic

semiconductor is based on intrinsic (undoped) semiconductors. The threshold voltage is generally nonzero because of dissimilarity in the energy barriers of the gate contact and the semiconductor and the presence of the remaining charges in the bulk of the semiconductor and traps at the interface between insulator-semiconductor.

A transistor is characterised by voltage-controlled (gate voltage) current induced in channel. Before explaining how the *FET* operates theoretically, a number of assumptions should be considered, and not all of these assumptions are correct in reality. Firstly, the transverse electric field that is induced by the gate voltage is bigger than the longitudinal one because of drain voltage. Secondly, the mobility assumed to be constant over the entire channel at different charge concentrations regions and electric field effect. Also, the thickness of insulator layers is smaller than the channel length. In addition, the bulk channel resistivity is higher enough than the resistivity of contacts.

The operation of a *TFT* can be categorised into three regimes with regard to the applied gate-to-source (V_{GS}) and drain-to-source (V_{DS}) voltages. These regimes are the sub-threshold, the linear and the saturated regimes.

Once the gate voltage is lower than V_{Th}, the drain current becomes exponentially proportional on the gate voltage which is so-called subthreshold regime. The subthreshold swing is represented by this equation,

$$(1\text{-}26) \qquad I_D = K\mu C_i \frac{W}{L}\left(1 - e^{-qV_{DS}/kT}\right)e^{qV_{GS}/nkT}$$

Where K is a constant related to the used materials and the structure of the device, k is the Boltzmann constant, T is the temperature, $n \geq 1$ is called the ideality factor and q is the basic charge.

The value of subthreshold is extracted from the plot of logarithm of drain current (I_D) versus V_G at constant maximum $V_{D,max}$. The quantity is called subthreshold swing taken according to,

$$(1\text{-}27) \qquad S = \frac{\partial log_{10}(I_D)}{\partial V_{GS}} = \ln(10)\frac{kT}{q}\left(1 + \frac{C_S}{C_i}\right)$$

This is a measure of how fast the switch between *off-* state and *on-* state is. The low value of subthreshold swing means that the transistor switches between two states over a very small series of gate voltages. However, the high value means that a slower transition from two states over a large range of gate voltages. The typical unit of

subthreshold swing is (mV per decade). Also, equation (1-27) describes the trap density C_s and the gate insulator capacitance C_i. In order to minimise the value of subthreshold swing, the values of C_s and C_i must be minimise.

Once a larger voltage than V_{th} is applied to V_{GS}, a uniform accumulation 'rectangular' layer of charge carriers is induced in the channel, as seen in Figure 9(a). This means that an accumulation layer that is (almost) equally strong near the drain as near the source. This operation defines the linear regime.

The linear regime describes the drain current (I_D), since I_D is propostional to V_D, in following equation:

$$(1\text{-}28) \qquad I_D = \frac{\mu C_i W}{L}\left((V_{GS} - V_{th})V_{DS} - \frac{V_{DS}^2}{2}\right) \qquad \text{for} \qquad |V_{GS} - V_{th}| > V_{DS}$$

Where V_{th} is the threshold voltage of the device, μ is the carrier mobility, C_i is the capacitance per unit area of the gate dielectric, W and L are the width and length of the channel, respectively.

The mobility can be calculated in this regime by the following equation,

$$(1\text{-}29) \qquad\qquad\qquad \mu_{lin} = \frac{L}{W C_i V_{DS}}\frac{\partial I_D}{\partial V_{GS}}$$

Increasing the drain voltage higher reduces the drain-gate voltage (while source-gate voltage remains the same), and therefore leads to a weaker accumulation layer near the drain. When $V_D = |V_G - V_T|$, the TFT reaches co- called "pinch off", as seen in Figure 9(c). Pinch- off limits drain current to a maximum even when drain voltage is further increased. This operation is called saturation regime.

Therefore, in saturation regime, the drain current is given by the equation:

$$(1\text{-}30) \qquad I_D = \frac{\mu C_i W}{2L}(V_{GS} - V_{th})^2 \qquad \text{for} \qquad V_{DS} > |V_{GS} - V_{th}| > 0$$

The mobility can be calculated in this regime by following equation,

$$(1\text{-}31) \qquad\qquad\qquad \mu_{sat} = \frac{2L}{W C_i}\left(\frac{\partial \sqrt{I_{Dsat}}}{\partial V_{GS}}\right)^2$$

The transconductance g_m is another essential concept, since it defines how the I_D is altered and modulated by V_{GS}.

$$(1\text{-}32) \qquad g_m = \frac{\partial I_D}{\partial V_{GS}} \ \ at \ \ V_{DS} = constant$$

The transconductance can be represented in linear and saturation regimes as following,

$$(1\text{-}33) \qquad g_{mlin} = \frac{W\mu C_i}{L}V_{DS} \ , \quad g_{msat} = \frac{W\mu C_i}{L}(V_{GS} - V_{Th})$$

When the gate voltage is higher than V_{Th}, these equations (above) can describe the operation of transistor.

The electrical behaviour of field-effect transistors is evaluated by the plot of the drain current versus either the drain-source bias which is called the output characteristics or the gate-source bias which is called transfer characteristics. More details about characteristics will be mentioned in sections 3.1.1.1 and 3.1.1.2.

Regardless of the considerable differences in the charge transport mechanism in inorganic and organic semiconductors, the operation of *TFTs* made of both semiconductors can be described by the same equations, above.
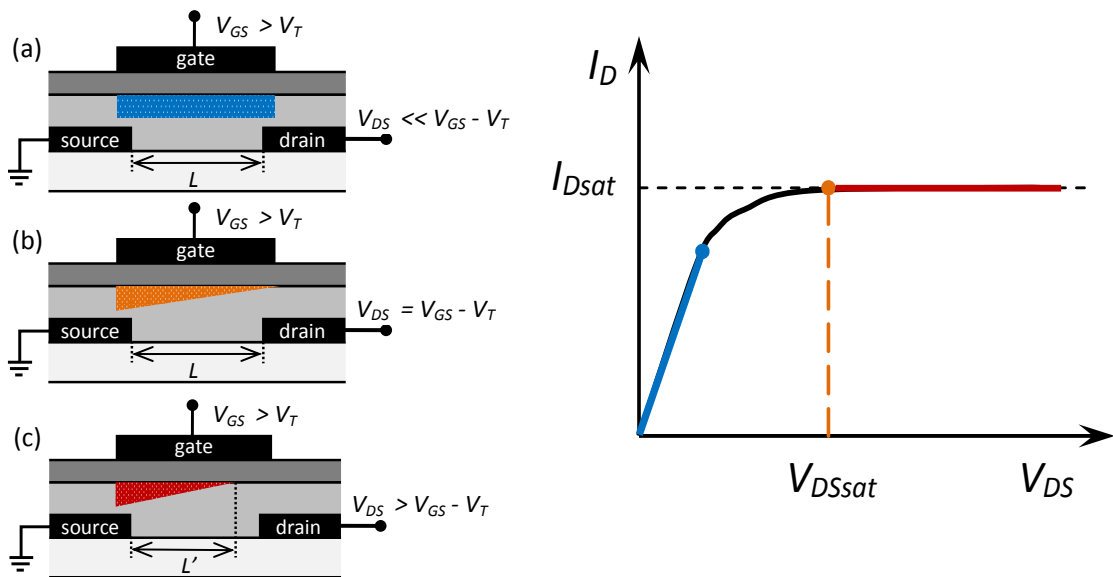
Figure 9, illustrations of the different charge distribution and voltage-controlled current characteristics in the different operating of FET: (a) the linear regime (**rectangular**); (b) the start of saturation at pinch-off; (c) the saturation regime.

1.5.3 Electrolyte as gate media

Electrolytes are materials that contain mobile ions. Many electrolytes are liquids, but solid state electrolytes are also known. As an example, dissolving salt in a polar solvent leads to dissociation of the ions into positive (+) ions (cations) and negative (-)

ions (anions). Also, some materials may undergo through the self-ionisation reaction (autoprotolysis), for example water,

$$H_2O + H_2O \rightleftharpoons OH^- + H_3O^+$$
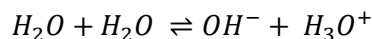
So, both dissociations contribute to build up electric double layers (*EDLs*). The exposure of water drops to atmospheric carbon dioxide (CO_2) increases H_3O^+.

The degree of dissociation determines, therefore, how strong or weak the electrolytes are, starting from a weak electrolyte (i.e. pure water) to an electrolyte in solid form. Electrolytes are electric conductors under alternating voltages, but under DC, Electrolytes become insulators due to the build- up of interfacial *EDLs*, as discussed in detail in section 1.5.3.5. To be used as liquid- medium- gated transistors, the essential property of an electrolyte is to tolerate an electrical voltage without electrochemical decomposition. In general, the specific capacitances' values of all electrolytes are between 1-10 µFcm^{-2} which depend on an electrode in contact with electrolyte. In the following, all liquids- media used for gating transistors are described, here.

1.5.3.1   DI Water

The source of ions in pure water comes from the fact that small part of the water molecule (only one in million) dissociates into hydroxide ions (OH^-) and hydrogen ions (H^+), as mentioned in the previous section. Under AC voltage, pure water is less conductive than tap water because small amounts of acids and dissolved salts raise the conductance dramatically. Tap water conducts at about 1000 (S cm^{-1})[33]. Moreover, when pure water is exposed to air, this action allows carbon dioxide[34] to dissolve and form carbonic acid which increases its conductance to 1 (S cm^{-1}). Another problem that may arise is the limited electrochemical window of water, and this may interfere with sensing analytes. However, there is a small electrochemical window of water about (1.23 V)[35].

1.5.3.2   Ionic liquid

An ionic liquid refers to a melting salt that has the melting point below or close to room temperature. Two ions with opposite charges constitute the ionic liquid (typically organic anions with bigger cations). Also, ionic liquid is a good solvent with no volatility and great stability thermally, chemically and electrochemically. In general, the ionic liquids are highly conductive reaching 0.1 (S cm^{-1})[36], since the

concentration of ions is higher and rather larger size comparing to dissociated water molecules. *EMI-TFSI* is the ionic liquid used here which stands for 1-ethyl-3-methylimidazolium-bis(trifluoromethyl-sulfonyl)imide (Figure 10) which has been used for gating TFTs before[37]. *EMI-TFSI* has large electrochemical window of 4.3 V and gives the capacitance about ~6.5 µFcm^{-2} at 1 Hz and ~5.17 µFcm^{-2} at 10 Hz[38]. Together, that means the maximum field we can go to (strictly, the maximum electric displacement, $D = C_i \times V_{window}$) can be almost 10 times bigger than for pure water gating. Consequently, the IL- gating organic semiconductor is built to achieve low voltage and fast- switching *FET* without sacrificing mobility.
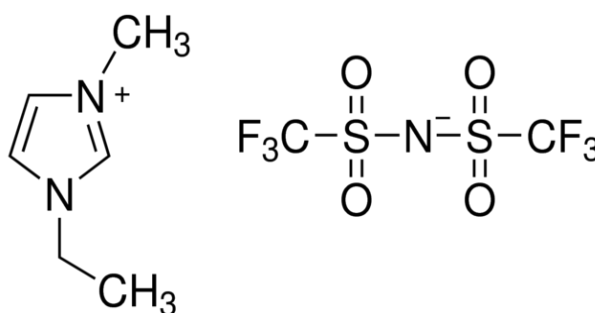
Figure 10, the chemical structure of 1-ethyl-3-methylimidazolium-bis(trifluoromethyl-sulfonyl)imide, (EMI-TFSI).

1.5.3.3 Solvent

It is a substance, usually liquid, that is used to dissolve a solute in order to have a solution. This solution must be homogenous not leaving any residuals of a solute. At the molecular level, such uniformly distributed solute in solvent is referred as miscibility; otherwise, it is called immiscibility. The solvent can give a mean to control temperature. Thus, it helps to increase the energy of collision of molecular (entropy) or to absorb the resultant heat from the reaction between solute and solvent.

For choosing the right solvent for solute, the simple rule is "like dissolve like" that means polar solvent will only dissolve the reactants with the same polarity which is polar reactants and vice versa. The polarity of solvent can be measured by three criteria: the solvent dipole moment; its dielectric constant and the miscibility with water. In general, the solvent possesses large dipole moment and high dielectric considered as polar; however, the one have small dipole moment and dielectric constant is categorized as non-polar. In more practical way, since water is polar liquid, it can be used to categorize polar and non-polar to evaluate the miscibility or immiscibility of solvent with water, respectively. Moreover, the polar solvent is divided into type: polar protic and polar aprotic. When a solvent contains a hydrogen

atom attached to an electronegative atom (i.e. oxygen), the solvent is called protic which is generally represented as R-OH (R is a chemical compound), such as Water (H-OH) and methanol (CH₃-OH). Thus, the dipole moment of this solvent comes from this (OH) bond. The aprotic solvent represents the solvent not containing (OH). However, some aprotic solvents still have large dipole moment originating from multiple bond (i.e. Acetone $(CH_3)_2$ C═O and Acetonitrile CH_3-C≡N).

1.5.3.4   Conventional insulators

In general, the transport of charge carriers in a *TFT* channel occurs at the semiconductor- gate insulator interface. The transistor characteristics get affected significantly by the properties of a gate insulator at the interface with the semiconductor[39]. The gate insulator with low- permittivity reduces the value of capacitance per unit area of gate insulator C_i as well as the transistor's performance. In contrary, high-permittivity one produces extra energetic disorder in the channel which leads to reduce the transport of charge carriers. The typical gate insulator material is SiO_2 which has electrons' traps affecting electron carriers. Chua *et al* suggested to use polyethylene in the surface of SiO_2 in order to reduce the presence of hydroxyls (-OH) (localised dipoles) which is thought to be a reason of trapping electrons[40]. It is usually suggested to treat the surface of a metal oxide with a self-assembled monolayer (*SAM*) (see section 2.2.4) as a buffer or a barrier layer between the gate insulator (or electrolyte) and the organic semiconductor.

The work- function of gate metal is not the main requirement for affecting the FETs parameters; however, the saturated drain current depends on C_i of gate medium. When the capacitance of gate increases, the value of threshold would decreases because of the capacitance's ability to accumulate a greater charge density. For having low-voltage operation, the used gate insulator should have a high capacitance whether by reducing the thickness of gate insulator or using gate insulator material having high permittivity or combining two ways, as showing in equation (1-25). Table 2 provides the values of relative permittivity ε_r, thickness and specific C_i of some gate insulators including solution- processed insulators. The given values of ε_r and C_i are applied to bulk (thick film), and these value may not agree with different thickness (low thickness) of the mentioned gate insulators.

Insulator	ε_r relative permittivity	Thickness (nm)	C_i (nF.cm⁻²)
PMMA	3.5	160	19.4
	3.2	560	5.1

PVP	6.4	450	12.6
PVA	10	500	17.7
TiO$_2$	41	97	373
	21	7-8	2420
Al$_2$O$_3$	9-11	6.5	650-700
	9	4.8	1660

Table 2, the relative permittivity values of common solution- processed gate insulator. All values are taken from the review of Kim *et al*[41] and A. Maliakal[42].

1.5.3.5 Electric double layers (*EDLs*)

Assuming a pair of metal electrodes is separated by an electrolyte, forming a capacitor. When a voltage bias is applied to the electrode pair, mobile ions will migrate towards the electrodes with the respective opposite electric polarity, leading to the formation of a thin sheet or 'cloud' of ions with polarity opposite to the electrode's polarity; such ions are known as 'counter- ions'. The combination of a biased metal contact and the sheet of ions with opposite polarity is known as *Electric Double Layer* (*EDL*).

Application of voltage bias to an electrolytic capacitor always leads to the formation of two opposing *EDLs*, an anionic *EDL* at the positively biased electrode (anode), and a cationic *EDL* at the negatively biased electrode (cathode). A number of ever more sophisticated models of the *EDL* have been devised over time to predict the precise distribution of ions, field, and potential, at the electrode/electrolyte interface, which will be briefly discussed below. However, all of these models qualitatively agree on a number of key properties of *EDLs*:

1. The EDL is very thin, in the order 1 nm[43]. Within this thin layer, carrier density is very high, in the order $(10^{13}–10^{14})$ cm^{-2}.
2. The field associated with the *EDL* is concentrated near the interface, the bulk of the electrolyte remains field- free. Consequently, the potential makes near step- like changes at the interfaces but is constant inside the electrolyte.
3. The build- up of the *EDL* after the application of a bias is much slower than the (almost instant) build- up of the field and potential distribution in a dielectric.

Properties 1 and 2 are illustrated on the right of Figure 11, where they are compared to the behaviour of dielectrics. The properties 1 to 3 explain the observed behaviour of *EDL* capacitors, and their differences to dielectric capacitors. Property 1

explains the very high capacitance of *EDL* capacitors, and property 2 shows why a capacitance is largely independent of the capacitors' bulk dimensions and also explains why electrolytes are DC insulators. Property 3 explains why they are AC conductors: If bias polarity is reversed faster than the characteristic time for *EDL* build- up, an electrolyte will be conductive.
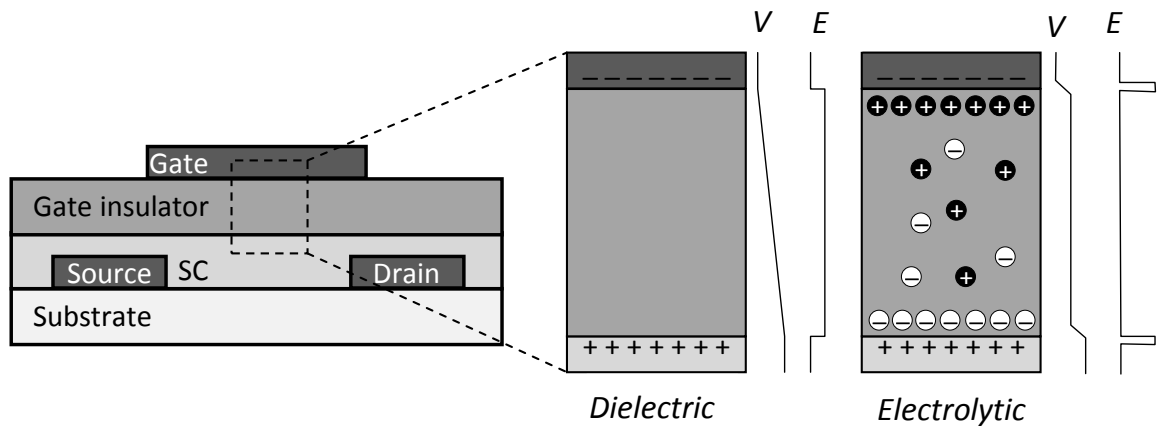
Figure 11, a diagram of the voltage (V) profile and the distributions of electric field (E), once a negative gate voltage is applied in a dielectric and electrolytic gate medium.[44]

To give a brief overview over the quantitative models that describe the *EDL.* Historically, the *EDL* was first discussed by *Helmholtz.* the *Helmholtz model* assumes that counter- ions are attracted to the surface of a biased electrode and formed a uniform thin sheet at distance (*d*) from the electrode until charge per area become balanced. From the electrical potential of surface, the potential drops linearly, reaching zero potential in the bulk of electrolyte at a limited distance. The distance between attracted counter-ions and an electrode is limited by the presence of the solvent molecules (i.e. water). This distance makes a boundary known as "outer *Helmholtz* plane". This model fails to show the dependency of a measured capacitance on the electrical potential of electrodes and concentration of electrolyte especially at lower concentration, and the rigid layers of charges do not exist in reality. Considering the thermal motion's effect on the distribution of attracted ions, the *Goüy- Chapman-Stern* (*CGS*) model suggests that the electrical potential falls exponentially away from the electrode forming two distinct layers which are the *Helmholtz layer* and the *diffusing layer* containing positive and negative charges. In spite of the prediction of the *CGS* model to the dependency of capacitance on the potential and concentration, the model does not match the experimental results, in particular the measured capacitance is much lower than that suggested from model. The *Stern model* combines the two previous models. Stern assumes that the attracted ions are not enough to fully balance the electrode by the *Helmholtz layer* alone, and the rest of surface charge of

the electrode is balanced completely by also a contribution of a *diffuse layer*. At the outer *Helmholtz layer*, the potential drops linearly followed by an exponential decay of the potential in the *diffuse layer*. Based on *CGS* model, the capacitance of a single electrode consists of contribution of two layers, as seen in following equation[45],

$$1\text{-}34 \qquad\qquad \frac{1}{C_S} = \frac{1}{C_S^{Hz}} + \frac{1}{C_S^{D}}$$

where C_S^{Hz} is the capacitance of *Helmholtz layer* which given by equation (1-25) with distance H representing a double layer distance between electrode and the centre of accumulative counter- ions, and C_S^{D} is the capacitance of *diffuse layer* that can be calculated[45] by complex equation including many parameters, such as electrical potential in the diffuse layer (ψ_D), z is the valency of electrolyte, e is the elemental charge molar concentration of the electrolyte in the bulk C_∞, Debye length λ_D with other constants (Avagadro's number N_A and Boltzmann constant k_B), as following,

$$1\text{-}35 \qquad\qquad C_S^{D} = \frac{4 z e N_A C_\infty \lambda_D}{\psi_D} \sinh\left(\frac{z e \psi_D}{2 k_B T}\right)$$

However, neither of these theories gives an account of the practically important dynamics of *EDL* build- up, and its dependence on ion concentration and electrode distance except *CGS* model. Wang et al[45] reported to the significant effect of the concentration of electrolyte to the capacitance of electrode using numerical simulations of electrochemical impedance spectroscopy, for example changing in concentration $C_\infty = 0.01$ mol/l to 0.001 mol/l give change in capacitance about $C_S^{D} = 12.7$ µFcm^{-2} to 40.3 µFcm^{-2}. As a result, the last fact must be considered, once the electrolyte- gated is used for sensor application in order to avoid misinterpretation of data coming from measurement.

The voltage profile and the distribution of electric field changes, once the negative voltage is applied at gate contact for dielectric and electrolytic. Figure 11 shows a remarkable difference in a dielectric, and an electrolyte. In a dielectric insulator, the electrostatic potential drops gradually, so the gate voltage generates a uniform and constant electric field. In electrolyte as gate medium, the applied voltage drops just near the interfaces and build up the Electric Double Layers (*EDLs*); as a result, the high electric field is only concentrated near the interfaces which have the high value of the electric field on the order of 10^9 (Vm^{-1})[46], and the bulk will be a negligible field effect and a constant value of applied voltage. Thus, the redistributing of ions comes first, and then the different field distribution is a result. Mathematically, the smaller

capacitance value in electrolyte- semiconductors interface would be dominant in the total of two *EDLs*, capacitors, connected in series. Since the typical value of dominant capacitor is on the order of 10 μFcm^{-2}, this would induce a large concentration of charge carriers about ($\sim 10^{15}$ cm^{-2}) in the channel of a transistor at low applied gate voltage (< 3 V)[47].

1.5.4 Electrolyte- Gated Organic FET (EGOFET) and operation principle

Different materials are used as a mean to separate electrically the channel of a transistor from the gate contact and also produce an electric field at the medium/semiconductor interfaces, such as dielectrics, organic layers, oxides and electrolytes. Moreover, Kergoat *et al*[25] reported a new approach to serve this by using pure water. Someya *et al*[21] claimed that *OFET* works in both standing (drops) and flowing water and also mentioned that this will open a new field towards transferring or passing chemical information by changing of electrical potential at active material/electrolyte (pure-water) interfaces to electric signals through devices. Water as a gate medium is capable of forming a nano- scale of electric double layer (*EDL*) that induces high capacitance in order to let transistor operate in low threshold *OFETs*.

Someya *et al*, Kergoat *et al* and others[21,25,48] confirmed that the main phenomenon exists which is the coexistence between field effect (electrostatic field-operated) mode (*FET*) and electrochemical mode (*ECT*), once the organic semiconductor is gated by water or electrolyte, in general. The former mode takes place in the interfaces between active organic materials and electrolyte because *EDLs*, so the uniformed electric field is produced. The latter mode happens, once ions pass through the interfaces and moves inside organic materials bulk and dope it, as seen in Figure 13. Consequently, the electrochemical mode and field effect mode are considered as depletion and accumulation mode[48], respectively. Kergoat *et al* believe that a water- gated *OFET* operates entirely at field-effect mode because of the present of high hydrophobicity and density materials. In contrast, Olle Inganäs *et al* prove that their transistors show both modes with high speed of switching, maybe, as they uses fiber-based electrolyte-gated devices that are different to conventional field- effect one.

Since *WGOFET* is considered, as well, as a capacitor where a channel with charge carrier is one of plates and the gate, above the channel, is another one, as seen in Figure 12.

Once the channel coated by layer that has an interactions with ions or molecules, the surface potential will change depending on these interactions[49]. This change of surface potential (electrical potential) can be realized or transferred to transistor characteristics and may be influenced either by threshold voltage[22] (V_{Th}) or mobility[21] (μ). Thus, this transistor may work as an electric transducer.
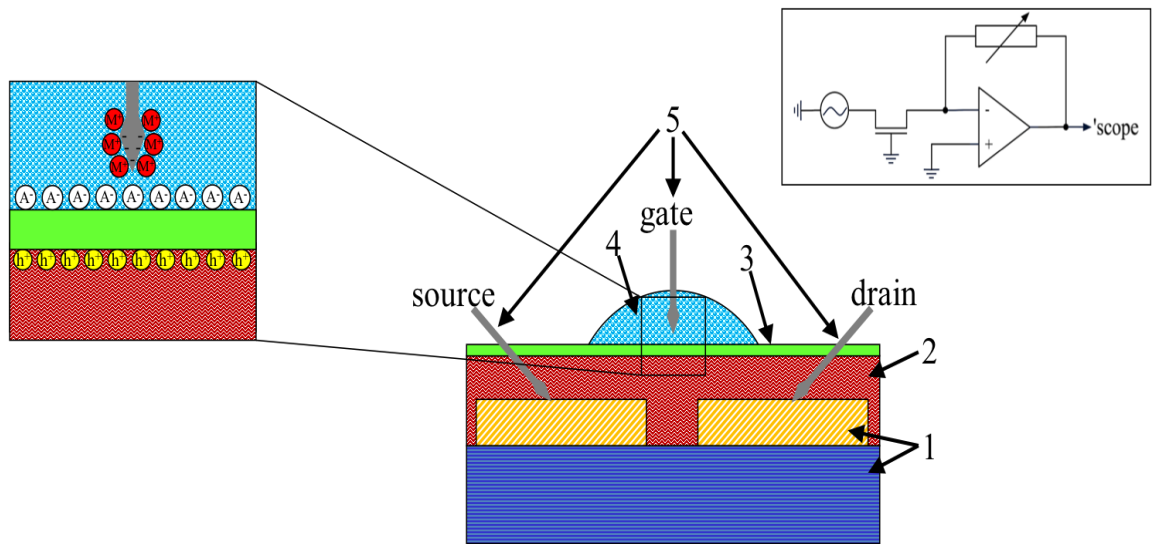
Figure 12, A calixarene as protective layer against doping, water- gated transistor, shown schematically. 1) Si/SiO$_2$ substrate and Au contacts; 2) *P3HT* layer; 3) Calixarene film; 4) Water sample; 5) Gate contact. The inset on the left is an enlargement of the calixarene interface under positive source voltage, showing a cationic *EDL* at the gate/water interface, an anionic *EDL* at the water/sensitiser interface, and a corresponding hole accumulation layer at the semiconductor/sensitiser interface. The inset on the right shows the electronic circuit we used to drive and measure water- gated transistors.
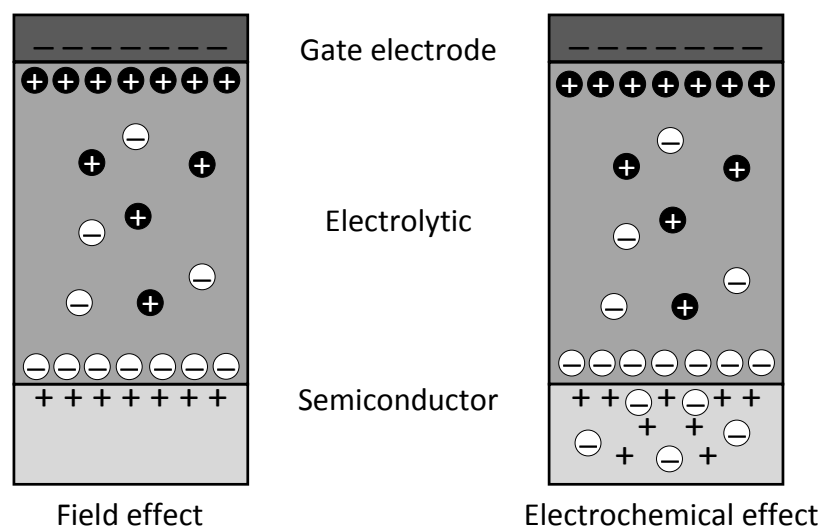
Figure 13, a diagram of an electrolyte- gated OCS film in Field Effect status (left), and in Electrochemical status (right)[47].

The source of signal transduction changing can be explained by two reasons. Firstly, an analyte interacts with organic semiconductors that, in turn, adsorb them in the grain boundaries seeding traps states inside the film. This leads to an increase in the resistivity of the charge transport between grains. Secondly, the accumulations of analytes on the dielectric layer above the conducting channel also cause electric field to be altered[50].

The transistor having electrochemical current can result in destroying[22,51], slow responding (switch on/off) of transistor[52] and may not have the capability to identify chemically the analytes. Chemical doping could increase the conductivity of bulk by electrochemical addition of ions from electrolytes to semiconductors. To reduce or even prevent this detrimental mode, immobile anions in polyelectrolyte in *p*- type *OFET* has been applied[53].

The field effect mode is desirable, since the phase transition from insulation stage of the organic material to conducting stage takes place so rapidly which just takes about < 10 (ms) to reach it.

1.5.4.1 Contact resistance and parasitic capacitance

For an ideal operation of transistors, the sheet resistance of contacts must be lower than the sheet resistance of the channel even in the presence of a strong accumulation layer, as seen in Figure 14. However, when contacts are formed by evaporated metals, this is not usually an issue. More critical is the demand that the transfer of carriers from the source electrode to channel (injection) and channel to drain electrode (extraction) shall also be of negligible resistance[54], which is not always true. An injection barrier (mismatch between electrode work function, and semiconductor transport level) often leads to high contact resistance, although such barriers can still be overcome by an applied gate voltage, in particular when *EDL* gate media are used in the 'top contact' geometry, as seen in section 1.2.3. Barrier- free contacts are called "o*hmic contacts*", but even *ohmic contacts* still represent a contact resistance that typically is significantly larger than the resistance in the bulk of the metal contact. The presence of a large resistance at the injecting or extracting contact can be diagnosed with the help of the *TFTs'* output characteristics, as discussed in section 3.1.1.1.

Parasitic capacitances are capacitances that come from the overlap between contacts providing unwanted capacitance; however, parasitic capacitances do not affect mobility. The important capacitances between the contacts are the capacitance of C_{GS} (gate-source) and C_{GD} (gate-drain). One part of these capacitance is due to the

parasitic capacitance overlapping between gate and contacts source/drain, and another part is due to the capacitance between gate and channel which is necessary for transistor's operation (Figure 14). Although, the channel is not considered as contact (terminal), the key capacitances are represented as following equation,

$$(1\text{-}36) \qquad\qquad C_{GS} = C_{GS,overlap} + C_{GS,channel}$$

$$C_{GD} = C_{GD,overlap} + C_{GD,channel}$$

The overlap capacitances do not depend on the applied voltage that can be estimated as fixed parallel capacitances represented as following,

$$(1\text{-}37) \qquad\qquad C_{GS,overlap} = C_{GD,overlap} = WL_{overlap}C_{gate,medium}$$

Where, $L_{overlap}$ is the overlap length, and C_{water} is the specific capacitance of a gate medium (in our case here, water).

The channel capacitance is voltage dependent. It is required to minimise the unwanted parasitic capacitance by reducing the length overlap, once fast switching of a transistor is necessary. Since we are limited in frequency anyway due to the slow build- up of the *EDL*, the parasitic capacitance is not that important. Anyway, we made a new design for contacts for reducing the length overlap, as seen in Figure 15.
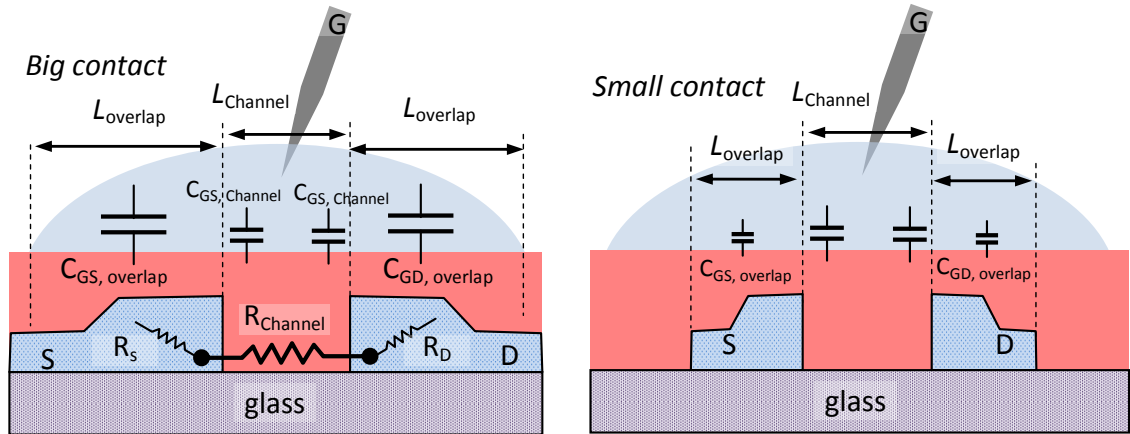
Figure 14, this shows the equivalent series resistance in source R_S, drain R_D and channel resistance. Also, it shows the gate-source (drain) capacitance C_{GS} (C_{GD}) and the parasitic capacitance due to the overlap between gate and source/drain.
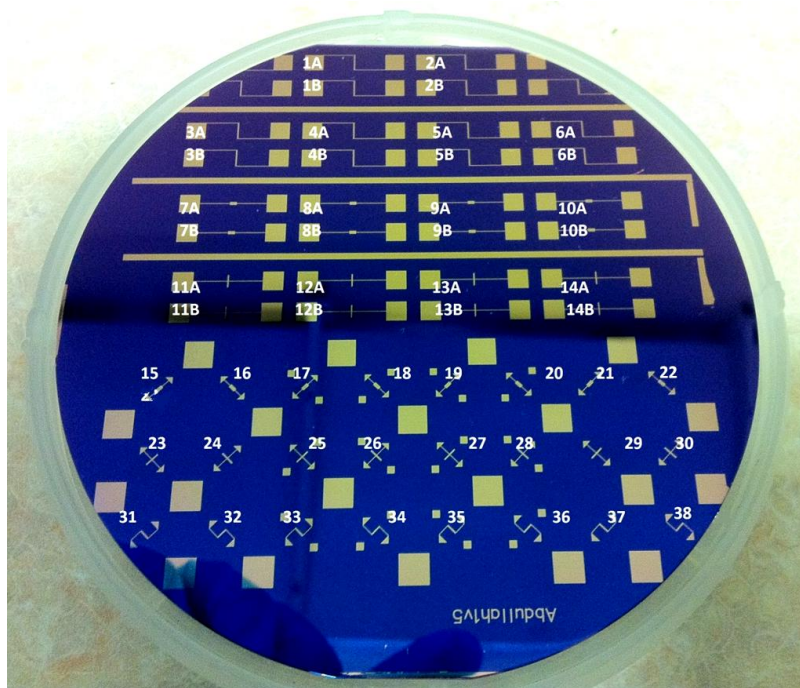
Figure 15, the design and the gold contact deposition made by Cardiff University.

1.6   Semiconductors materials used in this work

1.6.1   Zinc oxide film (ZnO)

ZnO film is the only inorganic material used in this work. *ZnO* can be found in nature as zincite mineral, but most of *ZnO* is produced synthetically, nowadays. It has been used for a range of potential applications including light emitting diodes (*LEDs*), field effect transistors (*FET*), spintronics[55], sensors[56] and piezoelectricity[57].

The common configuration structure of *ZnO* is wurtzite crystal structure in hexagonal form. The Zinc atoms are coordinated to 4 oxygen (*O*) atoms in tetrahedral sites, seen in Figure 16. As polycrystalline oxide semiconductors, *ZnO* is an *n-* type extrinsic semiconductor for two reasons. The *n-* type performance in *ZnO* refers to the result of oxygen (*O*) vacancies and/or Zinc (*Zn*) interstitials. There is still disagreement about which one is more dominant to identify *n-* type character[58]. Although, in undoped *ZnO* films, Hydrogen causes the *n-* type doping [59]. All these reasons causing electron transporting located about 0.01-0.05 eV below the conduction band make *ZnO* not easy to be reproducible and reliable device in terms of electric performance. At room temperatures, the *ZnO* phase is stable; therefore, it is not required to be stored in vacuum such as organic semiconductors, because *ZnO* gets doped under vacuum providing more oxygen vacancies in its structure. It is nearly insoluble in water "0.005 g/l" at 25 ^{O}C.
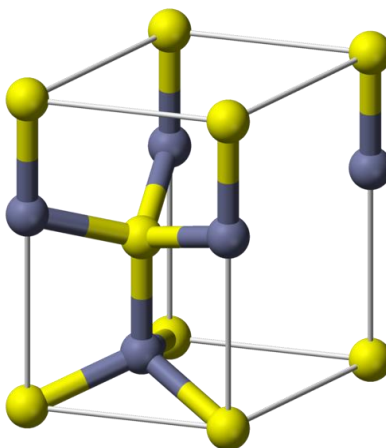
Figure 16, a wurtzite crystal structure for ZnO, (**yellow** ball, Zinc atom), (**grey** ball, Oxygen atom). The valence band of ZnO is located at -7.7 eV, and the conduction band is located at -4.4 eV.

In different heating temperature, *ZnO* gives rise of two distinct behaviours. At high temperature, *ZnO* becomes semiconductors because of decreasing of band gap energy; however, more dielectric behaviour of *ZnO* can be taken place at lower temperature. As described in Ong *et al* article, placing coated substrates by precursor at pre- heated hot stage would increase carrier mobility rather than step- heating process. This is because of increasing in crystallites size in film[60]. *ZnO* valence band is located unfavourably for hole injection from Au (*ZnO*, V_B = -7.7 eV *vs.* Au, work-function = 5.1 eV), whereas the conduction band at -4.4 eV is reasonably well matched for electron injection[61].

In 2003, the first transparent thin film transistor (*TFT*) of *ZnO* was revealed by works of Nomura at el [62]. In terms of mobility, *ZnO TFTs* generates approximately ~12 $cm^2V^{-2}s^{-1}$ comparing to currently- used for liquid crystal display a-Si:H *TFT* which produces less than 1 $cm^2V^{-2}s^{-1}$ at same conditions[63]. For more stable performance *TFT* of *ZnO*, Li- doped *ZnO* shows outstanding electrical properties in terms of high mobility, low threshold and more operational stability[64]. The previous transistors were designed in dielectric gate medium. Once the gate medium is replaced by solution- processed, for example ionic- liquid, the mobility increases dramatically with applying low voltage.

The *TFTs* of *ZnO* is capable of meeting the different requirements for future flexible plastic electronics that comprise a high- performance and electrical stability with low- cost, low- temperature fabrication (~300 ^{0}C) and solution-processability.

1.6.2 Low molecular weight organic semiconductors

In such molecular weight, they are relatively small molecules comparing to polymers. The electrical conduction (mobility) becomes high, when these low molecules are deposited by using thermal evaporation.

1.6.2.1 N,N'-bis (n-octyl)- dicyanoperylene-3,4:9,10-bis(dicarboximide) (PDI8-CN$_2$)

This low molecular weight material is an *n-* type organic semiconductor with mobility around 0.1 cm^{2}V^{-1}s^{-1} [65]. PDI8-CN$_2$ can be processed in order to make thin film using organic solvents or thermally evaporate it, and the chemical structure is shown in Figure 17. PDI8-CN2 has a remarkably low *LUMO* at 4.3e V which enables electron injection even from high work function metals (e.g. gold), and avoids electron trapping at 3.6 eV. It was demonstrated first with other modified perylene tetracaboxylic diimide (PTCDI) by Jones *et al*[66].
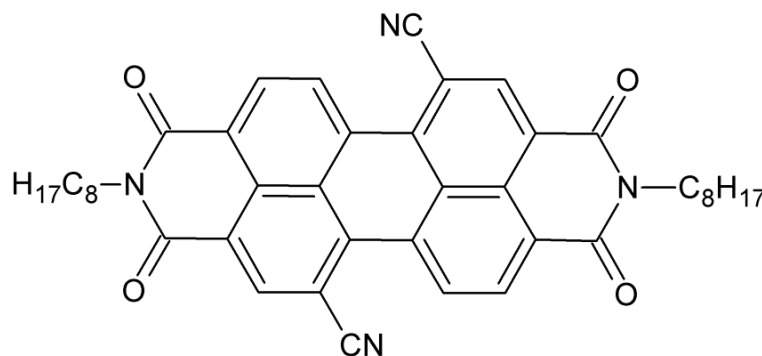
Figure 17, a chemical structure of (N,N'-bis(n-octyl)-dicyanoperylene-3,4:9,10-bis(dicarboximide)), for short (PDI8-CN$_2$).

1.6.3 Polymers

A repeatable of many subunits (monomer unit) constitutes a high molecular weight which is the definition of a polymer. Many pathways have been done to synthesize polymers, and each one of which provides various length's chains of polymer which is usually expressed as a molecular weight or as a degree of polymerization that computes the number of monomers integrated into one chain. The length of a polymer chain is a strongly essential factor to determine changes in physical properties of polymers, such as the increasing of the chain length would increase melting and boiling temperatures.

1.6.3.1   Poly(3-hexylthiophene-2,5-diyl), (P3HT)

As hole transporting polymer, P3HT is constructed by a long series of conjugated thiophenes, a cyclic compound of 5 atoms containing one sulphur atom (described in section 1.2.2), that are attached each with a hexyl chain as a side group, as seen in Figure 18. In fact, the presence of the sulphur atom improves crystallisation of resultant materials. As a result, the charge transport is improved by increasing long chain ordering. Moreover, the main purpose of appending alkyl side-chains to backbones of P3HT is to improve the solubility of the polymer in order to process the polymer by solution form in spin-coating, for example.
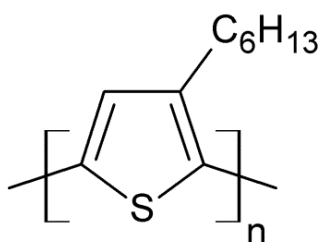
Figure 18, a chemical structure of P3HT (Poly(3-hexylthiophene-2,5-diyl)).

Three ordering formats can be built for the location of the alkyl chains on thiophene rings which are 2-5' (head to tail), 2-2' (head to head) and 5-5' (tail to tail). Mixture of ordering schemes is known as regiorandom. Consequently, twisting out of the plane of the thiophene rings leads to a decrease of the conjugation length. The longer conjugation length the polymers have, the better charge carrier mobilising throughout them. This applies, therefore, to scheme that have head to tail order which is identified as regioregular, and this enforces the thiophenes to be more rigidity in the structure and sitting in a plane. This scheme promotes for the polymer backbone to organised and constructs a lamella as sheet-like in two-dimensional. The Lamella ordering of polymers means that the individual polymer chains order themselves in such a way that the chain forms a parallel (ordered) section to several neighbouring chains and an unordered region above and below ordered section. The remaining spaces between ordered sections of lamella are filled with amorphous polymers.

The improvements of Thiophene polymerisation were attributed to McCullough[67] in 1992 and led to a much higher regioregularity.

1.6.3.2   (Poly(2,5-bis(3-hexadecylthiophen-2-yl)thieno[3,2-b]thiophene),
(PBTTT)

In 2006, McCulloch *et al*[68] reported firstly on PBTTT and how the size of crystalline domains, after annealing, is bigger comparing to P3HT, while the hopping

action of charge over grains boundaries becomes more efficient in ordered domains rather than disordered ones[69]. This is because of the fusion of two aromatic units (thiophenes) which aids to extend π electron systems and allows charge carriers to pass through close π-π interaction between intermolecular in higher density.

Moreover, the *HOMO* level of PBTTT becomes lower by 0.1 eV (seen in Figure 6), since the delocalization over the polymer backbone is reduced as a reason of the fusion. The increase of ionization potential improves the polymers in terms of crystallization, self-assembly and high stability in the presence of oxidising species[68].
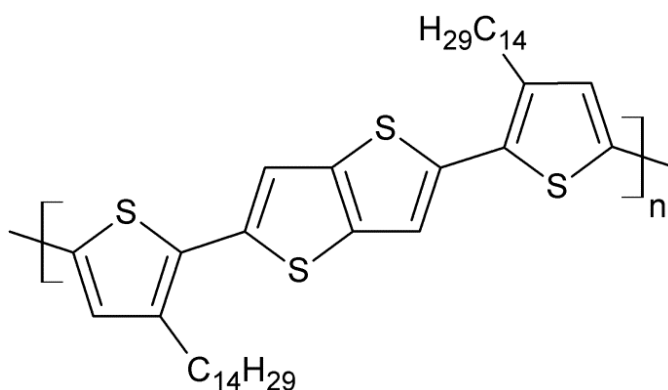
Figure 19, a chemical structure of pBTTT, (Poly(2,5-bis (3-hexadecylthiophen-2-yl)thieno[3,2-b]thiophene).

1.6.3.3   Poly(Benzimidazobenzophenanthroline), (BBL) nano-belts

Poly(Benzimidazobenzophenanthroline) is another *n*- type organic material that is normally known as *BBL*, but it is considered quite a remarkable organic semiconductor. *BBL* is a very stiff planar polymer, and also it does not have any flexible side in its chains. The lack of flexibility of its side chains means that processing and synthesising of *BBL* is really a very hard work, since it does not dissolve in typical solvents (i.e chloroform). However, Methane Sulphonic Acid (*MSA*) must be used to dissolve *BBL*[70]. *BBL* dissolves in *MSA* due to a chemical reaction between the acid *MSA* and the *BBL* polymer that acts as a base.

BBL was chosen, since its *LUMO* level is remarkably low. This distinctive feature gives *BBL* an ability to be very stable in ambient or humid conditions. Maybe, *BBL's* insolubility in usual solvents may also contribute to its feature of significant stability. The group of Briseno *et al* managed to fabricate *TFTs* of *BBL* that have remained stable for about 4 years in ambient atmospheric conditions[71]. They pointed out that the robust qualities of *BBL* are a result to two important reasons which are the morphology with closely- packed crystalline structure and high electron affinity of *BBL*. Furthermore, the closely- packed feature builds a kinetic barrier which shields

61

BBL against the diffusion of extrinsic molecules, and the molecules of *BBL* are energetically stable against chemical/electrochemical reactions because of the high electron affinity of *BBL*.

The structure with ladder shape of *BBL* (Figure 20) contributes to the more rigidity of the polymer than many other polymers. The rigidity strongly restricts the twisting motion and just allows continuing its rigid planar-shape contrasting its non-ladder cousin *BBB*. Moreover, this provides the two important purposes which are a decrease of the *LUMO* level and an assistance of the charge carrier transport[72]. Studies showed that chains pack of *BBL* is arranged as face-to-face perpendicular to the long axis of the nano- belt growth[73], as seen in Figure 21.

Although much research has been concentrated and done to investigate the *BBL* properties and applications[70,72-73], the synthesis and properties of *BBL* were recognized before in 1969. Arnold and Van Deusen[74] observed its thermal stability, and they also managed to produce films and fibre- forming properties. Unfortunately, their discovery and research were mostly forgotten until the late 90's.
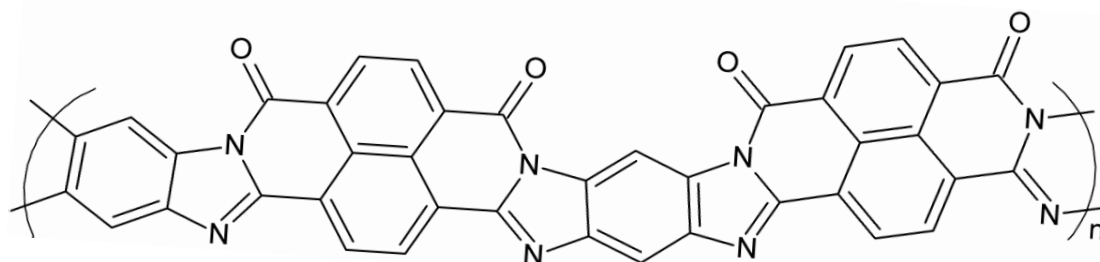
Figure 20, a chemical structure of BBL, Poly(benzobisimidazobenzo-phenanthroline).
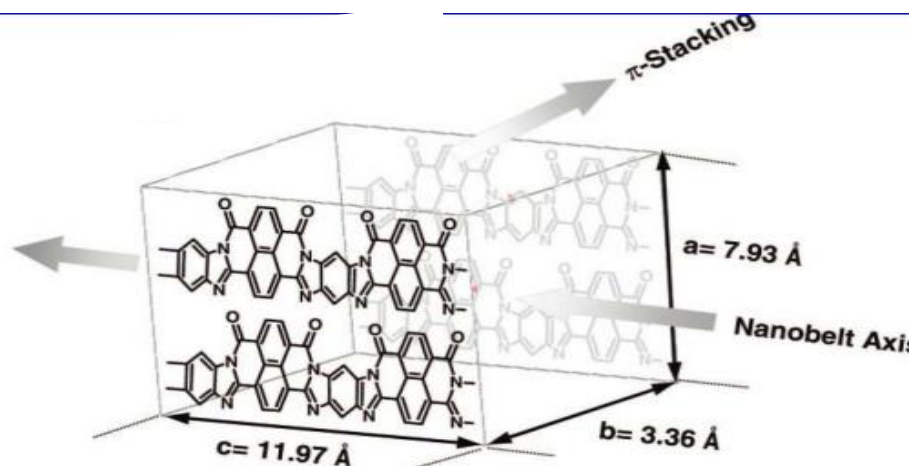
Figure 21, an illustration of the paking of BBL in nanobelts, taken from reference[73].

1.6.4 Nanowires (NWs) of Polymers

Either inorganic or organic materials, 1-D nanostructures (such as, nano-wires, -fibers, and etc.) have attracted a great interest. In this section, the focus will be about polythiophene nano- wires grown via the whisker method, and topics related to it, as seen in figure.

Ihn *et al*[75] was the first group who used whisker method to grow organic nano-wires by dissolving the organic polymer in pre-heated marginal (between good and poor solvent) solvent and then allowing clusters or aggregates to grow as the solvent is cooled gradually to room temperature. They found that P3ATs crystallise to form nanowires with width and height of tens of nanometres and few micrometers lengths. They point out that the used solvent depends on the side chain length (alkyl- side), so polymers with longer side chain require a poorer solvent in order to form nano- wires. At higher temperature, specific solvents become good solvents, but the solubility becomes poorer at lower temperature. A dual- behaviour of solvent with different temperature is a key factor to form crystallisation.

At same principle, Kiriy *et al*[76] group showed another way of producing P3HT nano- wires. After dissolving polymer in good solvent, drops of poor solvent was added to solution, at room temperature. This allows crystallising the solution, as seen in Figure 22.

After using whisker method, Oodterbaan *et al*[77] group recommended an Anisole solvent as an excellent solvent in order to grow P3HT nano-wires. They studied a correlation between many parameters affecting the growth of P3HT nano- wires, for example, refractive index of solvent and side chain length of polymers.

In 2007, a blend of P3HT nano- wires with [6,6]-Phenyl-C_{61}-butyric acid methyl ester (*PCBM*) for used in photovoltaic application as demonstrated by Berson *et al*[78]. Another group found that the efficiency of organic photovoltaic becomes greatly optimised after 60 hours of forming P3HT nano- wires in dichlorobenze solution. However, ageing time after 60 hours from making new solution shows an increase of large aggregates which, in turn, affects charge transportation between *NWs*[79]. By fabricating organic field effect transistor (*OFET*) devices, the electrical properties have been studied, as well. Using whisker method for growing P3HT *NWs*, Merlo and Frisbie looked into the electrical properties for several and single NWs in Nitrogen atmosphere. Also, the alignment of the long axis of *NWs* can be rearranged to be perpendicular to the magnetic field's directions[80].
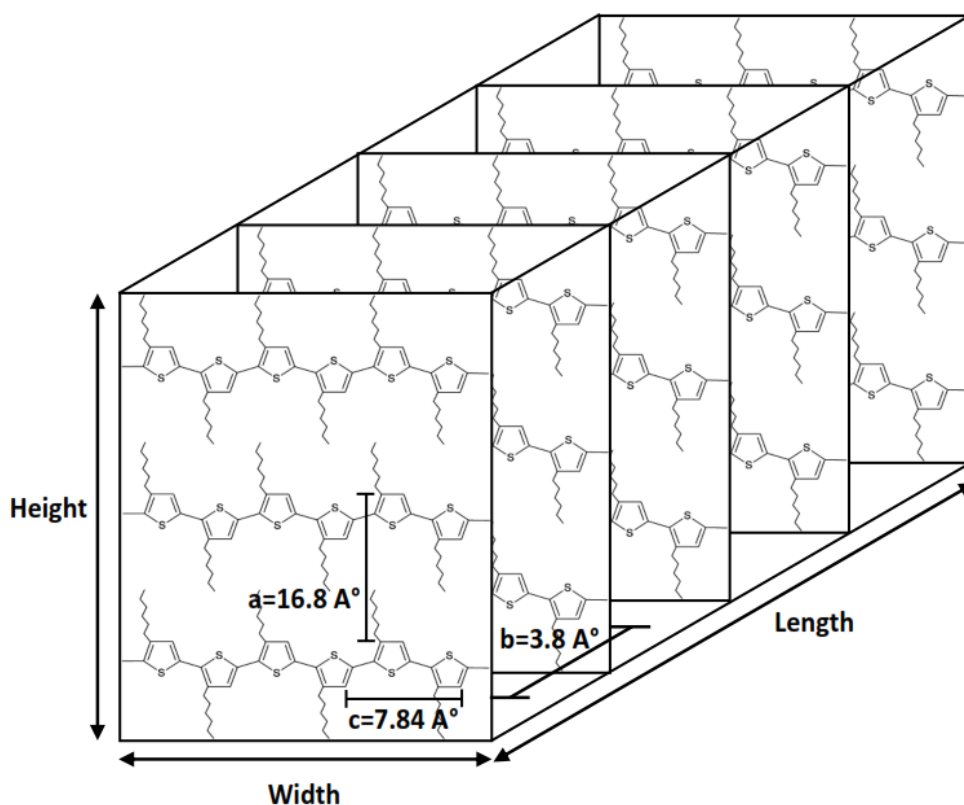
Figure 22, an illustration of P3HT nano-wires, taken from reference[81].

1.7 Calixarenes

In fact, Calixarene can be used as a receptor sites in a layer to enhance the selectivity towards analytes in gaseous or aqueous medium. Their properties are modified, once they bind to ionic guest with different event of recognition, as seen in Figure 23(b). Consequently, the binding event may leads or translates to an electrical signal using suitable circuits.

1.7.1 History
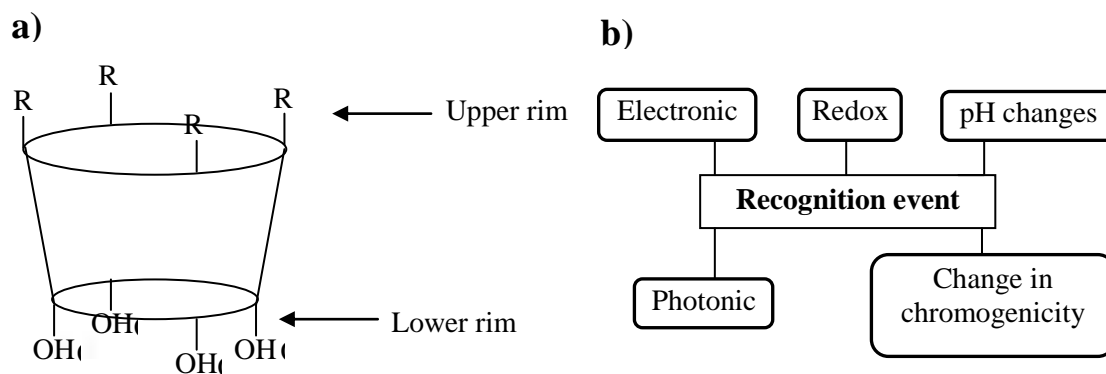
Figure 23: (a) the example here is calix[4]arene similar to Cup or basket-shaped, and the arrows indicate to the upper and lower rims with cavity shape. It is convention to have hydrophobic upper rim and hydrophilic lower rim, (b) Detection of the recognition event.

Calixarene, which is in order of nano- scale with unique conformation shape, basket-shaped Figure 23(a), has ability to sense and detect materials, such as pollutants and solvent vapours. Also, Calixarene have been used in many researches and project works to sense and extract the target analyte from medium. Calixarene is divided into two words, "calix" which means that a resemble of molecules possess a shape similar to a vase, and "arene" stands for the aromatic structure built by unit block, which is phenolic units connected by methylene group at *othro*-positions of phenol. What is interested in these basket- shaped macromolecules is that it can be tailored in such a way to get specific "man- made" receptor in order to be fit or sense a cations or molecular species[82]. The hydrophobic cavity sizes, functional groups at upper and lower rim are utilised as pre- prepared binding sites for varieties of cationic and natural guests for many previous uses[83].

The smallest calixarene that can be made is the one with four benzene rings which calix[4]arene. It has been used with ion selective electrodes[84]; however, the sensitivity was not that sufficient to sense low concentration of ionic species that usually present in real sample because of the problem related to electrode modifications[85]. For ion-selective field effect transistor (*ISFET*), the calix[4 and 6]arene have been evaporated thermally on the surface of gate insulator, and this work indicates that ion with small radius shows a clear interaction with cavity of calix[4]arene; however, bigger cavity, such as calix[6]arene, gives weak response[86]. Thus, even weaker response is expected for calix[9 and 11]arene[87].

In terms of the distribution of calixarene on the surfaces, the thermal evaporator is not the ideal choice because of the poor distribution coverage; however, films from Langmuir trough may play this role in order to provide us a well defined and a regular condensed array of calixarene on surfaces[88].

In this work, these Calixarenes will be utilized just as a buffer layer to blocks ions that could otherwise penetrate an organic material and dope it.

CHAPTER 2

Device Fabrication

This chapter describes the substrate preparation before deposition and the way of making thin film transistors of organic (including nano- wires of *P3HT* and nano-belts of *BBL*) and inorganic semiconductors. Also, the way of depositing semiconductors and the equipments used for this purpose are mentioned in more detail.

2.1 Substrate preparation

Uncleaned substrates result in poor adhesion of the deposited films, increasing *off*-current or even non- working devices. Thus, the cleaning procedures for substrates before depositing organic semiconductors are important steps to have the required and stable performance of deposited devices throughout the experiment. In the following section, the substrate cleaning techniques are explained.

2.1.1 Cutting substrates

Silicon substrates with a 100 nm thickness of thermally deposited oxide and glass substrates were cut manually. A cutter containing a diamond tip was used to carefully and deeply scratch the back of the polished side of wafer (non- polished side) or the pre-deposited-gold-contacts wafer. Finally, the remaining cracks from scratching were blown with dry nitrogen. The same step was done with glass substrates with the required size for both (1.2 X 2.4 cm^2). The advantage of glass substrates over silicon-oxide (SiO$_2$) is that glass guaranteed the minimal or zero off-current, since there is no sort of leakage going from source and drain beneath a channel like what usually may happen for SiO$_2$ after depositing Gold contact and diffusing towards Silicon layers.

2.1.2 Cleaning substrates

SiO_2 was cleaned in several steps, starting with acetone cleaning with clean- room wipe in order to get rid of any organic dirt of residuals, such as fingerprint. After drying substrates using dry nitrogen, they were cleaned by immersing them in a cleaned Petri dish with 1:100 diluted Hellmanex alkaline. After that, the Petri dish with diluted Hellmanex was sonicated in a sonic bath for 5 minutes. The next step is to remove Hellmanex alkaline and rinse substrates by de-ionised water. Finally, for 10 minutes, dried substrates were placed in a cleaned Petri dish with preheated Isopropanol (IPA) at 70°C on a hot plate. The same Petri dish with substrates was placed and sonicated in the ultrasonic bath for 5 minutes and were rinsed with clean IPA and dried with the aid of dry nitrogen, afterwards. In all time, these cleaning procedures were always done in clean-room labs, and the edge of substrates was picked up or touched by tweezers to guarantee a high level of cleaning, in addition of using gloves.

2.1.3 Ultraviolet-light-ozone cleaning (UV-O_3 cleaning)

The final step is cleaning all silicon and glass substrates with ultraviolet (UV) light ozone treatment (Bioforce Nanosciences Inc.) to remove the organic dirt that may still left behind on the surface of substrates. Usually, the substrates were held in ozone treatment up to 4 or 4.5 minutes. The principle of this treatment is to convert an organic compound on the surfaces into volatile substances (i.e. H_2O, CO_2 and N_2) by two different mechanisms which are a decomposition action of UV rays and a strong oxidisation by ozone (O_3) generated from ambient oxygen (O_2) by UV. The low-pressure mercury vapour lamp radiates two different wavelengths (184.9 nm and 253.7 nm). First wavelength is absorbed by atmospheric oxygen and forms O_3. Second wavelength decomposes O_3 to its original elements.

2.1.4 Reflux unit

This cleaning process was done for glass substrates, and it can be used for SiO_2, as well. The glass substrates were cleaned by immersing them in a cleaned Petri dish with 1:100 diluted Hellmanex alkaline and placing them in warm sonic bath for 5 minutes. After rinsing of substrates by DI-water and drying them, they were placed in a reflux cleaner containing isopropanol alcohol for 3 hours, as seen in Figure 24. Finally, refluxed substrates were dried with nitrogen gas. Some substrates are required to be hydrophobic prior to Langmuir trough and spin- coating deposition; hence, a further procedure well- known as silanization by adding 3 drops of

hexamethyldisilazane (HMDS) (more details about self- assembly in section 2.2.4) into a sealed Petri dish containing the substrates, for 24 hours.

Figure 24, the picture of Reflux unit.

2.2 The deposition techniques

In this section, various deposition techniques that are used for preparing a thin film of organic semiconductors, metal contacts and sensitizer layers of calixarenes are explained, in more detail.

2.2.1 Langmuir Trough

One of the simple and very useful deposition techniques to make monolayer film on the surface of the sub- phase (DI water in the trough) where the required material is deposited is called the Langmuir deposition. Then, the form and highly ordered monolayer is deposited on solid substrates.
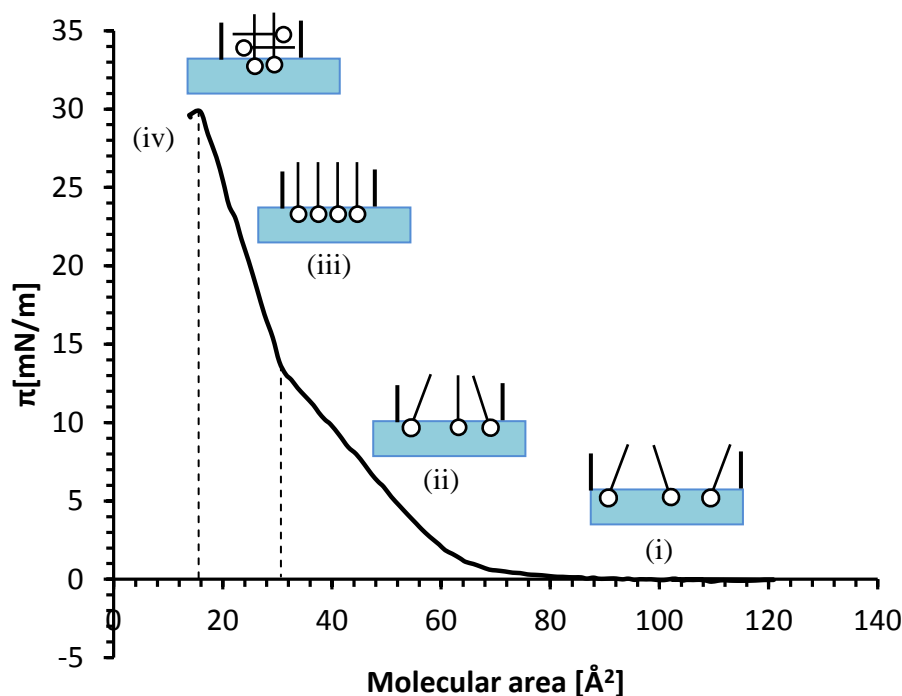
Figure 25, illustration of surface pressure- area isotherms of a Langmuir film showing the target molecules in different phases, where the molecular behaviour represent in (i) a gaseous phase, (ii) a liquid phase, (iii) solid phase and (iv) collapse mechanism. This demo data is taken from NIMA technology software.

For making Langmuir film, firstly, the required material, usually amphiphile materials (more details in section 2.2.1.1), is prepared by dissolving it with solvent (typically 0.1 mg/ml) that is not soluble in water and volatile after spreading on the sub- phase. The common solvent for that purpose is chloroform, but it is crucial to be a good solvent for the respective material. Then, a solution of material is spread over the sub- phase using a Hamilton micro- syringe. In inert and highly hydrophobic trough (Teflon), the barrier by same material of trough compresses the required monolayer on the surface of pure water. With the aid of Wilhelmy plate (a rectangular piece of a lab paper) measure, therefore, the surface pressure from the plot of (surface pressure– film area) as seen in Figure 25. Other phenomena related to surface can be extracted from surface pressure, such as effective dipole moment of molecules and area per molecules by knowing of the molarity of spread molecules and the surface area of the trough (typically 525 mm^2). The transitions between different film morphologies can be identified from changes in the slope of the isotherm.

Many forces affect on a Wilhelmy plate which are gravity, surface tension and buoyancy. The net force on the plate is represented by following equation[89]:

$$(2\text{-}1) \qquad F = \rho_W g l w t + 2\gamma(t + w)\cos\theta - \rho_L g t w h$$

Where the density of the plate material and the density of the sub- phase liquid are represented by ρ_W and ρ_L, respectively, g is the constant of gravity, l, w and t are the length, width and thickness of the plate, γ is the surface tension of the sub- phase, θ is the contact angle of the sub- phase to the plate ($\theta = 0$ for filter paper in water) and h is the length of plate that immerses in depth into the sub- phase.

When organic material is added to the sub- phase surface, the surface tension decreases which is indicated by the change in the force affecting the plate. Consequently, the changes in the surface tension as a result of changes in the net force on the plate are indicated by using following equation:

$$(2\text{-}2) \qquad \Delta\gamma = \frac{\Delta F}{2(t+w)} \approx \frac{\Delta F}{2w} \qquad \text{for} \qquad t \ll w$$

The changing of surface tension ($\Delta\gamma$) is related to surface- pressure Π (typical unit mN/m) that is given by following equation[90],

$$(2\text{-}3) \qquad \Pi = \gamma_o - \gamma$$

Where γ_o and γ are the surface tension of sub- phase without deposited film and film-covered surface, respectively. Nima 611D Standard trough is utilized for making calixarenes layers, as seen in Figure 26.
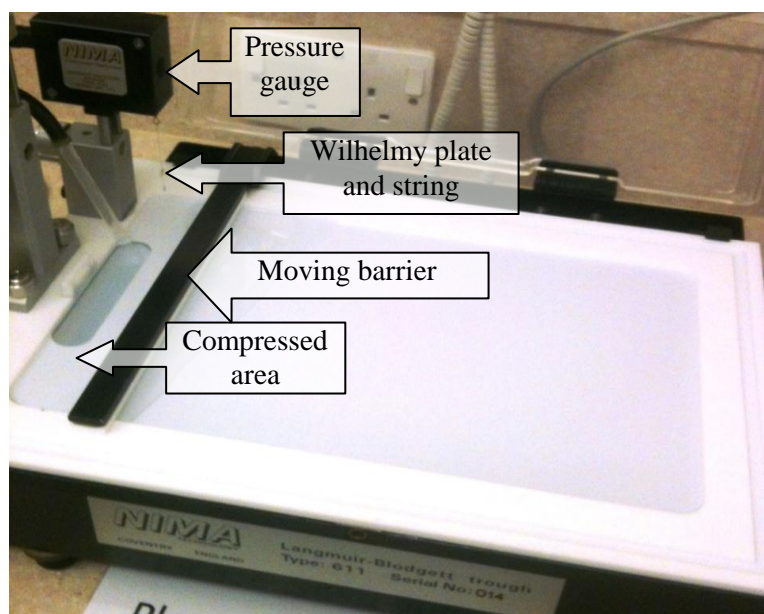
Figure 26, the picture of Nima 611D Standard Trough.

2.2.1.1   Amphiphiles

The dipolar moment of water is a result of withdrawing electrons towards oxygen atom causing uneven distribution of charges in the water molecule, as seen in Figure 27.
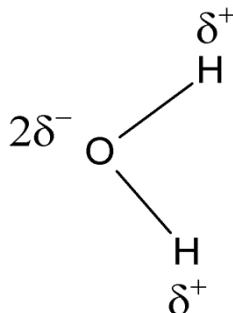
Figure 27, the polarity of water molecular.

Polar molecules are always attracted to the polar water, and they are called hydrophilic. Non- polar molecules that do not dissolve in water and repel the water are called hydrophobic. A typical monolayer molecule used in Langmuir trough should comprise a head group that possesses a polar molecular which is hydrophilic and a tail of molecular which is hydrophobic. This sort of molecule is called an amphiphile. The balance of hydrophobicity and hydrophilicity in an amphiphile leads the molecule to align and orient itself on the water surface in a well defined direction.

As seen in Figure 28, a general example of amphiphile is the fatty acid or Stearic Acid ($C_{17}H_{35}COOH$). Stearic Acid processes hydrophilic chains of long hydrocarbon with a methyl (CH_3) group at one end and a hydrophobic (polar) carboxylic acid group (CO_2H) at the other. The tail of the chain and the strength of polarity of acid group are key factors and should be balanced. If the balance is not precise, the amphiphile dissolve in the water.

$\sim 0.19 \text{ nm}^2$

H$_3$C

H$_2$C

CH$_2$

H$_2$C

CH$_2$

H$_2$C

CH$_2$

H$_2$C

CH$_2$

H$_2$C

CH$_2$

H$_2$C

CH$_2$

H$_2$C

CH$_2$

Tail

$\sim 2.5 \text{ nm}$

Polar head → HO O
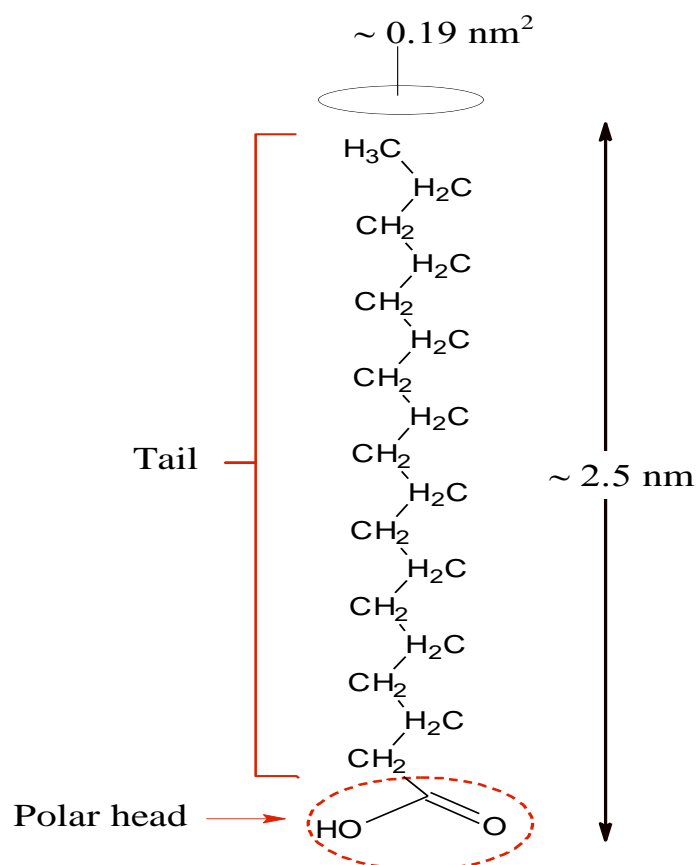
Figure 28, the Stearic acid molecule and approximate shape and size [91].

2.2.1.2 Different Langmuir Trough techniques (Langmuir- Blodgett Films, Langmuir- Schaeffer deposition)

After making the monolayer at target surface pressure that is in 'solid' phase but before collapsing of film on the trough, the monolayer can be transferred onto solid SiO$_2$ or glass substrates in two different ways which are Langmuir- Blodgett deposition (LB) and Langmuir- Schaeffer deposition (LS), as seen in Figure 29. The monolayer is compacted to an optional surface pressure using software. Also, surface-pressure is kept constant by the barrier following through during dipping, controlled by software. The different arrangement of monolayers is achievable, since the substrate can be dipped into the sub- phase whether vertically (LB) or parallel (LS) to the surface. To widen our arrangement options, the substrate can be placed inside the trough before pouring DI- water and applying the monolayer. Therefore, the molecule in the surface of substrate is organized by head to head, or tail to head, as seen in Figure 29.
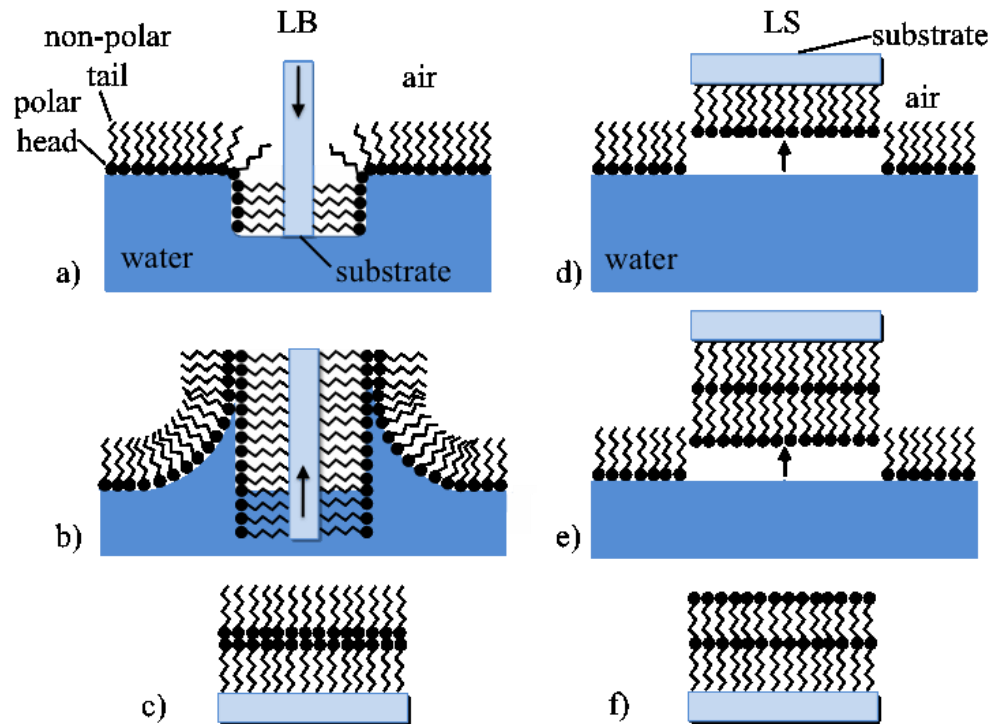
Figure 29, Comparison between Langmuir- Blodgett (LB) and Langmuir- Schäfer (LS) films. a)-c) and d)-f) depict the two steps for a two layer- deposition for LB and LS, respectively. The immersion (a) and emersion (b) of the substrate result in a LB film (c) in which the second layer of particles is disposed in the opposite way with respect to the LS film (f), obtained after two consecutive dips, (d) and (e).

2.2.2 Spin Coating

In this procedure, a thin film is deposited on the substrate by placing an amount of solution on it and rotating at high speed. The principle beyond this technique is spreading solution by centrifugal force. The volatile solvent is a good choice for leaving the thin film of organic material on substrates. However, the evaporation of solvent must leave enough time for organic material chain to crystallize and order themselves. Usually, polymer is spin- coated instead of low molecular weight, since polymers solutions are much more viscose. The used solvent has a strong effect on the thin- film quality (charge carrier mobility, for example) and thickness. The final film thickness can be calculated roughly using the following equation:

(2-4)
$$d \propto \frac{c\eta(c)}{\sqrt{\omega}}$$

Where: d is the resultant thickness, c is the solution concentration, $\eta(c)$ is a viscosity which depends on the concentration and ω is the spin speed.

Finally, the constant from this equation depends strongly on substrates adhesion, solvent and other factors.
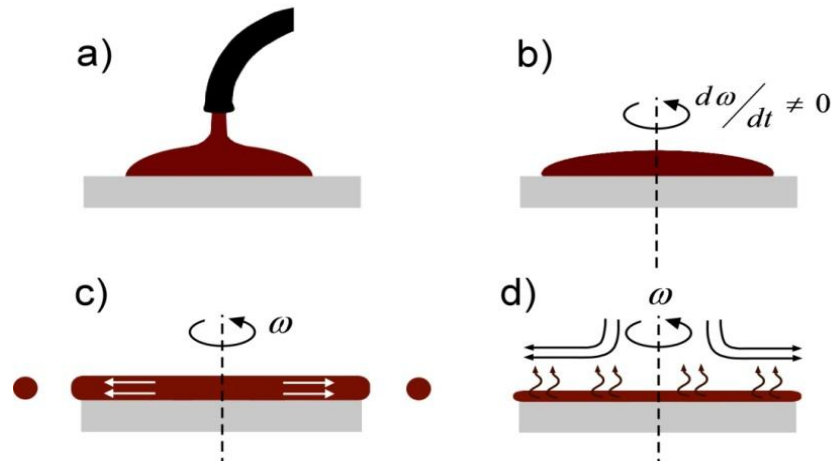
Figure 30, the different steps of spin coating. a) Applying solution. b) Start acceleration. c) Flow of fluid dominates. d) Evaporation of solvent dominates. From: http://large.stanford.edu/courses.

2.2.3 Thermal evaporation

This technique is widely used because vacuum assists significantly to transfer the solid phase of materials to the vapor phase at lower temperature. Vacuum also prevents oxidation, and increases mean free path, explained below. Thus, the deposition of thin film of metals on the substrates as electrodes and low molecular weight organic molecules are easily made by this technique. Evaporation from a hot source and condensation on a cool substrate are the two basic processes in thermal evaporation. High vacuum offers for evaporated particles a long mean free path which means that the vaporants travel towards the substrates without colliding with ambient or residual gas molecule inside vacuum chamber. The relation between pressure and the mean free path is given by:

$$\lambda = \frac{1}{n\pi d^2 \sqrt{2}}$$

(2-5)

Where d is the molecular diameter, n the number density of the molecules. From ideal gas law, $n = P/(k_B T)$, here P is the absolute pressure of the gas, k_B is the Boltzmann constant and T is the absolute temperature.

At typical pressure, for example, 10^{-6} torr, a partical with 0.4 nm diameter travels 60 m without collision, and the distance between substrates and hot source in our evaporation device is only around ≈ 15 cm.

The hot source used here is heated tungsten boat for low molecular weight materials and Gold (Au) and coils for Aluminum (Al) to make electrodes, and both of which has to possess a high melting point in order to reduce contamination. A high current DC is passed through the tungsten to heat up (Joule heating or resistive heating), as seen in Figure 31.
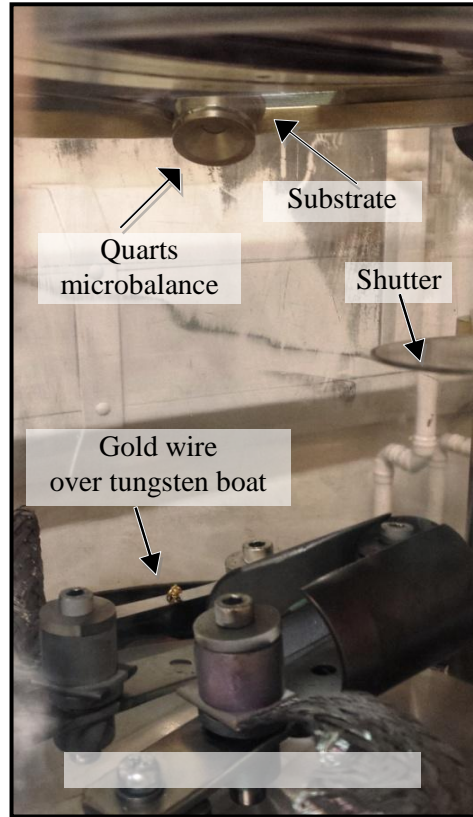
Figure 31, the configuration inside evaporator.

The quartz microbalance is utilized to monitor the rate of deposition and identify the final thickness of thin film on substrates. This monitor employs thin slices cut from a complete crystal with metallic electrodes. Once the quartz slice is exposed to the evaporant, its mass will increase consequently, and its resonant frequency associated with electronic oscillator will drop. Thus, the deposited thickness will be estimated, when the frequency changes and the materials density is known.

$$(2\text{-}6) \qquad\qquad \frac{\delta f}{\delta m} = \gamma (f_0 - \delta f)^2$$

where, resonant frequency f_0, frequency changes δf, mass changes δm and constant for the system γ.

The Edwards E306 Belljar Evaporator is used for depositing metal electrodes, and low molecular weight materials, as seen in Figure 32. Also, a removable glass bell jar,

sealed by a rubber, lies on the base of the apparatus. All electrical, gauges and vacuum and cooling piping are located at the metal bottom of the evaporator.

For the preparation of substrates inside the evaporator, the substrates were placed upside- down on two parallel steel frames. The magnetic sheet was placed on (rear) side of the suspended substrates. Thin shadow masks of ferromagnetic metals was positioned on the top side of each substrate, and shadow masks attached in place by the attraction action of the magnetic sheets. The whole collection including the frame, magnetic sheets and the substrates with the masks was placed on a stage inside the evaporator.

Figure 32, the picture of Edwards E306 Belljar Evaporator.

2.2.4 Self- assembly from solution

This is even much simpler way of deposition compared with Langmuir trough depositions. Monomolecular layers are formed by dipping proper substrates into a solution containing organic materials. An example of this kind of deposition is organosilicon compound formed on hydroxylated surfaces, containing -OH group on their surfaces, (i.e. SiO_2, Al_2O_3 and glass) depending on the idea of anchoring group (the head group of self- assembling molecule) interacting with substrates' surfaces. This slow process usually takes a long time around hours or days depending on several factors, such as the substrates, self- assemble organic materials, concentration and temperature.

We used two different self- assembling organic materials in this study. Firstly, on an Al_2O_3 surface, octadecyltrichlorosilane (*OTS*) is used depending on the idea that one of Cl atoms attached to the silicon of *OTS* leaves the molecule and bonds to the hydrogen atom of one of the -OH groups at the surface of the Al_2O_3. This creates the silicon forming a bond to the oxygen remaining on the surface while a molecule of HCl stays in solution, as seen in Figure 33. The self- assembly of *OTS* was performed by immersing the substrates having Al_2O_3 contact into *OTS* solution with cyclohexane under a nitrogen atmosphere in a glove box for 30 min. Every sample was cleaned in fresh cyclohexane in order to remove any non- bonded *OTS* with Al_2O_3 surface material and then kept them over warm Petri dishes unit they become dry.
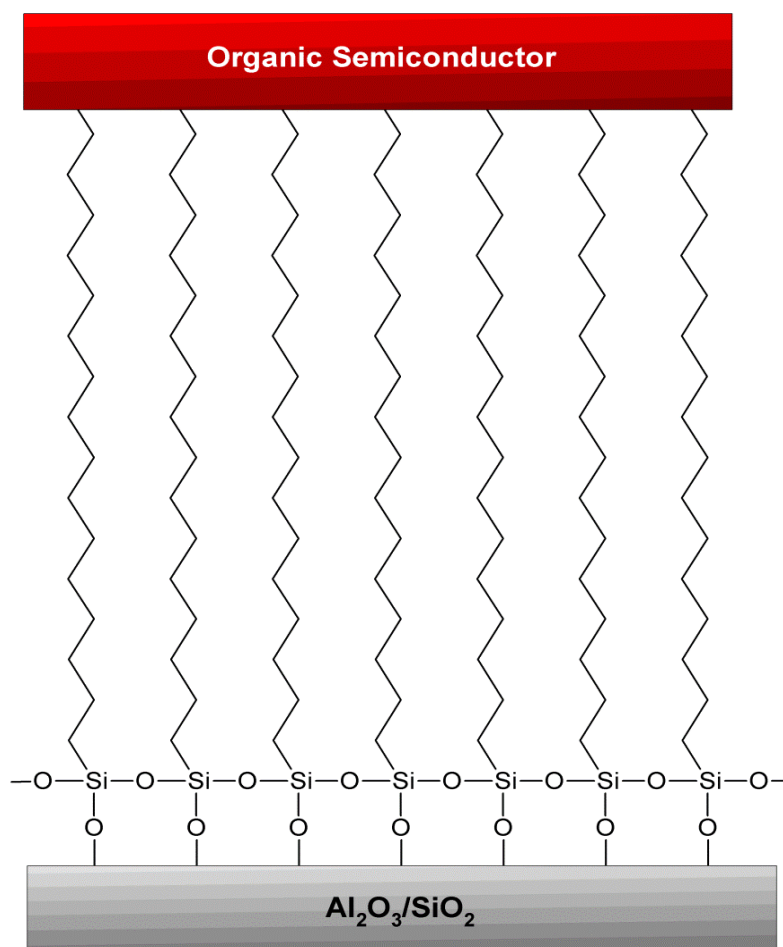
Figure 33, a diagram of OTS on Al_2O_3/SiO_2 with organic semiconductors.

Secondly, the hexamethyldisilazane (*HMDS*)[92] self assembly was achieved by placing the substrates (containing thin film of *ZnO*) into spin- coating, after that three or four drops of *HMDS* are placed over the substrates creating monolayer of *HMDS* after spinning at 5000 rpm for 60 s, as seen in Figure 34.
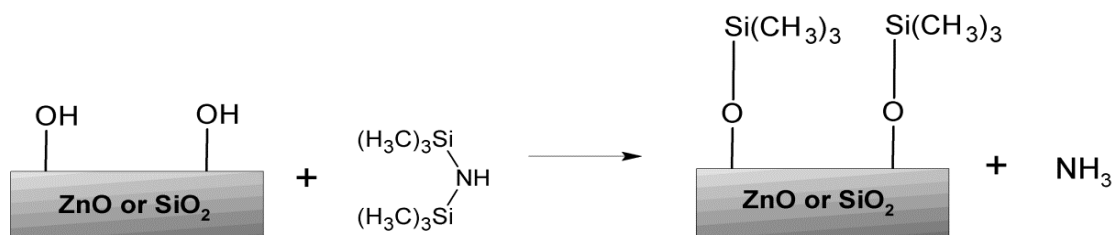
Figure 34, a diagram of HMDS on the surface of ZnO or SiO$_2$.

2.2.5 Metal Anodisation

This cheap and fast approach to create an oxidised layer of a metal is prepared by using it as working electrode in a bath with a fixed Platinum counter electrode and weak acid solution. Anodisation works only on those metals (or semiconductors) that show adhesion for layers of their oxides on their surfaces. These are known as 'valve metals', including Aluminium, Titanium, and Tungsten. On valve metals, a thin adhering oxide layer forms spontaneously under atmosphere, this is known as 'native' oxide. Native oxides prevent further oxidation of the valve metal bulk; the native oxide is usually an insulator (e.g. Al$_2$O$_3$), but some also are large bandgap semiconductors (e.g. TiO$_2$). Anodisation electrochemically grows a thicker layer of this oxide. After depositing a required metal to be anodised on the substrate, the deposited metal is connected as a counter electrode to fixed Platinum electrode in a bath of a weak acid, e.g. citric acid. Once a potential is applied across these electrode, the substrate must be more positive than the fixed electrode, as seen in Figure 35. Applied potential helps to dissociate the weak acid solution, and the flow of negative ions towards the anode (the substrate) oxidises the metal over the substrates (Aluminium, in our case here). Accordingly, the cathode (Platinum) receives the positive ions and converts H$_3$O$^+$ back into H$_2$O. Anode reaction is represented as following,

$$2Al \;+\; 9\,H_2O \rightarrow Al_2O_3 \;+\; 6\,H_3^+O$$
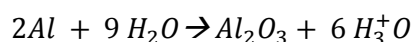
The more oxidised layer grows, the more its resistance increases until no current will flow through acid. The growth speed and thickness of the oxidised layer get affected by the magnitude and length of the voltage applied. In this work, the anodisation ratio of aluminium oxide is (1.3 nmV^{-1})[93] which means that a 5 V anodisation provides an oxidised film roughly 6.5 nm thick with a capacitance per unit area evaluated to be (640±30 nFcm^{-2})[94].
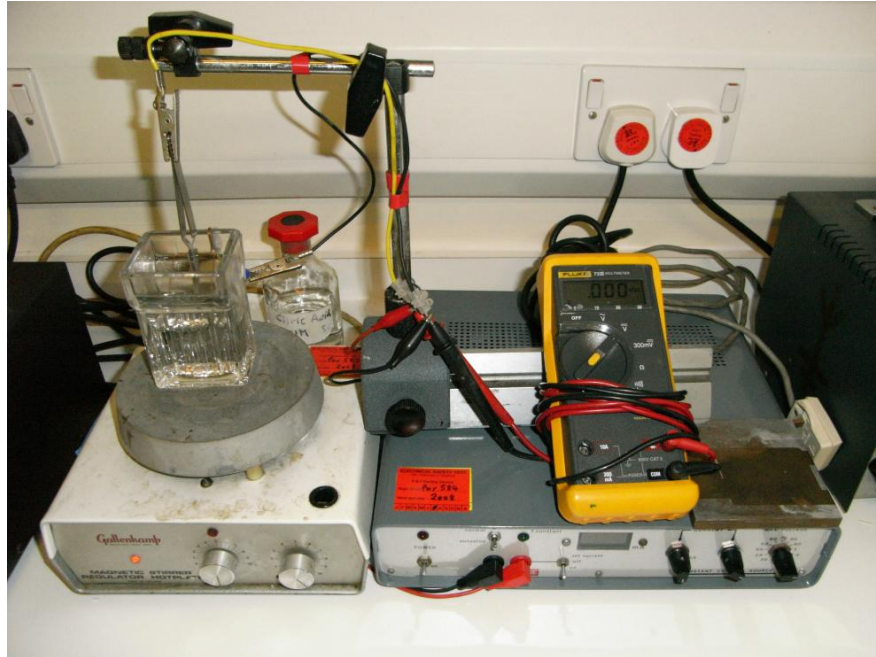
Figure 35, the equipment is used to anodise Aluminium metal.

2.2.6 Deposition of source and drain contacts

Cleaned substrates are loaded inside thermal evaporator. The gold wire is placed in the middle of a small tungsten boat. Shadow masks with 10 µm×2 mm of width and length, respectively, is employed to form contacts. As mentioned in section 2.2.3, the thickness of gold on substrates is monitored utilizing quartz microbalance to reach 50 nm thickness of source and drain contacts. Also, thermally deposited gold contacts over SiO_2 wafer that were made in Cardiff University were also used in experiments in order to reduce the parasitic capacitance and leakage of contacts, as seen in Figure 15.

2.2.6.1 Gold

Gold has attractive properties (i.e. the non- reactive chemically to other elements, the resistance to corrosion...etc.). Also, it is the material of choice for *p*- type semiconductor devices, because the ionisation potential of most *p*- type semiconductor matches relatively well with gold's work function which is around values from 5.0 to 5.3 eV[95]. Thus, low potential barrier is required to be overcome in order to get an efficient injection of charge carriers. The gold wire is used in this work and was thermally evaporated using a tungsten boat as a heating element. Appropriate dimensions of shadow masks were used for the patterning of the deposited electrodes.

2.2.6.2 Chromium as adhesion layer

The one major problem of using Gold is that Gold has low adhesion properties on glass or SiO_2 substrates which might result in peeling off the deposited gold thin films from substrates. This difficulty can be solved by depositing a few- nm- thick adhesion promoting layers made of other metals that have better adhesion than Gold and help Gold electrodes to stick to the surfaces, such as Aluminium or Chromium, prior to gold deposition. For some of the electrode used for electrolyte- gated OFETs presented in this work, another layer (i.e. Aluminium or Chromium) were deposited first on the SiO_2 surface before depositing gold electrodes. These layers were patterned following the pattern of specific shadow masks and have the same dimensions of the overlying gold electrodes.

2.2.7 Deposition of thin- film and nanowires semiconductors

In this thesis, we fabricated thin film transistor devices with a variety of solution processed semiconductors: one low- molecular weight organic semiconductor (PDI8-CN2), and two semiconducting polymers (P3HT, PBTTT) as thin films; other devices were fabricated from nano- wires of P3HT, and nano- belts of BBL. Also, we studied thin- film devices using the inorganic semiconductor ZnO. The processing of all of these materials is briefly introduced now.

2.2.7.1 Deposition of polymers OSCs

Polymers are prepared as solution to be spin- coated on the substrates. The unit of mg/ml solution always is used here which means the weight of polymer powder (mg) dissolved in a volume of solvent (ml). Stirring the solution under 50°C heating helps to dissolve polymers completely. Before spin- coating, the solution must be filtered with pore size of the filter (0.2 to 0.45) μm. During the whole procedure, covering bottle from light avoids any chemical reactions between solvent and solute, especially for P3HT. Spin coating is applied to P3HT and PBTTT as described in section 2.2.2. The typical concentration of solution is about 10 mg/ml. The solvents used in these work were generally described in section 1.5.3.3.

2.2.7.2 Deposition of low- molecular weight OSCs

On the other hand, low molecular weight OSCs, such as PDI8-CN2, were evaporated thermally, since casting of low molecular weight OSCs from solution results in poor quality films. A small amount of PDI8-CN2, say 6 mg, is placed in a

quartz boat and heated up to the vapor phase of used material until 50 nm thickness is achieved, as described in section 1.6.2.1.

2.2.7.3   Growth and deposition of BBL nano- belts

This section was done in collaboration with a project student, Mr. Richard Theo Grant. The preparation of *BBL* nano- belts films used as a semiconductor material in *TFTs* can be divided into two parts: growth and processing. Besides the extra safety precautions that must be taken into account when handling methyl sulfonic acid (MSA), *BBL* has no side- chains and, therefore, won't be soluble in common solvents, but it does dissolve in an organic acid MSA. The processing of the nano- belts in such a way that would remain stable after casting demonstrated to be greatly more difficult.

A solution concentration of *BBL* in MSA about 0.2 mg/ml was carefully measured and mixed and after that the solution is heated at 70°C for 10 mins to help the solubility of the *BBL* powder in acid. After dissolving the *BBL*, the solution's colour has a distinctive colour which is red, as seen in Figure 36. Another solution was prepared that contained the 4:1 ratio of Chloroform and Methanol in which the nano-belts would be produced. This solution was mixed with magnetic stirrer with speed about 1200 rpm, while small quantities about a 5 ml of the *BBL* and MSA solution were added using a pipette. The self-assembling of *BBL* nano- belts was taken place and recognised immediately to the naked eye as the drops of *BBL* and MSA solution entering the chloroform and methanol solution which changes the colour from red to dark blue. As the *BBL* molecules are forced by the poor solvents to self- assemble themselves and forming nano- belts of blue fibres. In such form, the nano- belts are very stable that can be kept in suspension for long time.

Figure 36, a solution concentration of BBL in MSA about 0.2 mg/ml with red colour (left), and a same concentration of BBL nano- belts after a mixture of Methanol, Chloroform and MSA with dark blue colour (right).

Nevertheless, nano- belts in this form cannot be drop- casted directly upon substrates because the different constituents of the medium in which they were dispersed evaporate at different rates. Thus, the chloroform and methanol evaporate relatively quickly comparing to the MSA because of its high boiling point of 167°C that remains present on the substrates. Once the nano- belts drop- casted directly over substrates causes problems, such as dissolving Au contacts because the high acidity of MSA and the nano- belts changing back to red colour which means MSA redissolves the nano- belts.

We, therefore, had to first 'wash' BBL nano- belt suspensions from residual MSA. So far, the growth process mentioned was done according to the process outlined in Briseno *et al*[73]. Attempts were done to execute the washing process for removing any traces of the MSA, but still a number of obstacles were observed.

Using a pipette, the BBL nano- belts are collected, transferred to special vials of centrifuge, and then they are washed with pure methanol at 3000 rpm for 10 minutes. Then, the BBL clusters transferred again to new vials containing deionised water and washed twice. When attempting to repeat these processes, the BBL nano- belts stick to the wall of the vials after adding deionised water.

To avoid this problem, the better results were attained by avoiding the steps of using the deionised water. Instead, the BBL clusters were washed by the different solvent (i.e. methanol, ethanol, or isopropanol) three times at 5000 rpm for 10 minutes, as seen in Figure 37. Variations of different washing media were tested to observe which one of solvent has a better performance when used as semiconductors in electrolyte- gated transistor.

Removing any remaining excess solvent in samples needs great care in order to not lose any of the formed nano- belts and avoid disturbing the nano- belts using pipettes and syringes.
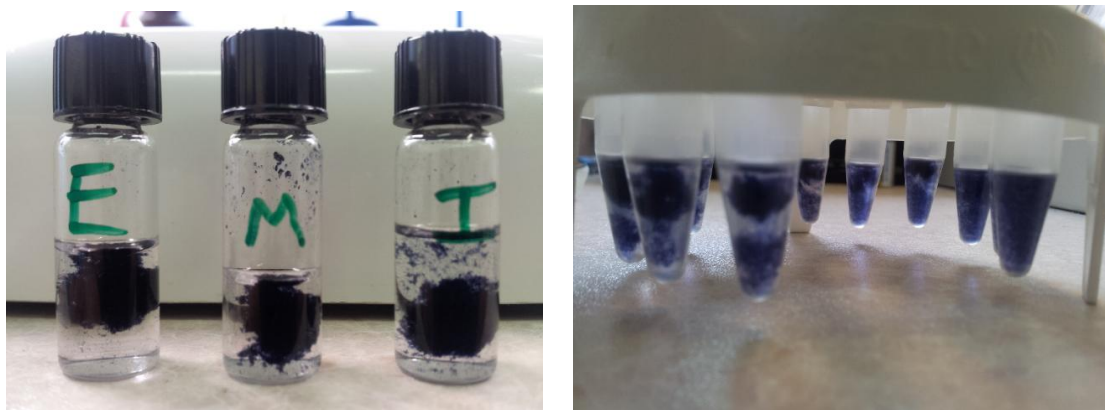
Figure 37 a) BBL nano- belts during washing in different agents to remove any remaining MSA, b) Concentrated clean samples of BBL nano- belts stored in Ethanol, Methanol and Isopropanol

2.2.7.4   Growth and deposition of P3HT nanowires

Two different routes of making P3HT nano- wires were used in this work. Firstly, the P3HT dispersion was prepared following the 'whisker' method. The P3HT (sourced from ADS dyes) was dissolved in anisole (5.2 mg/mL). The solution was heated to 90 °C until fully dissolved, and then the solution was allowed to cool down to room temperature. The solutions were kept in sealed vials and stored in the dark for 3 days for the nanowires to be formed. NWs derived by this route are called 'Anisole- P3HT' NWs. This vials of P3HT nano- wires were prepared and provided by our collaborating partners, Mark Hampton and Dr. J Emyr Macdonald, in the University of Cardiff.

Secondly, 'CB- P3HT' NWs route were grown from regioregular poly(3- hexylthiophene), rrP3HT (sourced from Ossila) in 5 mg/mL chlorobenzene (CB) solution. CB was initially heated to 80 °C and agitated to dissolve the solution, and the solution was then filtered through a 0.45 μm PTFE syringe mounted filter and then left to mature in the dark at ambient temperature for several weeks or months. This P3HT nano- wire was prepared and provided by Mr. Adam Hobson, in the University of Sheffield.

2.2.8 Deposition of ZnO thin film

All the thin films of ZnO used here are formed from a liquid precursor routes. This precursor goes through a chemical change at a substrate surface after thermal treatment which, in turn, leaves a solid thin layer on substrates. Spin- coating is used to deposit the liquid precursor over substrates at spin speed around 1200 rpm, and then the substrates heated at 450°C for 15 min. Repeated depositions (up to three times)

can be carried out to raise the thickness of films at desired thickness which maybe around ~10 nm.

Purchased from Sigma Aldrich, the precursor of zinc acetate dihydrate [$Zn(CH_3COO)_2 \cdot 2H_2O$] (Sigma Aldrich) is dissolved in Ethanol to make concentration about 20 mg/ml, and this is called as Ethanol route. The ammonia route is another way of making thin film of ZnO and prepared by dissolving 1 mMole of zinc oxide (Sigma Aldrich 99.999%) into 12 ml of ammonium hydroxide (aq) (Alfa aesar, 99.9%).

2.2.9 Deposition of Calixarene layers

The example is mentioned here to show how to make a nano- scale layer of different calixarenes. The nitro-ester calix[4]arene (5,17-(34-nitrobenzylideneamino)-11,23-di-tert-butyl-25,27-diethoxycarbonylmethyleneoxy-26,28-dihydroxy-calix[4]arene), shown in the inset of Figure 38, was used and known as Mat16, and it was manufactured as described by Supian. F. *et al*[96]. This calixarene contains a conjugated push- pull electron system at upper rim.
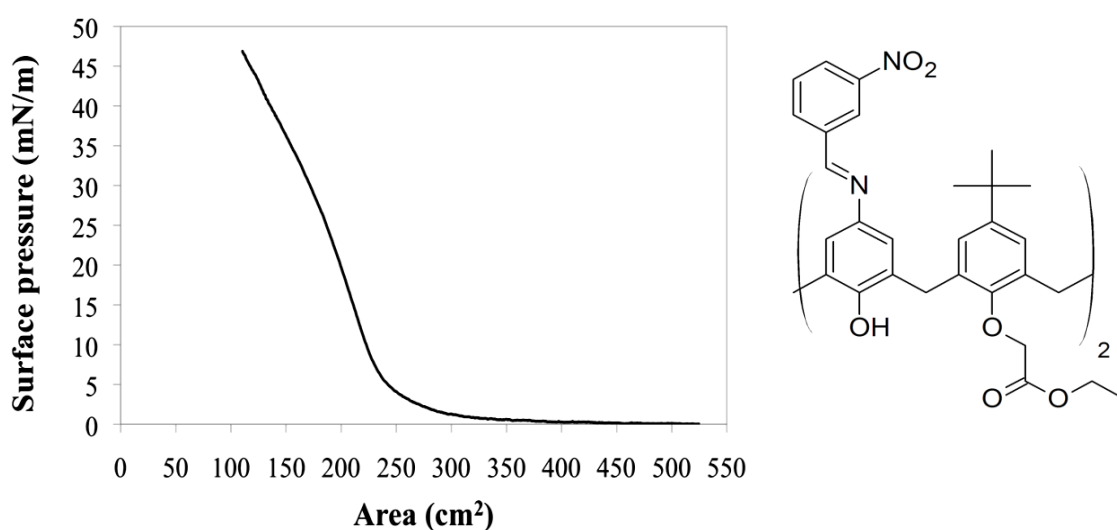
Figure 38, Langmuir isotherm of the calixarene used as ultrathin interfacial layer, chemical structure in the right- side.

Mat16 was diluted in chloroform (0.1 mg/ml), and about 350 μl of solution was spread on the water surface (sub- phase) of a Langmuir trough (Nima 611D Standard Trough) to form a monolayer. Langmuir isotherms (Figure 38) were recorded. The monolayer collapse takes place at a surface pressure of ~ 40 mN/m. We, therefore, always deposited calixarene films by either the Langmuir- Blodgett (*LB*) dipping, or Langmuir- Schaefer (*LS*) printing technique at slightly lower pressure, ~ 35 mN/m, to have dense monolayers on the surface of semiconductors.

2.3   Building liquid flow cell

The need of flow cell increases, when one intends to study the sensing ability of TFTs with the presence of different concentrations of analytes in order to precisely record the transistor's responses. The home- made flow cell is built to be sure constant stream of liquid (DI- water, usually used) flowing on certain channel area in order to have as much stability as possible and give a transistor channel chance to respond (recover) faster to (from) analytes. Two injecting syringes (NE-300, New Era Pump Systems, Inc.) are used, as seen in Figure 39.

First syringe contains a base liquid to mix it with second syringe which contains concentrated analytes but within their solubility. The sum of total flow rate for both syringes is fixed to be at 1 ml/min. Thus, Changing pump speeds of both pumps allowed access to a range of concentration spanning approximately 2.5 orders- of- magnitude. This flow cell was prepared and made by Mr. Saud A. Algarni, in the University of Sheffield.

Figure 39, the home- made flow cell (left), and the NE-300 syringe from New Era Pump Systems, Inc. (above).

2.4   Gate contact needle materials

In the case of electrolyte- and water- gated *OTFTs*, the choosing the right gate electrode material is essential and has an influence on important device parameters[25,97]. On the other hand, in the case of conventional, let's say "dry *OFETs*", the material selection is nothing to do with functional considerations and just to connect to the Keithleys instruments or to I-V converter (measurement system). In this work, *OFET* examples are separated into two different architectures. In the case of electrolyte- gated *OTFTs*, the samples are made as top- gate architectures using

Tungsten contact needle to immerse in the electrolyte, but dry *OFETs* have a bottom-gate. Aluminium was used as a bottom- gate. The properties of these materials are briefly discussed in following sections.

2.4.1 Tungsten

Tungsten was used in electrolyte- gated OTFTs because it as lower off- current comparing with Gold and any other needle used[25]. Kergoat *et al* points out that the shift of threshold is related to the variation of work function of the gate contact needle immersed into a drop of water. During taking data, it is better to have no much effect on *off-* current which, in turn, would gives a correct and not misinterpreting result. Also, another reason of choosing tungsten is that it resists the attacks from oxygen, acids, and alkalis, but not chlorine.

2.4.2 Aluminium

For all bottom- gate OFETs, Aluminium was used as gate contact material, since Aluminium is anodised to form a thin film of the Aluminium oxide gate, as described in section 2.2.5. The Aluminium material came in wire form, and a tungsten coil was used to heat the Aluminium wires to evaporate over Silicon substrates. A 10 cm of aluminium wire was cut into small wires and fitted inside the coil which helps for the growth a thin film of aluminium up to 150 nm thick on the substrate. The coil is connected to a manually controlled current source. Before the thermal evaporation began, the evaporator chamber was pumped down to a high vacuum of $< 5 \times 10^{-7}$Torr.

CHAPTER 3

Experimental Methodology

3.1   Electrical characterisation of TFTs

Once the devices were fabricated, they should be tested before they could be used for any application. Testing the devices is an essential step to find out the best fabrication procedures in order to reach a higher performance, stability and resist unwanted effects coming from gate leakage and other issues that will be explained later. Fabricated devices were characterised by two standard ways to reveal the output currents *vs.* voltages profiles of TFTs which are output and transfer characteristics. However, the alternative real- time characterisation of TFTs was made for measuring and extracting essential parameters during monitoring the presence of pollutant either in gas or liquid phase. The later characterisation would give more imperative information of how the target pollutants interact with a bulk of different TFTs or a deposited sensitiser layer. All of which will be explained in the next section.
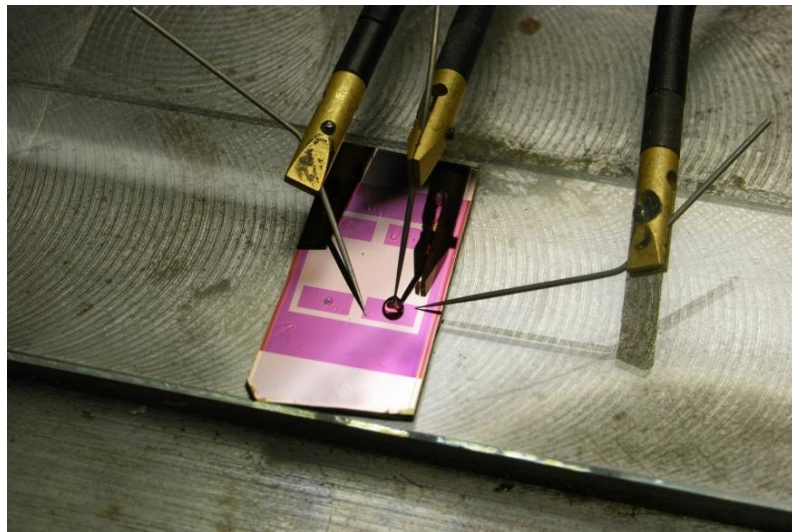
Figure 40, three Tungsten needles connected to TFT device.

3.1.1 Electric source- measure units

We used electric source- measure units for the electrical characterisation of transistors. Such units were used to apply discrete different voltage values to source and gate terminals of a transistor device under test (DUT) and at the same time in order to measure the current responses. These measurements represent output characteristics and transfer characteristics, respectively, as will be explained in section 3.1.1.1 and 3.1.1.2. These are most reliable instruments to provide precise results of electrical characteristics.

Our measurement setup constitutes of two devices of Keithley 2400 source measure units connected to three Suss microtec PH100 probe- heads via coaxial cables, as seen in Figure 41. This instrument is controlled by a computer program written in test- point (Labview-code, Figure 43 and Figure 45) using two GPIB-PCI interfaces. During the test, the OFET device is connected to Keithley through three tungsten needles, as seen in Figure 40. Two of these needles are connected to electrodes (source and drain) and the third is immersed in electrolyte to act as gate contact.
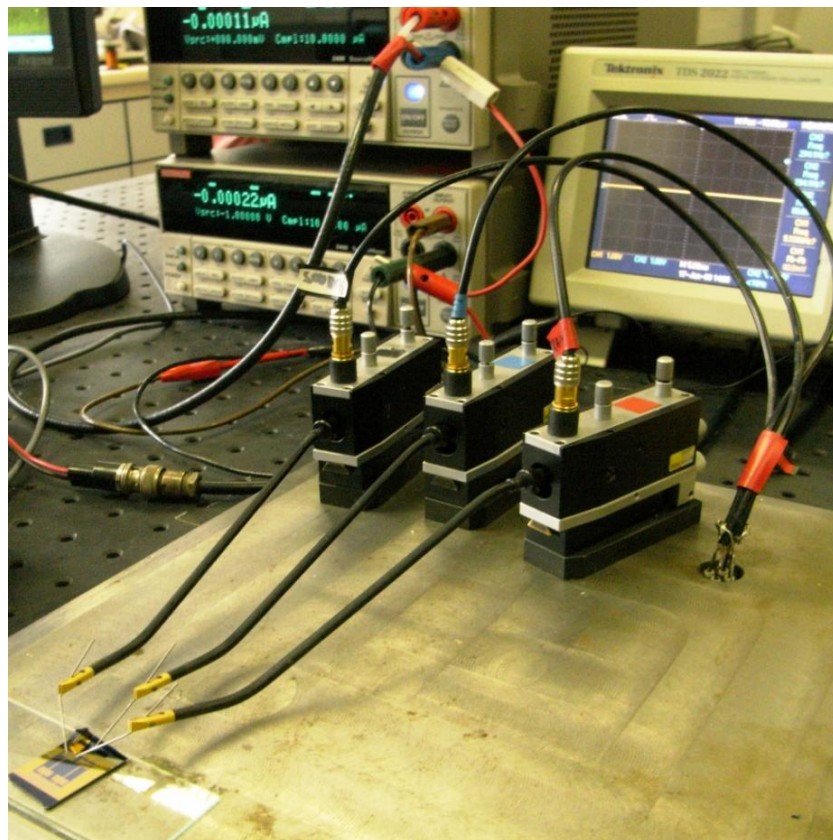
Figure 41, a picture of the Keithleys and probe- heads.

3.1.1.1 Output characteristics

The output characteristic is measured by applying a set of discrete drain voltages (V_D) at different fixed values of gate voltages (V_G) which, in turn, produce a drain current (I_D). The output characteristic is plotted between I_D at Y-axis and V_D in X-axis, as seen in Figure 42. Under a fixed gate voltage, every sweeping of V_D starts from 0 to a maximum voltage and goes back to 0. The same sweeping at same steps is repeated, but the increased value of V_G is applied until it reaches the maximum value of V_G, as well. One important restriction for applying the gate and drain voltages is that the value of both voltages V_G and V_D do not exceed the electrochemical window of an electrolyte used for electrolyte *TFTs* or, in general, the dielectric breakdown of the gate insulator. The output characteristics do not provide the quantitative analysis as well as the transfer characteristics do. Still, its qualitative information can be utilised to diagnose the common problems that same *TFT* device suffering from. For example, the linear of the "ideal" output characteristics is not supposed to have any curvature. If such curvature is observed, this indicates a contact problem in terms of non- ideal injection. Also, when the saturation region of I_D fails to stay at a fixed value for high V_G values but keeps increasing gradually, this means that this *TFT* suffers from doping. Another example of these problems is the hysteresis (different values of I_D between increased and decreased V_D or V_G) that indicating traps or impurities exist in bulk of *TFT* or at interfaces at the semiconductor and insulator.
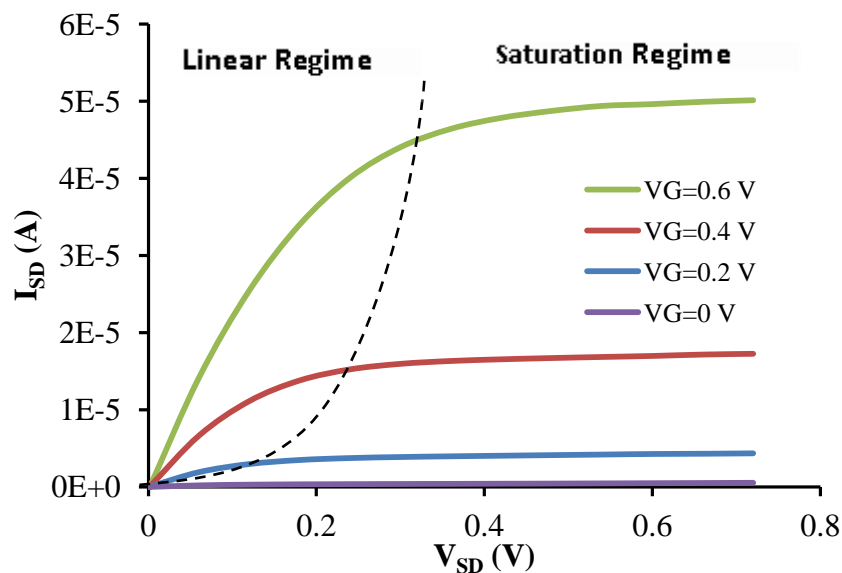
Figure 42, an output characteristic showing the linear and saturation regimes.
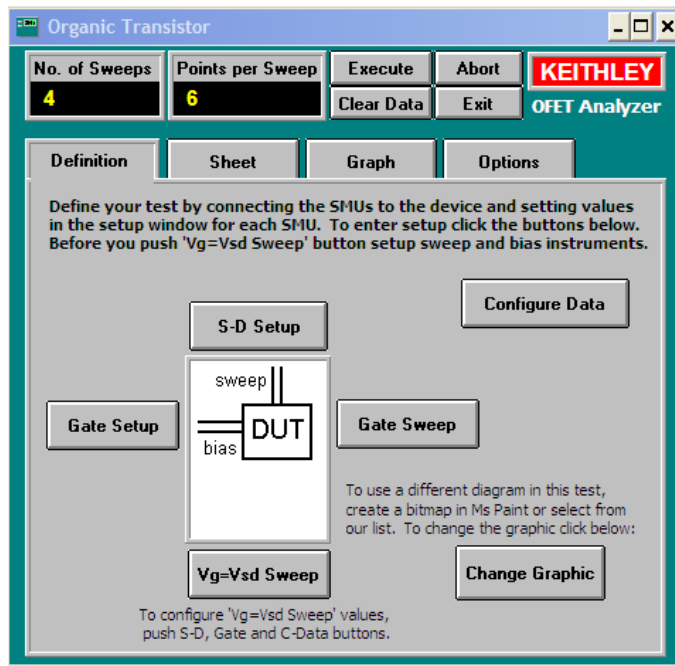
Figure 43, a screenshot of the test- point (Labview-code) of the output characteristic.

3.1.1.2 Transfer characteristics

For transfer characteristics, V_G is swept for fixed V_D. Linear and saturated transfer characteristics are recorded for a very small V_D ($V_D << V_{G,max}$: linear transfer characteristic), and large V_D ($V_D = V_{G,max}$: saturated transfer characteristic). The response of I_D is plotted versus V_G. For saturated transfer characteristics, I_D is typically shown twice, on both a logarithmic, and a square root scale. An example of a saturated transfer characteristic is shown in Figure 44.

The key *TFT* performance parameters (i.e. carrier mobility μ and threshold voltage V_T) can be taken from such a plot of a saturated characteristic by simple fitting and extrapolation procedures. Working on the square- root of I_D, extrapolating a line starts from the linear part of the transfer characteristic (blue- line) to the V_G axis (x-axis), and extrapolating a parallel line to x-axis starts from the lowest part of "*off*" current's plot. The intercepted x-axis value at the intercept of the two extrapolations will give the value of V_G (in Figure 44 case, $V_G = 0.31$ V). By using Equation (1-31) with the slope of the extrapolated line (blue-line), μ can be calculated. The test- point controls the voltages applied to *TFT*, as seen in Figure 45, All other parameters can be calculated by using $\log(I_D)$ scale (red-line) and given in following sections, as in Figure 44.
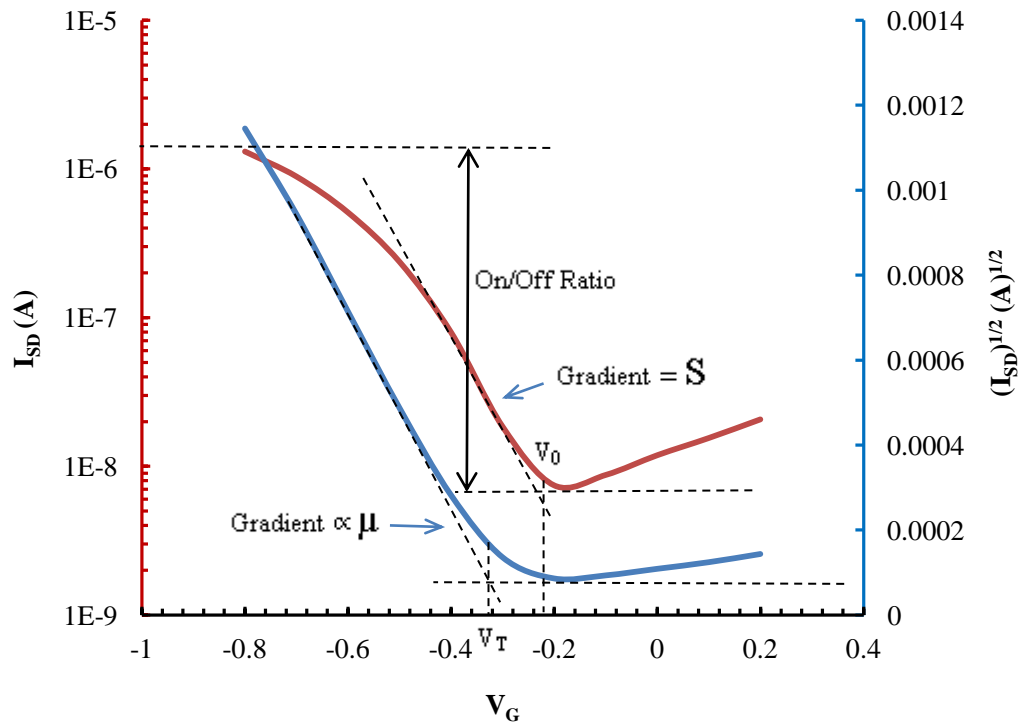
Figure 44, a saturated transfer characteristic with μ, V_T, V_0, S and the *on/off* ratio indicated. The value of $V_D = -0.6$ V.
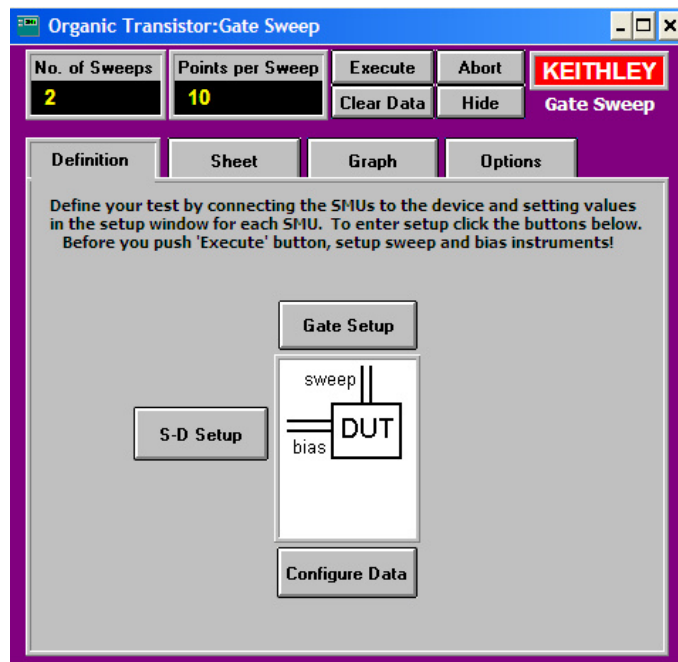
Figure 45, a screenshot of the test- point (Labview-code) of the transfer characteristic

3.1.1.3 *OFET* parameter calculation

This section explains the ways of calculating all parameters of *TFTs* that were used in this study.

3.1.1.4 Saturated Drain Current and *On/off*- current ratio

The saturated drain current ($I_{D, Sat}$) is measured for all values of $V_G > V_T$ in a saturated transfer, but whenever $V_D > V_G - V_T$. This is the definition of saturation.

The *on/off* ratio is a parameter defined as the ratio between the highest possible value of I_D in the saturated regime with I_D in the *off*- state. The bigger value of this ratio represents how effective the gate medium is to gate *TFTs*. The ratio depends strongly on doping levels. The *on/off*- current ratio is calculated as following,

$$(3-1) \qquad \frac{I_{on}}{I_{off}} = \frac{I_{D,V_{DS}=Max,V_{GS}=Max}}{I_{D,V_{DS}=Max,V_{GS}=0}}$$

Usually, the plot of transfer characteristics is taken at $\log(I_D)$ scale (red-line), as in Figure 44. *On/off* ratios are dimensionless (and ideally, large) numbers often expressed as a power of ten.

3.1.1.5 Mobility

As seen in Figure 44, the slope of the extrapolated line (blue-line) is used to calculate the mobility. By using equation (1-31), the slope is calculated as,

$$(3-2) \qquad Slope = \sqrt{\mu C_i \frac{W}{2L}}$$

After reordering the parameters, the mobility becomes as following equation,

$$(3-3) \qquad \mu = \frac{2L}{C_i W} Slope^2$$

Where, C_i is the capacitance per unit area of the gate dielectric and the device dimensions (*W*idth and *L*ength).

3.1.1.6 Hysteresis

This phenomenon may take place in both characteristics of *TFTs*, and hysteresis shows a shift of I_D values in upwards and downwards sweeping either in gate voltage or drain voltage. Thus, the direction of sweeping voltages would affect the direction of shift. In the presence of hysteresis, the combination of the upwards and downwards shifting creates both curves as an open loop. In Figure 46, the values of downwards I_D

(from the maximum voltage to zero) are noticeably higher than the values of upwards direction.

The importance to this phenomenon is its relation to the existence of traps in the interfaces between semiconductor/dielectrics and mainly in bulk of the semiconductors[98]. The way of calculating this phenomenon is not clear after calculating TFTs parameters. Thus, from now on, all TFTs parameters will be calculated from data taken from upwards sweeping of voltage in order to have consistent results.
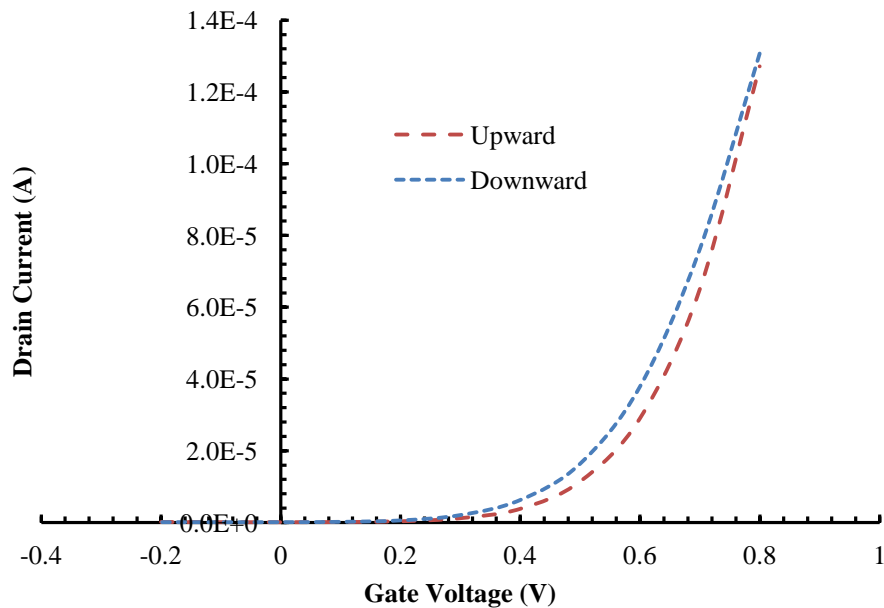
Figure 46, an example of hysteresis.

3.1.2 I-V Converter method

The I-V converter circuit was used as another option for measuring the electrical characterisation of Organic Field Effect Transistors (*OFETs*) rather than Keithley instruments. This circuit has been developed by Lee Hague *et al*[99]. The unique advantage of this circuit is to measure saturated characteristics of transistors in real-time. Thus, the I-V converter can record multiple parameters with many continuous data- points, when the channel get affected by any external influences, such as toxic in gaseous and liquid form. Many modifications were made to develop the I-V converter unit and integrated to Labview program by Dr. Antonios Dragoneas. The electrical circuit, operation and the calculation of parameters of the I-V converter are discussed in following sections.

3.1.2.1   Circuitry and operation

By applying a suitable alternating (sinusoidal) drive voltage to the *TFT* source contact from a signal generator, the circuit shown in Figure 47 delivers a saturated transfer characteristic parametric in time, thus providing an efficient tool to characterise instantly the changes of threshold and mobility almost instantly.
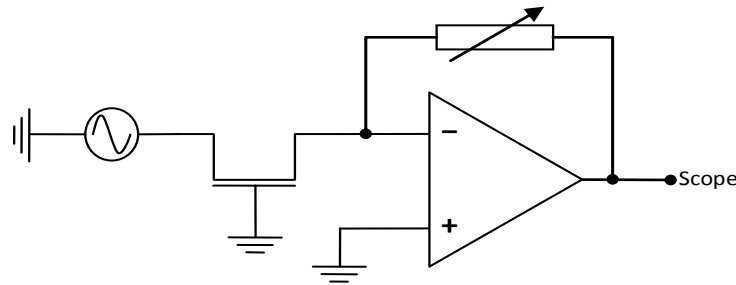
Figure 47, a simplified schematic of the I-V converter measurement system. The model of operational amplifier is a high- voltage op-amp from Texas Instruments number (OPA445AP).

The I-V converter and Keithley show a consistency in results in terms of *FET's* parameters, so I-V converter is reliable, measuring parameters in real- time and such a portable device that can be taken to outside labs, supplied electrically by economical batteries. Figure 48 shows typical Water- gated *OFET* characteristics taken from Picoscope software.
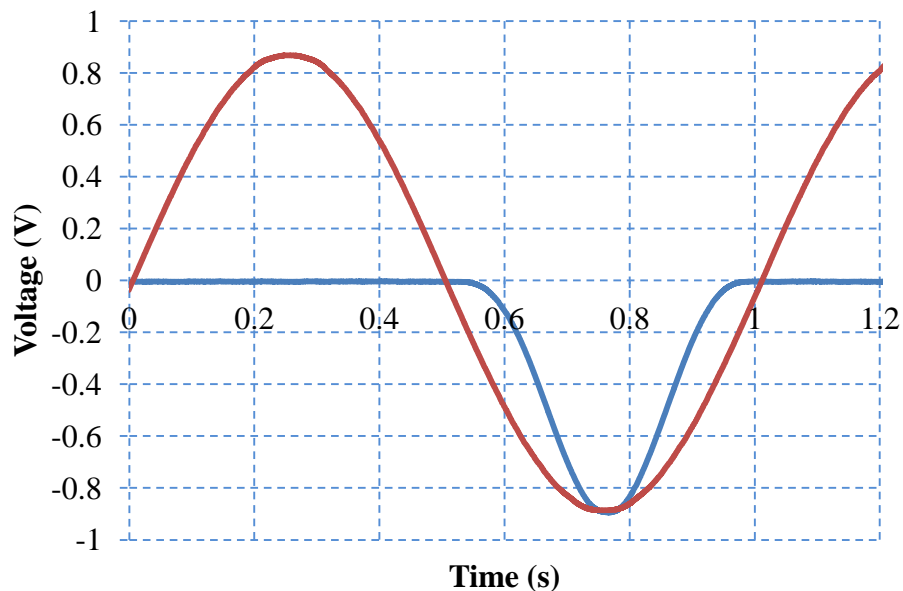
Figure 48, typical electrolyte- gated TFT of PBTTT, taken directly from picoscope software at frequency= 1 Hz and R_f =18 kOhm. Red sine- wave represents the voltage applied to a transistor (V_{in}) or (V_s), and blue sine- squared- wave represents the response of the transistor (V_{out}).

The drive voltage $V_S(t)$ (usually a sinusoidal) is applied into the source of the *TFTs* being tested using a programmable signal generator and voltage follower, the gate is linked to the electrical ground and the drain is connected to an op-amp through inverting input. This input of the op-amp is considered as a virtual ground as the op-amp's the non- inverting input is linked to the real ground. The op-amp's output voltage $V_{OUT}(t)$ is fed back into the inverting input of the op-amp through a feedback resistance R_f. The value of R_f can be changed by using an external resistance box connected to the circuit. $V_{OUT}(t)$ of the op-amp was recorded, since it is proportional to the saturated drain current $I_{SD}(t)$ according to the following equation,

(3-4)
$$V_{OUT} = -10R_f \, I_{SD}$$

Together, $V_{out}(t)$ and $I_{SD}(t)$ constitute the TFT's saturated transfer characteristic parameters with time, as seen in Figure 50. It is important to mention that a factor *x10* is applied because of the x0.1 attenuation of the drive signal, and minus (-) is applied, as well, because of the inverting of drive signal. For more explicit representation of the both voltages (input and output) signal on the oscilloscope screen, both voltage signals should appear at the same as the maxima at same time coordinate (x-axis) by adjusting the value of the feedback resistance, more detail about this system reported in Hague L. *et al*[99].

The main advantage of using sinusoidal signal as symmetrical bias is to make sure that the gate dielectric is exposed equally to positive and negative voltage bias in order to reduce the effect of *bias- stress* over the gate dielectric. The effect of gate- bias is demonstrated in several studies especially the effect on the threshold voltage[100]. There is no information about gate leakage, because the gate electrode is grounded. Thus, the system cannot notice the current flow between the source and the gate.

Figure 49 shows an overall picture of the actual system being used in this work including resistance box, Picoscope (Pico Technology Picoscope 2204) and characterisation board (I-V converter). The portable system is using *USB* port to connect to *PC* containing a two- channel (*A* and *B* channels) digital oscilloscope and signal generator.

Figure 49, the complete system, from top to bottom, resistance box, Picoscope and characterisation board (I-V converter).
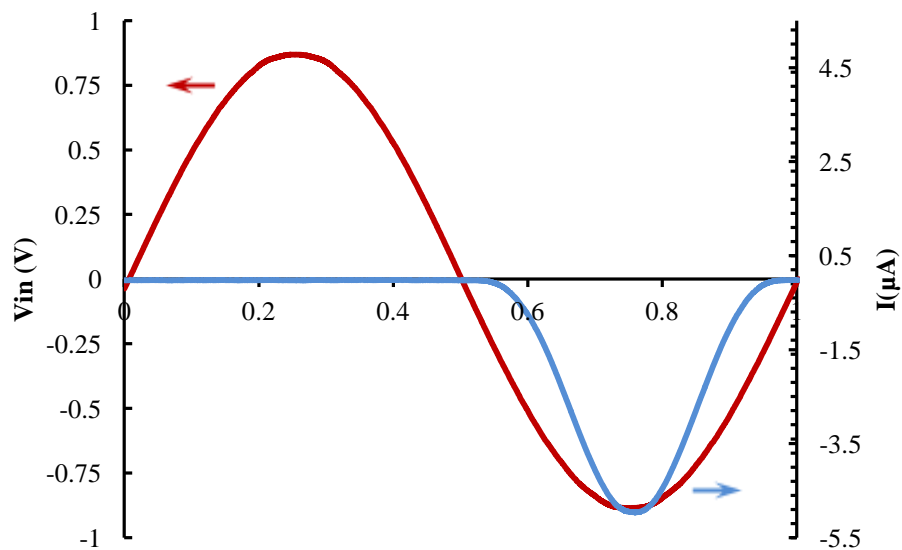
Figure 50, I_{SD} calculated from Figure 48 by applying value of R_f =18 kOhm in equation (3-5).

3.1.2.2 Consideration for electrolyte- gated TFTs

When this scheme is applied to electrolyte- gated TFTs, it is important to consider that the properties of tested device affect the output's results taken from *I-V* converter in terms of a shifting in phase. This is because of the presence of the combination between a channel resistance with high value ($\sim$MΩ/GΩ) and the parasitic

capacitance. This combination acts as low- pass filter which are connected in parallel to the *I-V* converter. Thus, at high frequencies, the oscilloscope detects sometimes the lagging and leading of V_{out} over V_{in} depending on the value of the feedback resistance and the parasitic capacitance. To control this issue, the taken measurements from this scheme were adjusted to have no phase- shift by applying a low frequency about (0.5-1Hz). However, the dry transistors do not suffer from a phase- shift at high frequency reaching 100 Hz. Considering, as well, the slow building up of electric double layers (*EDLs*), the chosen frequency was very low about ($f = 1$ Hz). Also, the peak of the drive voltage V_S was set to (0.6-0.9) V to remain within the electrochemical window of all the electrolytes used, thus avoiding electrolytic decomposition of the gate medium.

3.1.2.3 Saturated drain current calculation

The equation is used to calculate the saturated drain current, according to,

$$(3\text{-}6) \qquad I_{D_{max}} = \frac{V_m}{10 \times R_f}$$

where V_m is the peak output voltage.

3.1.2.4 *On/off* ratio calculation

The ratio of *TFTs* is simply calculated by dividing the positive (maximum) peak of output voltage over the negative (minimum) peak in case of an *n-* type semiconductor device. For a *p-* type semiconductor device, the ratio is inversely calculated, according to the following equations,

$$(3\text{-}7) \qquad \frac{I_{on}}{I_{off}} = \left| \frac{\text{max peak } (V_{out})}{\text{min peak } (V_{out})} \right| \qquad \text{For } n\text{- type}$$

$$(3\text{-}8) \qquad \frac{I_{on}}{I_{off}} = \left| \frac{\text{min peak } (V_{out})}{\text{max peak } (V_{out})} \right| \qquad \text{For } p\text{- type}$$

3.1.2.5 Threshold voltage and mobility calculation

Two different ways to extracting threshold voltage and mobility using this scheme are discussed, here.

3.1.2.5.1 Conversion to conventional saturated transfer characteristics

Data taken from the I-V converter are usually plotted as input (V_S) and output (V_{OUT}) voltages (Y-axis) versus time (X-axis), as seen in Figure 48. The same data can be plotted as conventional saturated transfer characteristics by eliminating the time parameter, and plotting the input voltage (x-axis) versus the output voltages (Y-axis), seen in Figure 51. The output voltage is converted into a drain current using equation (3-6), and the drain current square- rooted to be $(I_{SD})^{1/2}$ as done by Hague et al[99].

From Figure 51, the threshold voltage and mobility can be calculated as the same way as the section 3.1.1.2 mentioned. There remains one difference between the converted saturated transfer data and the standard transfer characteristic. In the converted saturated transfer data, the applied value of V_{DS} is continuous (not constant) while the V_{GS} range is swept having the same value to V_{DS}, so $V_{DS}=V_{GS}$ is applied at all times. Generally, this means that *I-V* converter fulfils always the condition of saturation, $V_{DS} > |V_{GS} - V_{th}| > 0$, and there will be no quantitative difference between I/V converter- and conventionally measured characteristics as long as we are dealing with a 'normally off' FET; *i.e.* one with negative (positive) threshold for p-type (n- type) semiconductor.
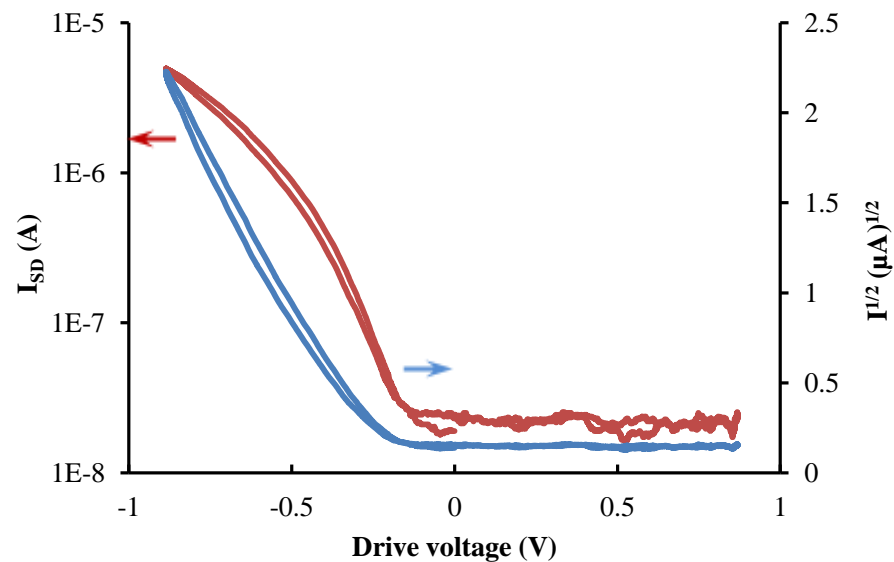
Figure 51, shows the Saturated Transfer conversion from I-V converter's data, for PBTTT water- gated TFT.

3.1.2.5.2 Sinusoidal method

This is another way for measuring threshold and mobility directly from *I-V* converter data, without first eliminating time. As seen in Figure 52, a straight line is

fitted the middle point of the rising flank of the output voltage. The intercept of this line on x-axis is projected on the input voltage in order to give the threshold. Since these data are taken in saturated regime, the mobility is calculated using the following equation,

$$(3\text{-}9) \qquad \mu = \frac{1}{10 R_f C_i} \times \frac{2L}{W} \times \frac{|V_m|}{(|V_0| - |V_{th}|)^2}$$

Where, V_0 is the amplitude of the sinusoidal drive (input voltage) and V_m the peak of output voltage. They can be same value, once they are matched by adjusting feedback resistance.

Using measurement data from I-V converter is considered as an advantage, because of the larger data points produced comparing to the standard transfer characteristic. This gives a high certification and accuracy for the values of TFT's key parameters. Later, this advantage is used to build real- time measuring by integrating to Labview program (see section 3.1.2.7).
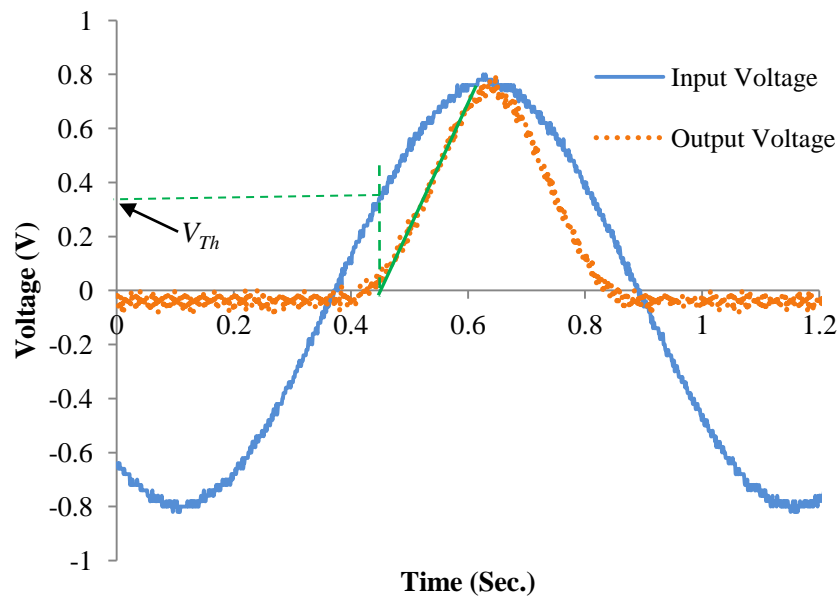
Figure 52, a linear fit and extrapolation on the data taken from oscilloscope.
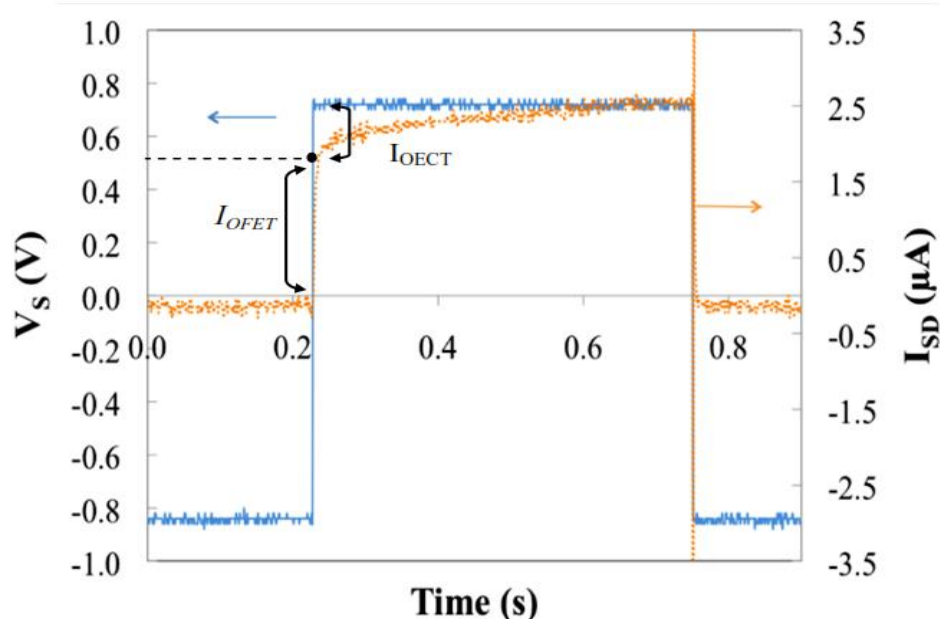
Figure 53, a square- wave signal applied on TFT, and the field effect and electrochemical operation regimes are indicated.

3.1.2.6 I_{OECT}/I_{OFET} ratio calculation

Applying square drive in an *I-V* converter assists to verify whether the field effect or electrochemical regimes operate in *TFT*. The field effect regime switches fast from *off* to *on* in (<msec.), but the electrochemical operates more slowly (typically reaching within sec.) depending on the rate of the diffusion ions going in or out the channel of a semiconductor[101]. Laiho *et al* point out that the semiconductor's operation depends on the organic materials and the applied gate bias[101]. During the square- wave voltage, the constant voltage was applied to both drain and gate electrode (*V_DS=V_GS* which are same in *I-V* converter) in order to record the response of output voltage, as seen in Figure 53. Thus, the I_{OECT}/I_{OFET} can be measured by taking the height of the slow switching (I_{OECT}) divided by fast switching (I_{OFET}).

3.1.2.7 Real time measurement of OFET parameters

The advantage of I-V converter was used to develop the software that is able to extract automatically the parameters of transistors in real time, as seen in Figure 54. Labview program is connected to Picoscope by Microsoft Windows dynamic- link library. The applied signals and collected data are transferred between Labview and the I-V converter using a USB connection. A number of parameters (i.e. the capacitance of the gate dielectric C_i, the channel's length and width, the type of semiconductors whether n- type or p- type, the frequency of signal, an amplitude and a shape of signal and the feedback resistance R_f) must be identified before

starting measuring key parameters, such as mobility, threshold, on- current, off- current and the ratio between on/off. The saturated transfer conversion (section 3.1.2.5.1) and sinusoidal method (section 3.1.2.5.2) are used to calculate the mentioned parameters. The Labview code was developed by Dr Antonis Dragoneas.
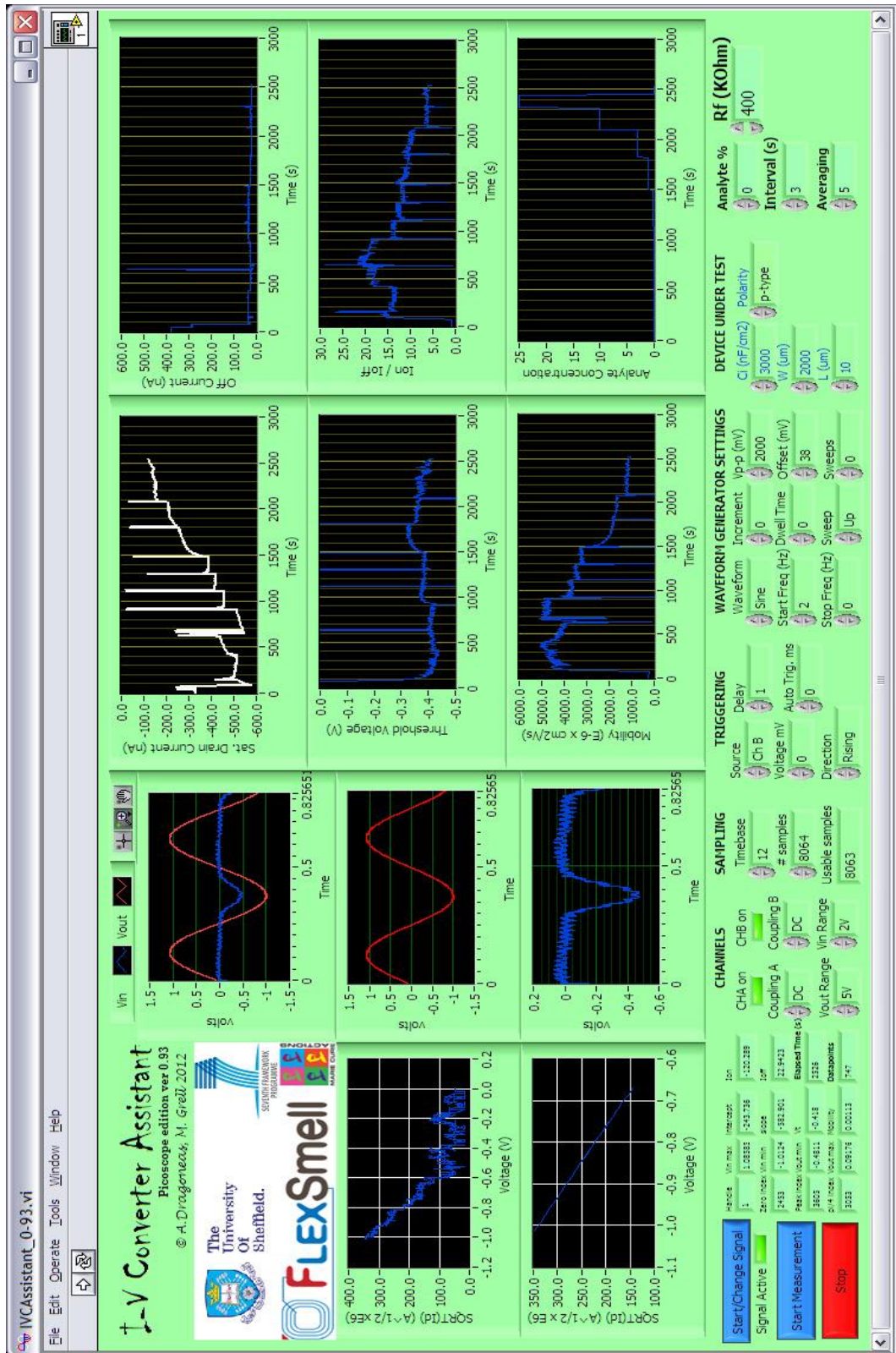
Figure 54, a screenshot for real- time characterisation taken from Labview program.

3.2   Optical characteristics

3.2.1   Contact angle

Surface tension quantifies cleanliness and the hydrophobicity of substrate surfaces. In order to quantify surface tension between solid and liquid phases, the contact angle technique is the best choice because of its simplicity. The shape of a drop of water on a surface results from the balance between forces of three phase boundaries. Young's equation[102] is used to represent this balance, as following,

(3-10)
$$\gamma_{lv} \cos\theta = \gamma_{sv} - \gamma_{sl}$$

Where, γ_{lv}, γ_{sv} and γ_{sl} stand for the interfacial tension of the liquid- vapour, the solid-vapour and the solid- liquid interfaces, respectively.
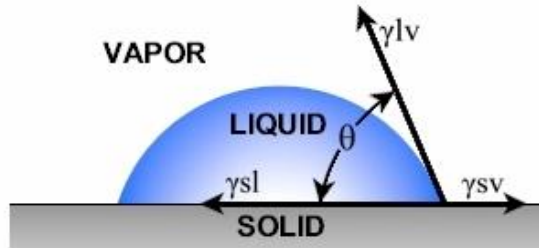
Figure 55, the geometry of the drop of water with different interfacial tension.

The left hand side of the equation (3-10) can be taken from experiment, but the right hand side is unknown. As a result, γ_{sl} is required to obtain γ_{sv}. A mathematical method can be done to achieve that. To measure the contact angle, the (KSV instruments attension theta) was used and equipped with a high contrast camera that is connected to computer software that has a fitting option.

3.2.2   Ellipsometry

This optical technique has the ability to measure the thickness and the optical properties of thin transparent films on reflective substrates by computing the change of the polarization of light (amplitude ratio ψ and phase shift Δ). These changes take place once light gets reflected from the material coated on the substrate. Therefore, when the incident light beam is linearly polarized light (containing superposition of *s*- and *p*- polarization) and reflected from a thin film, this light beam is converted to elliptical polarization because of phase shift Δ and amplitude ratio ψ, as seen in Figure

56. It is known that light has two components of electric field which are parallel (*p*) and perpendicular (*s*) of polarized light with the plane of incidence.
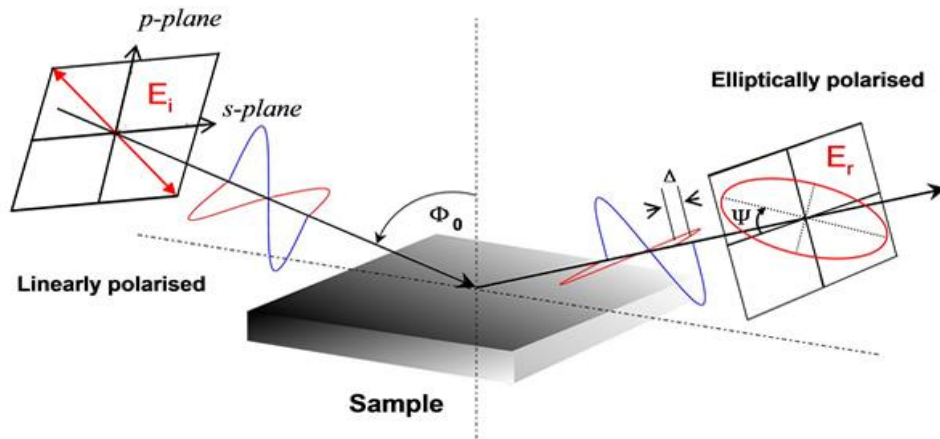
Figure 56, the setup of an Ellipsometer experiment.

Since, the wavelength of light is longer than the investigated thin layers, this gives access to vital information related to the sample morphology and the film's thickness (d), and its refractive index (n) by measuring a complex quantity called the reflectance ratio (ρ) between the amplitudes of r_s and r_p after being reflected and normalized, as written in following equation[103],

$$(3\text{-}11) \qquad \rho = \frac{r_p}{r_s} = tan(\psi)e^{i\Delta}$$

The model of Ellipsometer used is M2000V (J. A. Woolam) that is equipped with a fitting program with different fitting equations, and the wavelength range is applied between 370-1000 nm.

3.3 Morphological characterisation

3.3.1 Atomic- force microscopy (AFM)

AFM works by sensing the atomic forces between a surface and tip in gentle contact with each other[104], and AFM is, therefore, categorised as a scanning probe microscopy (SPM). The resolution of this type of microscope is about of a fraction of nanometer. It was developed in 1986 by Binnig and Gerber[105] after building a scanning tunnelling microscope (STM) which was invented by Gerd Binnig and Heinrich Rohrer who both won the Nobel Prize in Physics later in 1986. In AFM, the feedback signal takes place from the atomic forces including, not limited, Van der Waals forces, electrostatic forces, magnetic forces, adhesive forces and even solvation

forces, in liquid, which means an interactions between the molecules of a solvent and a solute.

Three basic components control the operation of an AFM, as seen in Figure 57. Firstly, piezoelectric elements are utilized to move the probe in three directions (X, Y and Z axis). For scanning sample, the probe move across the sample in two dimensions (X and Y), and Z direction is manipulated by a control system in order to maintain the desired forces or modes between probe and the sample. Thirdly, the cantilever on which probe is mounted is used to measure and detect the interactions between the sample and the probe, and the cantilever is excited into resonant oscillations. The photodiode records the illuminating laser's reflections from the back of a cantilever as a sensitive force transducer seen in Figure 57.
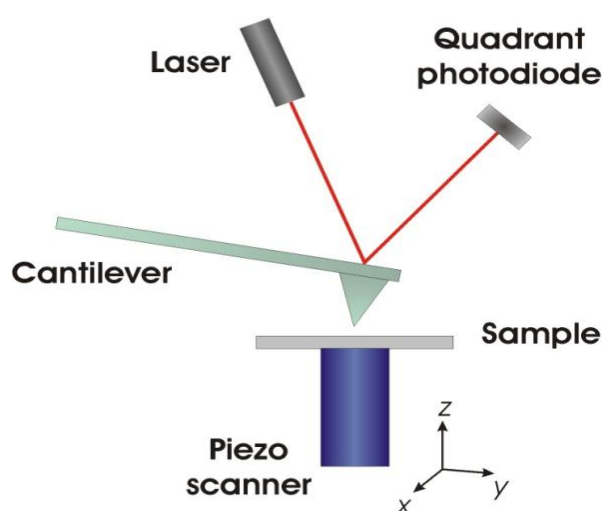
Figure 57, the principle of AFM.

AFMs can be operated in three possible modes known as contact mode, non-contact mode and tapping mode. At molecular level, other forces are active; however, van der Waals forces are still a dominant force. From Figure 58, weak repulsive van der Waals forces takes place first on the probe and results in tip deflection, when the probe is in contact with the sample. Once the tip goes away from the surface, the non-contact mode increases attractive Van der Waals forces until electron clouds electrostatically repel each other. The former mode is the primary mode of operation. The surface tension force is used here to scan across the surface quickly with good topography of the rough samples. The latter mode depends on the oscillation of the cantilever to scan across the surface with low resolution, since the amplification's response of electronics constituting AFM and lowest resonant frequency of system are usually the limiting factor to have high resolution scanning. The third mode is called

tapping mode, as it is the intermediate- contact mode between modes before. Tapping mode still provides high resolution scanning even with soft or fragile samples, such as organic semiconductors and biological samples. The imaging of AFM is produced by the feedback signal due to a change in the oscillation amplitude or phase of the cantilever. The change of oscillation's phase is used to distinguish between different materials on the sample's surface.
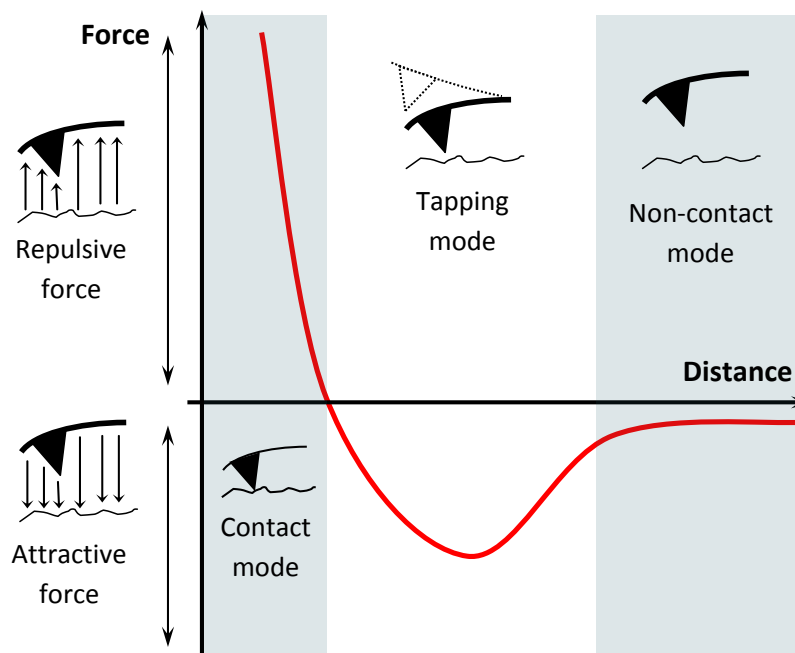
Figure 58, Tip- sample interaction force (Y-axis) vs. distance (X-axis).

For nano- wire AFM characterisation, a Veeco Dimension 3100 was used to obtain height and phase images of spin- cast P3HT NW films. The controller used on all AFM images was a Nanoscope IIIa controller with a Basic Extender. For all images, we used a standard tapping mode cantilever (Bruker TESPA, k=42 N/m, a resonant frequency 320 kHz). The full specifications for these cantilevers can be found at Bruker AFM Probes website[106].

3.3.2 X-ray photoelectron spectroscopy (XPS)

In the middle of 1960s, XPS, known before as ESCA (Electron Spectroscopy for Chemical Analysis), was developed and introduced by Kai Siegbahn and his colleagues at the University of Uppsala (Sweden). In 1981, the Nobel Prize was awarded to Kai Siegbahn for his contribution to XPS. The law of the photoelectric effect discovered by Albert Einstein was behind the idea of XPS. The purpose of XPS is to identify the chemical state of elements constituting the surface of a thin film[107].

The technique beyond XPS is to excite the surface of thin film with photons or ions in order to have a highly excited state of core electrons producing different decays, such as fluorescence (radiative) decay or *Auger* (non- radiative) decay. Thus, the kinetic energy of emitted core electrons due to the incident of X-ray beam is measured, as seen in Figure 59.
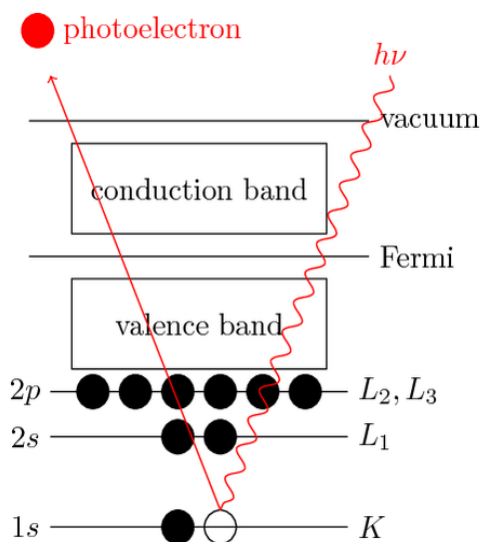
Figure 59, photoelectric process to explain XPS principle.

The core electron escapes from an atom that is on a sample's surface, if the photon energy is bigger than the binding energy E_b of the core electrons. The kinetic energy of escaped electrons is correlated to the energy level of specific elements and is calculated by the following equation,

(3-12) $$E_k = h\nu - E_b - \varphi$$

Where h is Planck's constant, ν is an exciting radiation frequency and φ is the work-function of the spectrometer (not the sample).

Theta Probe Thermo-VG Scientific instrument was used for executing the XPS measurements (from the University of Bari). A monochromatic source of Al Kα with particular settings such as 15 kV, X-ray spot size 300 mm, taking off angle about 37° and base pressure 10^{-9} mbar was utilized. The wide- scan survey of binding energy around (0–1 200 eV, BE) were gained at the pass energy of 150 eV. Thermo Avantage software was used to analyse and produce a fitting for XPS data.

CHAPTER 4

In following chapters, all results taken from fabricated TFTs are presented with discussions and conclusions for every chapter.

4.1 The Water- gated Organic TFTs with interfacial layers of calixarene

Using a drop of water as gate electrolyte in principle offers an attractive alternative for organic transistor- based water sampling, wherein the sample is a functional part of the sensor device. Water- gated *TFTs* thus offer themselves as transducers for the sampling of waterborne analytes, with applications to biomedical or environmental samples. However, two major challenges remain. Firstly, organic semiconductors are not themselves specifically sensitive to particular bio- molecules or ions[108]. Gating requires either an anionic, or a cationic, *EDL*, depending on the type of organic semiconductor (anionic/cationic for a hole/electron transporter), but is otherwise indifferent to the chemical identity of the ion. Secondly, in water- gated organic semiconductors, there may be a number of other currents competing with field effect, such as electrochemical effect[25,101], as discussed in section 1.5.4 and Figure 13.

This section reports on a technology platform designed to overcome these challenges related to the existence of the electrochemical current I_{OECT}. We introduce an ultrathin interface layer of Langmuir- deposited calixarenes at the organic semiconductor/water interface. A wide range of calixarenes are known that can selectively bind e.g. to particular cations[109], thus can specifically sensitise a water- gated transistor for the selective detection of cations. Crucially, we show that a small number of Langmuir- deposited calixarene layers result in films that do not compromise *EDL* gating, but can block the ionic doping currents that lead to *OECT* behaviour. We can delineate the field effect from the other currents observed in water-

gated devices, even when we use ordinary tap water rather than DI- water as gate medium, to simulate a realistic environmental sample.

4.1.1 Experimental details

The experimental part of this section was performed in collaboration with Dr. Delia Puzzovio. A water- gated organic transistor is a relatively simple device, comprised of gold contacts, an organic semiconductor film, and a droplet of water with a gate contact needle inserted into it. Source- drain gold contacts (channel length L=10 μm and width W=2 mm) were thermally evaporated on clean Si/SiO_2 substrates (described in section 2.1.2) under 10^{-6} Torr vacuum through shadow masks (described in section 2.2.3). As organic semiconductor, we used two different batches of the common hole transporting organic semiconductor, poly(3-hexylthiophene-2,5-diyl) (P3HT): one was purchased from Sigma- Aldrich (electronic grade 99.995%, average M_n 15000-45000), the other from Ossila (regioregularity 96.6%, average M_n 32000). Both materials showed similar performances, and are, therefore, not discussed separately. We dissolved 10 mg/ml of P3HT in dichlorobenzene (*DCB*) under stirring and heating to 60°C for about 15 min, and filtered through a PTFE membrane syringe filter. The reason of choosing *DCB* with P3HT is that the solvents having a low vapour pressure contribute remarkably to more ordered and close packed film in *TFTs* and increase the lifetime of produced device[110]. We spin cast solutions (2000 rpm for 1 min) onto the described substrates. Cast films were dried under dynamic vacuum at 40°C for 1h. The deposited calixarene (*Mat16*) was used as described in section (2.2.9) and shown in Figure 38. The reason of choosing this calixarene is that it was known to be specifically sensitive to Fe^{3+} as a cation[111].

To represent an environmental water sample, we used local tap water without purification. We placed a 2 μl droplet of tap water on the channel with the help of a micro- litre syringe, and inserted a tungsten (W) needle as gate contact. Source and drain were also contacted with W needles, avoiding direct contact with the droplet. Figure 12 shows the overall device architecture. Data may require some processing (filtering 50 Hz, subtraction of '*off*'- current) before they can be analysed, but processing, as well as extraction of mobility and threshold, are straightforward.

4.1.2 Results and Discussion

Figure 60(a) and (b) show the drive voltage, V_S, and the drain current, I_D, (derived from V_{OUT}) under square- and sine- wave drive, respectively, of a water- gated *OFET* without any calixarene surface layers. Under square wave drive (Figure 60a), in the

positive V_S half- cycle, we find I_D initially 'jumps', then slowly increases further over time, until V_S is reversed. This signal reveals contributions from both field effect and electrochemical transistor behaviour: the initial quick jump is a response to field effect (I_{OFET}, which takes less than 10 ms to appear), and then electrochemical doping gives rise to a slowly increasing current, I_{OECT}. These observations are very similar to those by Inganäs et al[48,101]. In the negative V_S ('off') half- cycle, contributions from both field effect and electrochemical doping are zero; however, a small I_D is nevertheless observed. This reveals contributions from either, or both, ionic leakage currents from source to drain across water (I_{leak}), and permanent doping of the organic semiconductor (I_{perm}), as mentioned in Table 3. These currents are also present during the positive ('on') half cycle, adding to the transistor currents; however this is unimportant as long as they are comparatively small. Under sine wave drive (Figure 60b), characteristics look very similar to those observed for 'dry' transistors[99]. We extract the ratio of field- effect to electrochemical current (I_{OFET}/I_{OECT}), and the transistor's *on/off* ratio, from Figure 60a, and threshold (V_T) and μC_i from Figure 60b and equation (3-9). All characteristics of this transistor are summarised in the first row of Table 3.

Figure 61 shows the corresponding result for a water- gated OFET where the P3HT surface had first been coated by 4 LS layers of *Mat16*. Figure 61a shows that current *on/off* ratio is significantly reduced; this is not due to a significant increase of the *off*- currents (I_{perm}, I_{leak}), but due to a reduction of 'on' currents, note the different current scales in Figure 60 and Figure 61. We conclude that the application of the LS layers has significantly reduced carrier mobility in the accumulation layer, which affects the transistor currents, but not doping or leakage current. This reduction of carrier mobility is not due to an increase or decrease of the threshold, as seen in Table 4. Figure 61a also shows that current in the 'on' half- cycle now no longer slowly increases with time. We conclude the 4 LS layers block the gate- driven flow of anions from the electrolyte into the semiconductor, hence I_{OECT} is suppressed. To calculate threshold, and μC_i, from Figure 61b, we have first subtracted the current observed during the 'off' (negative V_S) half- cycle from the 'on' current, to correct for contributions from I_{leak} and/or I_{perm}, before evaluating V_T and μC_i.
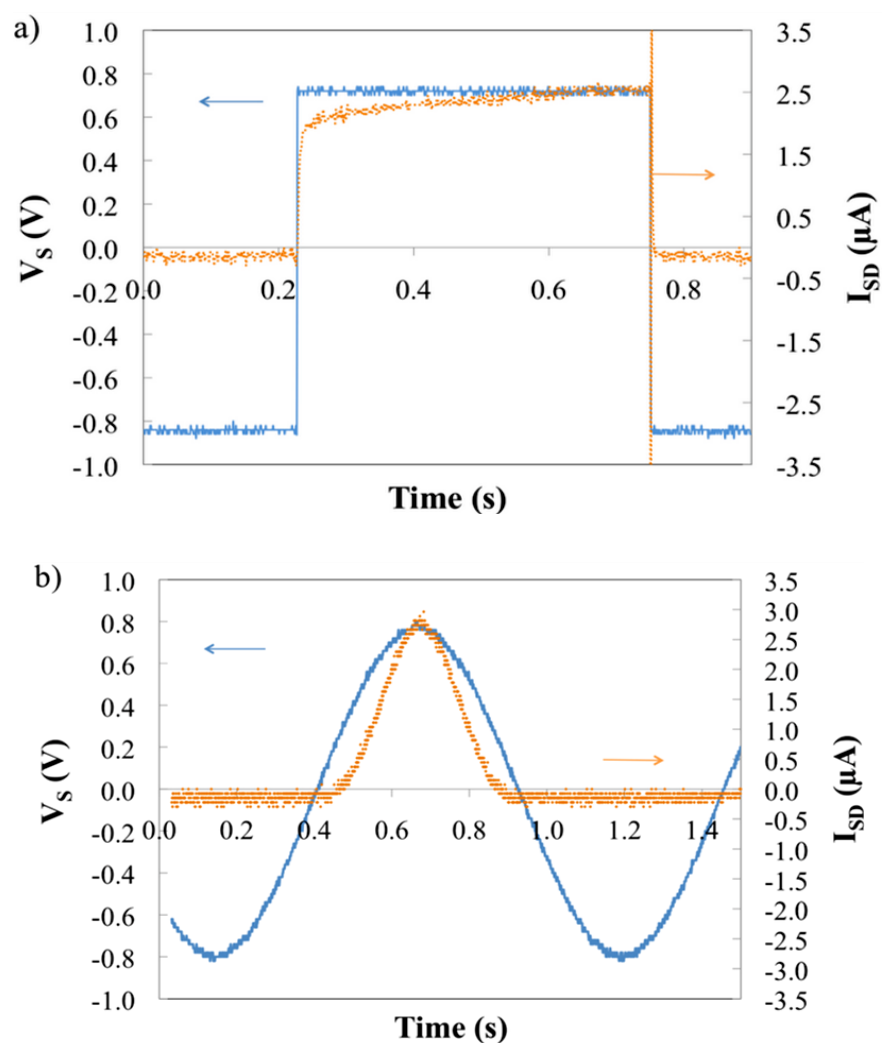
Figure 60. AC characterisation of a P3HT uncoated transistor: square- wave drive (a) and sine- wave drive (b). The blue signal is the input voltage, V_S, and the orange is the drain current, I_D, derived from the output voltage, V_{OUT}.

Type of current	Carrier	Caused by	Gate driven?	$I(V_S)$ or $I(t)$ characteristic
I_{OFET}	holes	Field effect from electric double layer	Yes	$\sim (V_S - V_T)^2$
I_{OECT}	holes	Electrochemical doping by anions from electrolyte	Yes	Slow increase with time (>10 ms to s)
I_{perm}	holes	Permanent chemical dopants (e.g. catalyst residue)	No	$\sim V_S$ (ohmic)
I_{leak}	ions	Non- perfect insulation between source / drain contacts and electrolyte	No	$\sim V_S$ (ohmic)

Table 3. The different currents found in electrolyte- gated organic transistors with hole-transporting organic semiconductor, and their I/V or $I(t)$ characteristics. V_S is a drive voltage applied to source, with drain and gate grounded. Biased currents are only observed during the 'on' half- cycle of the drive voltage, unbiased currents flow in the 'off' half- cycle, as well.
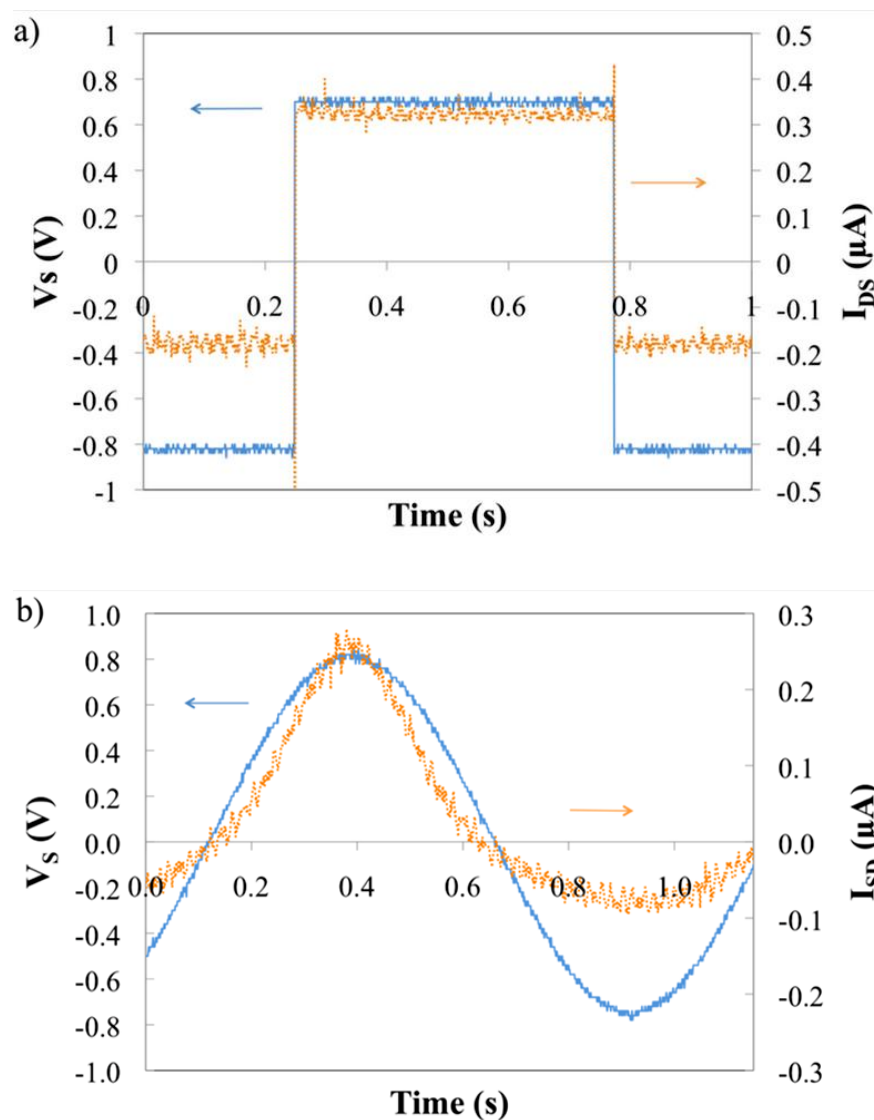
Figure 61. AC characterisation of a P3HT transistor coated with four LS layers: square- wave drive (a) and sine- wave drive (b). The blue signal is the input voltage, V_S, and the orange is the drain current, I_D, derived from the output voltage, V_{OUT}. FFT filtering was applied.

Sample	I_{OECT}/I_{OFET}	I_{on}/I_{off}	V_T (V)	μC_i (CV^{-2}s^{-1}) *10^9
Uncoated P3HT	0.31±0.03	19.8±1.8	0.28±0.03	113±14
4 LS- coated P3HT (1)	0	3.33±0.3	0.16±0.02	6.35±0.8
4 LS- coated P3HT (2)	0	2.46±0.3	0.26±0.03	3.02±0.4
4 LS- coated P3HT (3)	0	4.11±0.4	0.18±0.02	2.18±0.26
2 LS- coated P3HT	0	2.5±0.25	0.14±0.01	5.74±0.7
1 LS- coated P3HT	0.13±0.012	1.6±0.15	0.1±0.01	3.82±0.5
4 LB- coated P3HT(1)	0.42±0.04	4.22±0.4	0.38±0.04	3.97±0.5
4 LB- coated P3HT(2)	0.55±0.047	3.31±0.34	0.36±0.04	10.4±0.95

Table 4. Data read and derived from AC characterisation for uncoated and coated transistors. Columns 1,2 are read from transistor currents under square- wave drive. Column 1 gives the relative contributions to 'on' current from electrochemical doping. Column 2 gives the transistor's *on/off* ratio. Columns 3,4 are read (V_T, column 3), or calculated (μC_i, column 4, using equation (3-9) from currents under sine drive.

We find that threshold is in fact reduced as a result of applying 4 LS layers to the P3HT surface, which implies that 4 calixarene LS layers are thin enough not to compromise the high capacitance of the EDL. However, as we already concluded from comparison of Figure 61a to Figure 60a, mobility in the accumulation layer is substantially reduced, about 18- fold on the assumption that C_i is not affected by the LS layers. Data are summarised in the second row of Table 4. We carried out similar studies for transistors coated with two and one LS calixarene layers, instead of four. Resulting transistor characteristics looked similar to those shown in Figure 61, and were evaluated in the same way, to give the data shown in rows 3 and 4 of Table 4. Data and conclusions for 2 LS layers are very similar to those for 4 calixarene LS layers; for 1 LS layer we find that the blockade of electrochemical doping is no longer complete, although the I_{OECT}/I_{OFET} ratio is still smaller than without LS coating.
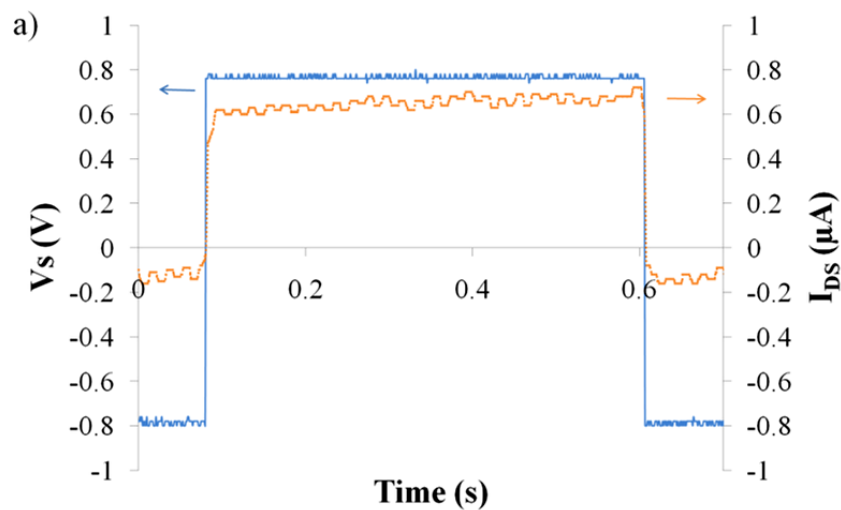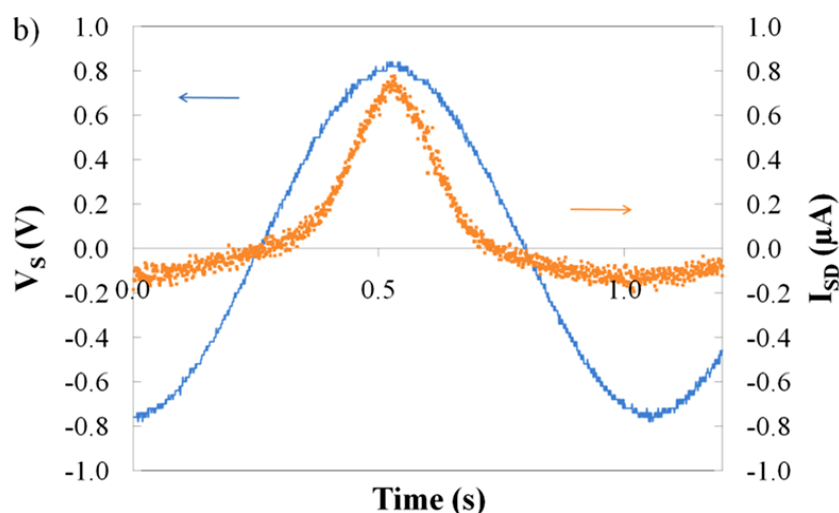
Figure 62. AC characterisation of a P3HT transistor coated with four LB layers: square-wave drive (a) and sine- wave drive (b). The blue signal is the input voltage, V_S, and the orange is the drain current, I_D, derived from the output voltage, V_{OUT}.

4.1.2.1   LB vs LS deposition

When a transistor is coated with four layers of calixarene through LB deposition, rather than LS printing, we observe a different behaviour compared to the LS samples. Electric characteristics are shown in Figure 62 and are evaluated in the same way as before to give the final row in Table 4. Again, carrier mobility is significantly reduced, and threshold now is increased compared to the uncoated sample.   Also, even 4 LB layers cannot completely block electrochemical doping. The LB- coated transistors are also harder to work with practically, as the surface is rather hydrophilic, and the gating water droplet tends to wet the surface. This is explained due to the different orientation of calixarenes in LB films, compared to LS films[88]; LB films present the hydrophilic upper rim to the surface, while LS films present the hydrophobic lower rim (Figure 29c and Figure 29f). This was confirmed by contact angle measurement. After measuring 4 times, the average contact angel for one LS deposition on the surface of P3HT gives about $\theta_{avg.}= (98.2\pm7.4)^0$, while one LB deposition gives $\theta_{avg.}= (87.9\pm6.7)^0$. Also, it seems that the total dipolar moment in case of LS is enhanced and blocks the ions; however, the total dipolar moment in LB coating is cancelled out which, in turn, allows ions to penetrate and dope the semiconductor materials.

4.1.3 Summary

This section demonstrates a technology platform that enables the development of new organic transistor sensors. It shows that an organic semiconductor can still be water- gated within the electrochemical window of water even after the Langmuir deposition of up to four calixarene layers to its surface, because such layers are thin

enough not to compromise the high capacitance of an *EDL*. Since many calixarenes are known to selectively bind waterborne cations, this allows sensitising a conventional organic semiconductor with a physically deposited layer for the specific recognition of waterborne cations. Thus the functionalities required for transistor sensors, i.e. charge carrier transport and specific recognition, can be met by combining currently known materials by physical deposition methods, without the need for synthesis of new materials with dual functionality, or chemical grafting of sensitisers onto semiconductor films. When two or more LS (rather than LB) layers are deposited, these block the electrochemical doping of the organic semiconductor, which usually competes with field effect in water- gated organic transistors. Since electrochemical doping is not specific to the chemical identity of the doping ion, such doping is parasitic with respect to ion recognition, and the observed blockade is a desirable feature, which can be achieved by as few as 2 LS layers. This conclusion was proved by Cotrone *et al*[112]. After they used biological film, so- called phospholipids films, the impedance spectroscopy results indicated that phospholipids films helped to reduce the penetration of ions in OSC TFTs. Since LS films also wet better than LB films, we therefore recommend LS printing over LB dipping as the method- of- choice for the sensitising of organic semiconductors with cation- specific calixarenes.

CHAPTER 5

5.1 Electrolyte- gated inorganic thin film transistors

The next step will address the remaining drawback of the method developed, so far. The organic semiconductor P3HT we used here is a hole transporting material, and therefore turns '*on*' under an anionic *EDL*, while most reported calixarenes selectively bind cations. Thus, it is required to replace P3HT with an electron-transporting material, which implies problems, because hydroxyl (-OH) groups are known as electron traps, and -OH groups are present both at the lower rim of the calixarene, and water. However, high electron affinity electron transporters (*LUMO* below 3.6 eV) have been reported to be not susceptible to such traps[13], and such materials are now commercially available[113]. For such devices, it is expected to have a strong impact on the measured transistor characteristics when a 'target' cation binds to a sensitiser calixarene. For example, it is expected a change of hysteresis, mobility and threshold, as bound cations will continue to sustain a carrier accumulation layer at the semiconductor surface even after the applied voltage has dropped back below threshold.

Currently, it is still difficult to immobilise suitable sensitisers for specific target analytes at the organic semiconductor/water interface, because commonly used organic semiconductors have apolar surfaces, means that organic semiconductor surfaces offer no specific binding sites for sensitisers. Polythiophenes (PTs) with carboxylic acid (-COOH) side groups have been used to bind to amine groups in DNA sequences, that perform as sensitisers[114]. However, DNA- sensitised water- gated PT-COOH *TFTs* displayed poor electric performance, and the response to target analyte is tentative. Also, water- gated organic *TFTs* often display effects of electrochemical doping in parallel to field effect drain current modulation[115], which may be difficult to separate, and no *n*- type water- gated organic *TFT* has been reported, as (-OH) groups strongly trap electrons in organic semiconductors.

In parallel to the development of water- gated organic *TFTs*, there is a current effort to develop electrolyte- gated *TFTs* with solution- processed inorganic (rather than organic) semiconductors, because these display higher carrier mobility, better environmental stability and other advantages. Fortunato *et al*[116], among others, have manufactured transistors that in their architecture and electric characteristics closely resemble typical organic *TFTs*, but used magnetron- sputtered films of un- doped (intrinsic) ZnO as electron- transporting semiconductor (ZnO: CB = -4.4 eV, VB = - 7.7 eV, bandgap 3.3 eV[61]). This approach has been advanced by Ong *et al.*[60], who prepared intrinsic ZnO in- situ on a *TFT* substrate by thermal conversion of a solution cast precursor, zinc acetate dihydrate. They reported electron mobility > 5 $cm^2V^{-1}s^{-1}$. However, the high conversion temperature (500 ^{o}C for optimum results) makes precursor- route ZnO unsuitable for flexible substrates. Recently, there has been progress in materials and preparation procedures towards lower conversion temperature by combustion process[117], heating under ultraviolet ray[118] and oxygen plasma treatment[119]. Since, the surface of ZnO as an inorganic oxide has -OH groups, this may give an advantage over the organic materials in order to immobilise sensitisers for specific analytes.

Here, it is demonstrated that ZnO films perform as high mobility *n*- type *TFTs* using precursor- route under water drops as *EDL* gate medium, establish an optimised gate electrode geometry for best results. Also, ZnO films that are produced from two different routes showed almost same results.

5.1.1 Experimental details

Onto the cleaned substrate with Au contacts, as described in sections 2.1.2 and 2.2.6.1, we spun a solution of 20 mg/ml zinc acetate ($Zn(OAc)_2$) (from Sigma Aldrich) in ethanol at 1000 rpm, and converted into ZnO on a pre- heated hotplate at 400 ^{o}C for 30 minutes under ambient atmosphere. This route is called ethanol- route.

Another used route that we called ammonium- route was done by dissolving 0.001 mole of ZnO powder with purity 99.999% (from Sigma Aldrich) into 12 ml of ammonium hydroxide that was diluted in water with purity 99.9% (from Alfa aesar). 25% of that solution, therefore, contained just ammonium hydroxide. To increase the solubility of this solution, it was refrigerated for 5 h. Then, we spun a solution at 1000 rpm by spin- coating, and the film was converted into ZnO on a pre- heated hotplate at 400 ^{o}C for 30 minutes under ambient atmosphere. This route was taken from Park *et al*[120]. The gradual- heated hotplate gave low performance with very small carrier mobility comparing to pre- heated hotplate[116].

These processes of spinning the solution over the substrates and converting into ZnO by pre- heated hotplate were repeated at least three times for a thicker ZnO film (see section 5.1.2.3). We found the electrical resistance of such films was ≈ 500 kΩ, corresponding to a sheet resistance of 100 MΩ/square, which shows ZnO prepared as described here is largely an intrinsic semiconductor, just like sputtered ZnO[116].

However, films were hydrophilic, and low water contact angle hinders the application of a droplet for gating. We have therefore treated the ZnO surface of such samples to turn them hydrophobic. This was done in either of two ways: firstly, by spin casting neat HMDS (3000 rpm for 1 min.), as this couples to -OH groups on inorganic oxide surfaces and turns them hydrophobic[121]. HMDS effectively eliminates the –OH group from the hydrophilic surface of SiO_2 and substitute them with –Si-$(CH_3)_3$ which is more hydrophobic[122].

Alternatively, we modified ZnO surfaces with one layer of stearic acid by the Langmuir- Schäfer (LS) technique. We spread 250 µl of 0.3 mg/ml stearic acid solution in chloroform on a Nima Langmuir trough filled with DI- water (15 MΩcm resistivity) as sub- phase, and compressed to 40 mN/m to form a dense layer. The resulting Langmuir isotherm, and LS technique are illustrated in Figure 63. This is similar to the work of Spijkman et al, who modified ZnO surfaces with a self-assembled octadecylphosphonic acid layer, a large molecule they chose to introduce an insulating layer[123].

For fabricating *TFT* device of PDI8-CN2, as described in section 2.2.7.2, a small amount of PDI8-CN2 (sourced from Polyera Corporation, well- known as ActivInk N1100), say 6 mg, was placed in a quartz boat and heated up to vapor phase of used material until 50 nm thickness is achieved. The evaporated film was deposited at substrates containing Au contacts. One of such substrates was surface- treated with spin- casting neat HMDS (3000 rpm for 1 min.), and another substrate had not such treatment for comparison.

For water gating, we dispensed a drop of about 2 µl DI- water over the channel with the help of a microliter syringe. As gate contacts, we used tungsten (W) needles, either with a straight tip, or bent into *L*- shape, with the foot of the *L* overlapping the width of the channel. To apply water as the gate medium, we either dispensed a drop of about 2 µl DI- water over the channel from a microliter syringe, or threaded the gate needle through a water reservoir in the shape of an upturned cone with its tip cut open, held a few millimeters above the ZnO surface, see Figure 64. In the latter case, evaporation was replenished from the reservoir, so there was no need to work in a

humid atmosphere[25]. Source and drain were also contacted with W needles, avoiding direct contact with the droplet. To record *TFT* output- and transfer characteristics, we used two Keithley 2400 source/measure units to control gate (V_G) and drain (V_D) voltage, and measure drain current (I_D).

For IL- gating, a 2 μl drop of *EMI-TFSI* (sourced from Sigma Aldrich) was placed over the channel with the help of a microliter syringe. The tungsten (W) needle was bent into *L-* shape and immersed in IL as close as possible to channel with avoiding touching of contacts or channel.
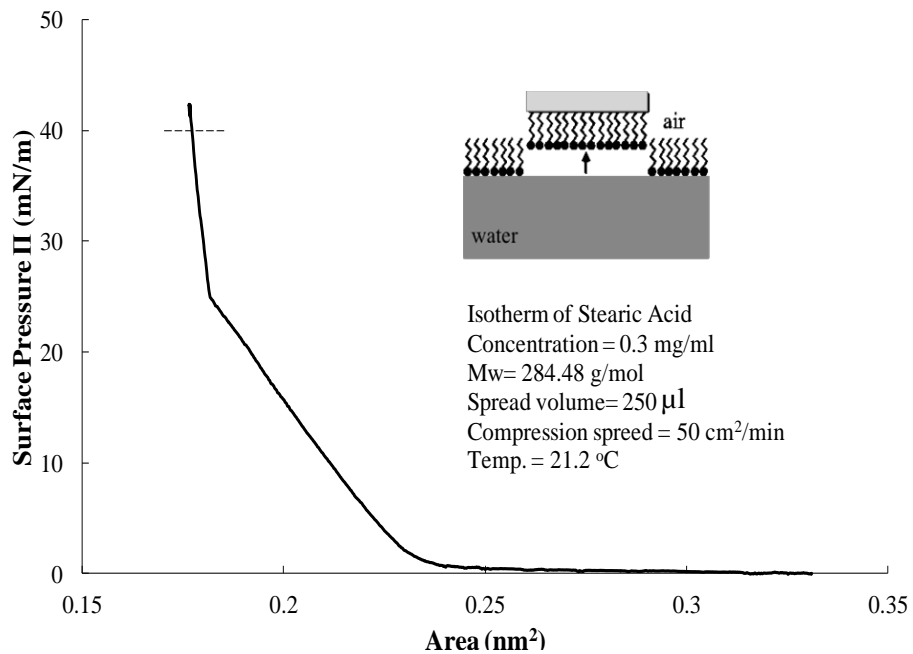
Figure 63, compression isotherm of stearic acid Langnuir monolayer, and the insert shows the LS deposition.
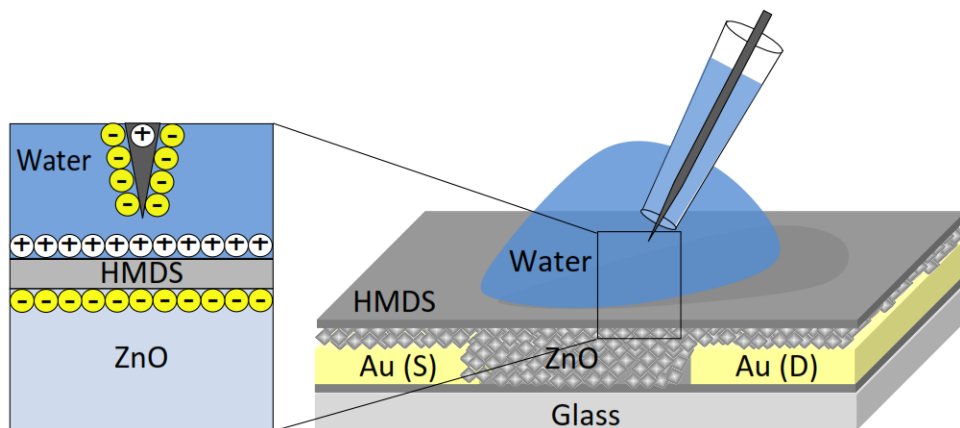
Figure 64: an illustration (not to scale) of the water- gating *TFT*, as described. Inset: applying positive bias on gate needle causes the accumulation layer of electrons at the ZnO surface. Also shown are the anionic *EDL* in the water near the gate needle, and the cationic *EDL* in the water near the ZnO surface.

5.1.2 Results and Discussion

5.1.2.1 XPS results

Figure 65 show XPS data proving the chemical state of elements constituting the ZnO surface. This data was taken by Mr. Mohammad Yusuf Mulla in The University of Bari in Italy. The sample's data was for ZnO fabricated in ethanol- route without surface coating. The resulting percentages of individual atom were taken from three different points of the surface of samples. The carbon is considered as contamination detected on the surface of film at 290 eV. The main peak is assigned as O1s and can be fitted as the superposition of two peaks centred at 529.5 and 530.8 eV. The prominent peak at 529.5 eV represents metal cation- oxygen bond (ZnO). In many published papers, the binding energy located in 530.8 eV represents the oxygen vacancy (O_{vac}) or CO bond[124].
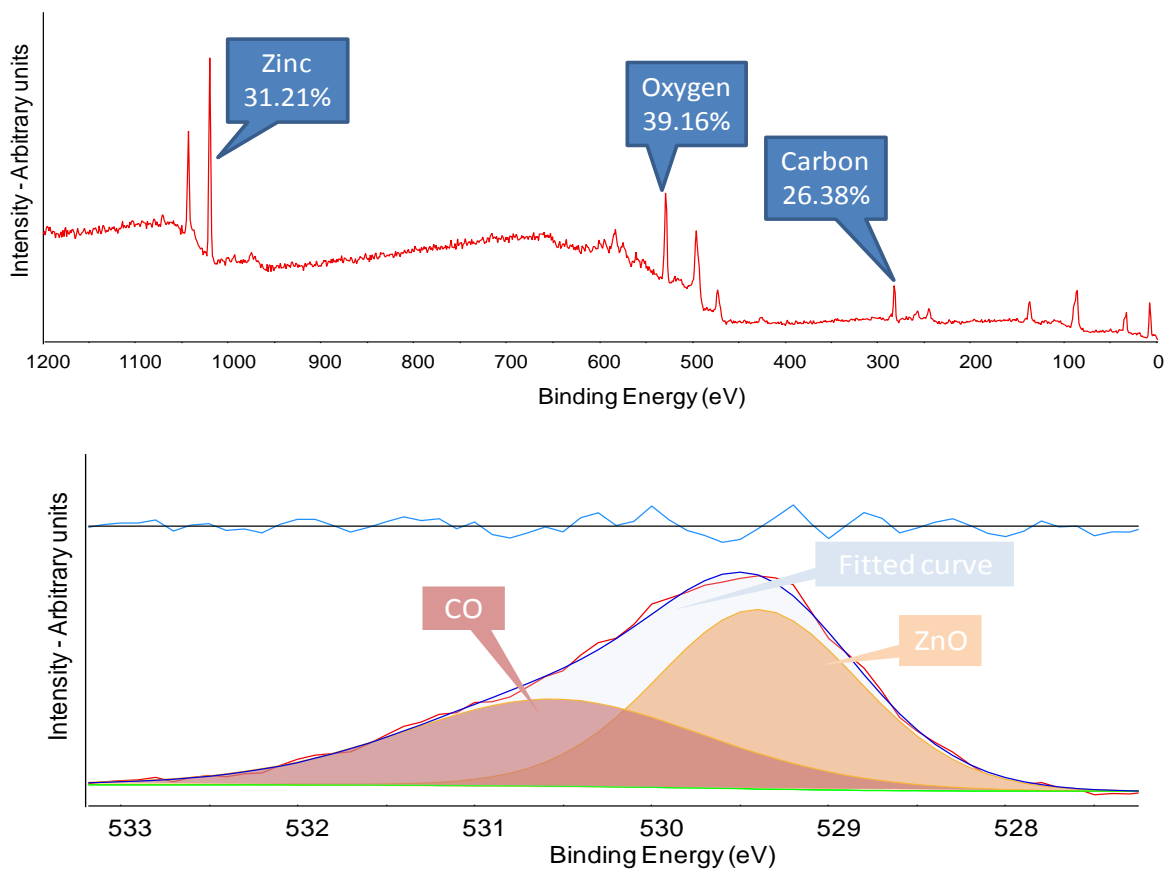
Figure 65, taken by XPS equipment with fitting that identify the binding energies of ZnO bond and the CO bond.

5.1.2.2 Contact angle study

Using the contact angle as a quantitative tool gives a clear indication of forming the coupling between -OH groups on inorganic oxide surfaces and self- assembled techniques mentioned before to turn metal oxide surfaces hydrophobic.

After fabrication of ZnO films made from ethanol- route, a small drop, about 2 μl, of DI water (15 MΩcm resistivity) was placed on the surface. The shadow of the droplet is projected to a high contrast camera, and then a computer with fitting program provides the contact angle.

Figure 66 shows different hydrophobicity (wetting) that results from different surface treatments. For as prepared- ZnO, the value of average contact angle was $\theta_{avg.}= (30.05\pm4.2)^0$. After coating with HMDS, the surface became more hydrophobic (less wetting) reaching about $\theta_{avg.}= (66.7\pm4.6)^0$. Contact angle went up again reaching about $\theta_{avg.}= (98.9\pm7.5)^0$ for 1 LS layer of stearic acid.
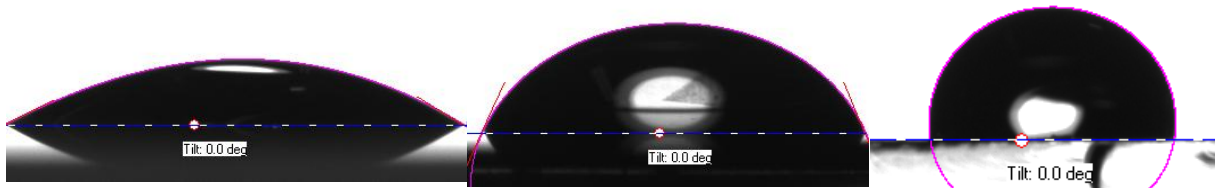
Figure 66, screenshots of ZnO surfaces, (starting from left) as prepared- ZnO, ZnO coated with HMDS and ZnO coated with 1 LS stearic acid.

5.1.2.3 Ellipsometer study

The thickness of ZnO was taken by applying Cauchy dispersion model, since it gives the best fit and small root mean square error (RMSE). While, each layer is characterized by complex refractive index $(N = n_i + jk_i)$, the model used for analysis is written as following[103],

$$(5\text{-}1) \qquad n(\lambda) = A + \frac{B}{\lambda^2} + \frac{C}{\lambda^4} \qquad\qquad k(\lambda) = a \exp\left[b\left(\frac{1240}{\lambda} - E_g\right)\right]$$

where, A, B, C, a and b are fitting parameters, and E_g and λ are the energy gap and the wavelength, respectively.

The key requirement for best fitting is to build multilayer model containing, in series, SiO_2, ZnO film, roughness layer and finally HMDS layer. The resulting fit parameters are shown in Table 5.

Since, ZnO films and HMDS deposited over SiO_2 and Si, the optical constants for both silicon oxide and silicon was taken from Grundke $et.$ $al.$[125], while the refractive index of HMDS in the visible light range was set to $n(\lambda) = 1.41$, as suggested by Murray C. et al[126] with the extinction coefficient $k(\lambda)$ set to zero.

sample	A	B	C	a	b
Ethanol- route ZnO	1.982	-0.0653	0.019	0.01714	-0.002
Ammonia- route ZnO	1.995	-0.0665	0.01788	0.021	-0.002
HMDS- SiO2/Si	1.41	0	0	0	0

Table 5, the fitted parameters of Cauchy model for different samples.

As shown in Table 6, a different thickness of ZnO is formed over substrates with different routes that were used. There was no a certain value of $HMDS$ thickness, and the values in Table 6 shows the indication of the thickness of $HMDS$ over either silicon oxide or bare silicon. $HMDS$ certainly is very thin, as it should be. It is expected that the measurement using Ellipsometry becomes difficult at films that are only 1 nm or less thick.

	Sample 1	Sample 2	Sample 3
Ethanol- route ZnO	11.66±0.65 nm	12.23±0.43 nm	10.36±0.75 nm
Ammonia- route ZnO	15.30±0.62 nm	15.01±0.37 nm	16.20±0.75 nm
HMDS- SiO_2	1.17±0.1 nm	0.89±0.06 nm	1.02±0.063 nm
HMDS- Si	2.78±0.12 nm	3.02±0.24 nm	3.14±0.18 nm

Table 6, the analysed data from Ellipsometer, every sample was measured three times at different positions.

5.1.2.4   Output and transfer characteristics results

Figure 67 shows the output (a) and transfer (b) characteristics of a water- gated HMDS- ZnO film (Ethanol- route) under positive gate voltages, using an L- shaped gate needle. The foot of the L was lowered as closely as possible to the TFT channel (approximately 0.1 mm), but avoiding direct contact. Figure 67a shows typical n- type TFT behaviour: For positive V_G above threshold (V_T) (here, at and above +0.4 V), I_D first increases with increasing V_D, and then saturates at high V_D.
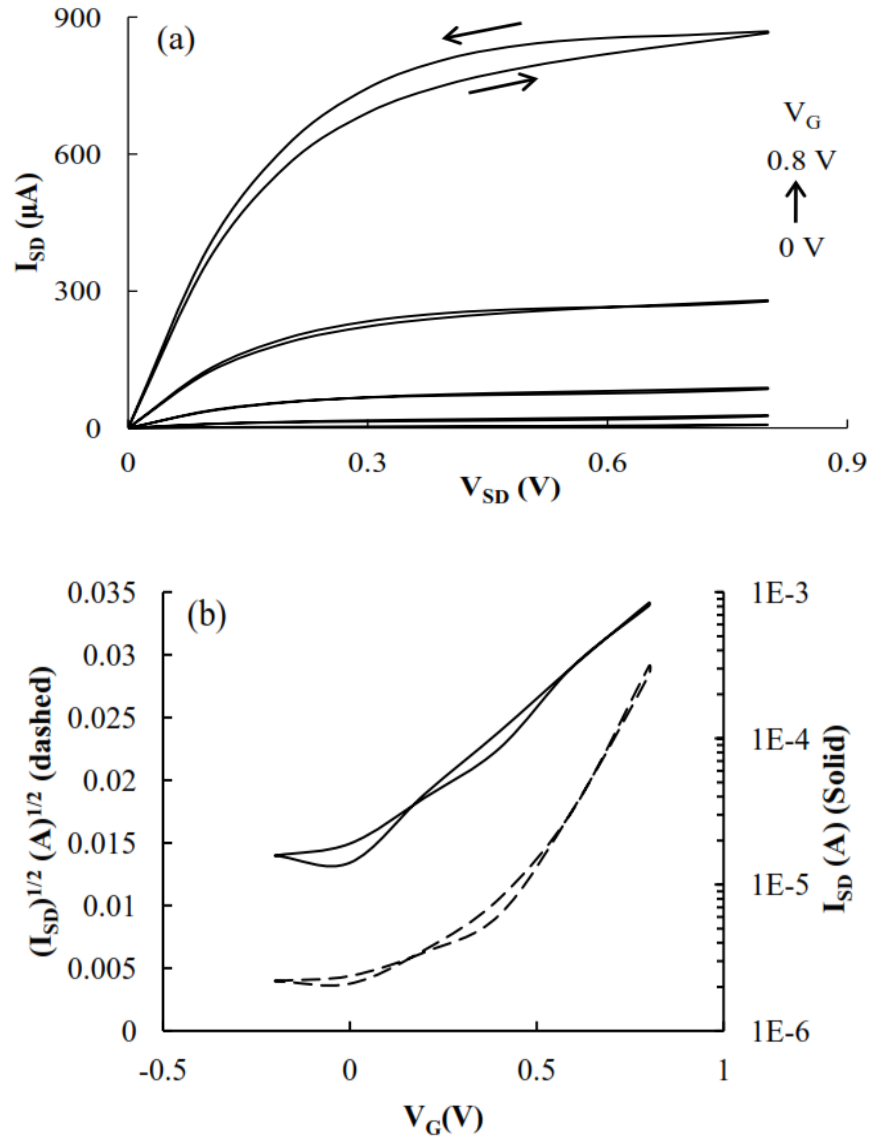
Figure 67: Ouptut (a)-and saturated transfer (b) characteristics of water- gated HMDS- ZnO TFTs. Gate voltage step between different output characteristics in Figure 67a was 0.2 V. In Fig. 2b, the source- drain voltage for the saturated transfer characteristics was 0.9 V. The dashed (solid) line in 2b refers to the $I_{SD}^{1/2}$ (log I_{SD}) scale, respectively.

We observe 'hard' saturation, just like for magnetron- sputtered ZnO with dielectric gates[116]. Hysteresis is small, which suggests the absence of electrochemical doping by ionic species[48]. Electron injection from the high work function gold (5.1 eV) also is no major problem, probably because the high capacitance of the *EDL* gate across a very thin ZnO film gives field- assisted injection. For high gate voltage, saturated I_D ($I_{D,sat}$) reaches almost 1 mA, considerably more than commonly observed for water- gated organic TFTs of similar geometry[25,114-115]. For a quantitative analysis, we evaluated the saturated transfer characteristic (Figure 67b). The *on/off* ratio read from the log I_{SD} *vs*. V_G saturated transfer characteristic is rather low ($<10^2$), albeit dry ZnO displayed very high sheet resistance, i.e. low doping. We believe *on/off* ratio is

somewhat compromised by a source- to- drain leakage current across the water droplet, which we intend to minimise in future by an optimised source/drain electrode geometry with low electrode/water overlap. We evaluated saturated transfer characteristics in the form $(I_{SD,sat})^{1/2}$ vs. V_G in the same way as Kergoat et al.[25]. We find a threshold of V_T = 0.36 V. Modulus of threshold is similar to those observed previously for water gated hole transporting organic TFTs with W gate contacts[25,115], but with opposite sign due to the opposite sign of carriers. To evaluate mobility, we need to assume a specific gate capacitance C_i; Kergoat et al[25] give alternative low-frequency water EDL capacitances of 20 μF/cm^2 (for Au / DI water / Au capacitor) and 3 μF/cm^2 (for Au / P3HT / DI water / Au capacitor), respectively (wherein P3HT is an organic semiconductor). They chose 3 μF/cm^2 to evaluate mobility in their (P3HT / DI water / Au gate) TFT, but it is not clear which of these values applies to our (HMDS- ZnO / DI water / W gate) TFT. Assuming either 3 or 20 μF/cm^2 for C_i, we find electron mobility μ_e = 8.8 cm^{2}V^{-1}s^{-1} or 1.32 cm^{2}V^{-1}s^{-1}. Either way, electron mobility in water- gated HMDS- ZnO is considerably higher than hole mobility in water- gated polythiophenes[25,114-115], but similar to the 5.25 cm^{2}V^{-1}s^{-1} that Ong et al. report for a 'dry' gated precursor- route ZnO TFT[60]. We conclude that electron mobility in ZnO is not compromised by water gating. When comparing TFTs made from different batches of ZnO films prepared in nominally the same way, we find some variation in $I_{SD,sat}$ (up to 50%); however, for a given ZnO film, $I_{SD,sat}$ is rather stable over time: When gating with a droplet, we observe drain current slowly drops by about 15% over 10 min., but this is due to the evaporation of the gate droplet, and $I_{SD,sat}$ fully recovers when water is replenished. When a gate water droplet is allowed to dry up completely, and then is replaced with a new droplet, we find $I_{SD,sat}$ within 5% of the prior value.

5.1.2.5 The diverse performance for different protection layers and the distance between gate and channel

For comparison, we have also gated HMDS- ZnO and stearic acid- ZnO films using the tip of a straight W gate needle, rather than the L- shaped needle. The tip was again positioned as closely as possible to the channel. Resulting output characteristics are shown in Figure 68a (HMDS) and Figure 68b (stearic acid). Compared to Figure 67a, Figure 68a shows an output characteristic with reduced source- drain current, and stronger hysteresis. We believe these differences result from the dynamics of EDLs in different gating geometries. The original rationale for using electrolytes rather than dielectrics for gating was that the EDL is extremely thin (therefore, its capacitance is very high), independent of the geometric separation between gate electrode and TFT

channel[127]. Unlike for dielectric gates, there is therefore no need to work with ultrathin films to achieve high capacitance. However, note that here, electrode/channel distance was in the order 0.1 mm, considerably larger than a solid electrolyte film (100 nm)[127], which is again much thicker than the thinnest dielectric gates (< 10 nm e.g. for *SAM* dielectrics[128] or anodised valve metals[129]).

At the 1 mm distance scale, *EDL* capacitance may be dominated by slow dynamics: From the study of ionomers, it is known that the time constant for build- up of 'electrode potential' (that is an *EDL*) scales linearly with electrode distances in the order (0.1 and 1) mm[130]. The distance between the tip and the edges of the channel is larger than 1 mm even when the tip itself is very close to the centre of the channel, while this is not the case for the *L*- shaped gate electrode. Kergoat *et al*[25] observed that water *EDL* capacitance is strongly frequency dependant, with capacitance increasing with decreasing frequency even below 1 Hz- a water *EDL* builds up very slowly, and does not reach its 'static' (zero frequency) value even after applying a voltage for 1 second; the 'low frequency' value of 3 $\mu F/cm^2$ Kergoat *et al* use to evaluate mobility can therefore only be an estimate. Unfortunately, capacitor thickness is not reported by Kergoat *et al.,* but is likely to be less than 1 mm. We believe that here, *EDL* build- up may be incomplete even on the time scale of a source/measure unit voltage sweep when only the tip of a gate needle is used to contact the water droplet, thus leading to reduced $I_{D,sat}$.
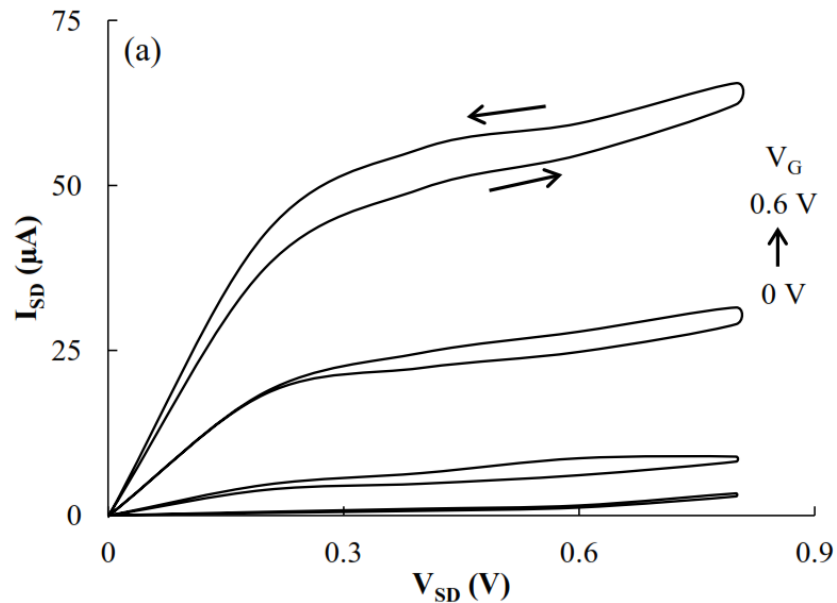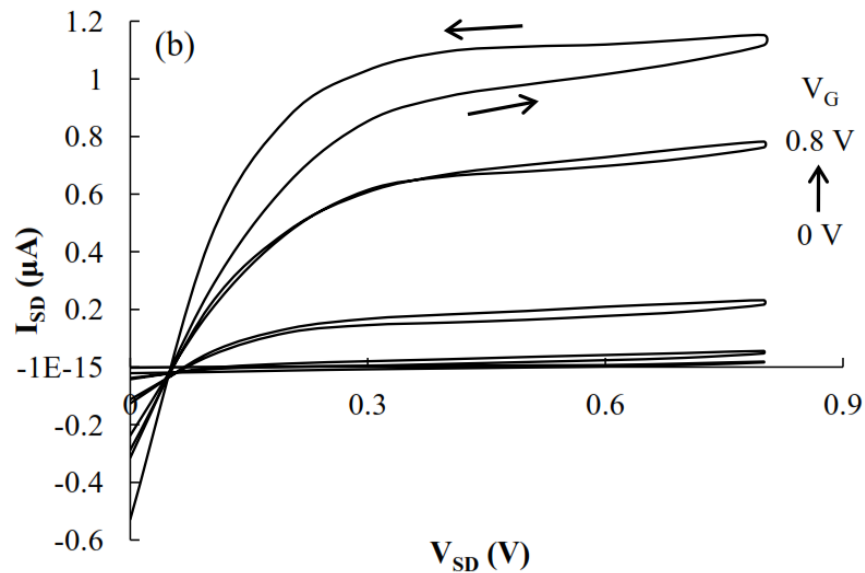
Figure 68: Ouptut characteristics of water- gated ZnO *TFTs*, using the tip of a straight tungsten needle. a), HMDS- ZnO. Note the smaller drain currents, lack of saturation and stronger hysteresis, compared to HMDS- ZnO gated with *L*- shaped needle (Figure 67a). b), stearic acid- ZnO. Source- drain currents are smaller still, and there is visible source- to- gate leakage.

Figure 68b shows the output characteristics for a stearic- acid modified ZnO film gated by a water droplet. Compared to Figure 67a, and even Figure 68a, these characteristics show much reduced I_{SD}, and stronger hysteresis. Also, we observe apparently negative I_{SD} at low V_D and high V_G, which indicates source- to- gate leakage across the water droplet. Similar leakage currents would be invisible in Figure 67a, due to the much larger current scale. We conclude the large stearic acid molecule at the water/ZnO interface introduces a serial capacitance smaller than *EDL* capacitance, and thus significantly reduces overall capacitance, similar to the observations of Spijkman *et al*[128]. The gating then is via a conventional dielectric film contacted by an electrolyte, like in an electrolytic capacitor, rather than via the *EDL* itself. This was not the case on surfaces modified with the much smaller HMDS.

5.1.2.6 Ionic liquid- gated HMDS- ZnO

As mentioned in section 1.5.3.2, ionic liquids (*ILs*) are the electrolyte gate media best suited for low threshold and fast- switching *FET*. *ILs* typically display near- zero volatility, and good thermal, chemical, and electrochemical stability, which makes them suitable for applications, gas sensors and ion selective sensors, for example[131]. Also, its biocompatibility with proteins and enzymes attracts interests towards using *ILs* in biosensors devices[131]. We have therefore applied an IL as gate medium to the same HMDS- ZnO films that were studied under water gating in section 5.1.2.4.

a)

Legend:
- Isd Vs=1.6 V (A)
- Isd Vs=3.1 (A)
- Isd Vs=3.6 (A)

Time (s)

I_{SD} (A)

b)

Legend:
- Isd Vs=1.6 V (A)
- Isd Vs=2 V (A)
- Isd Vs=2.5 V (A)

I_{SD} (A)

Vs (V)
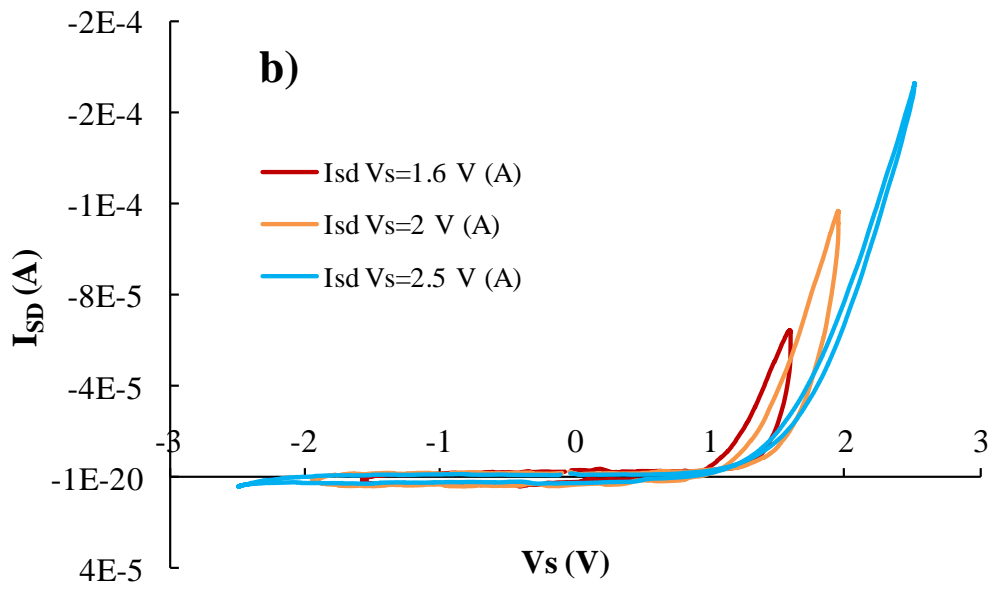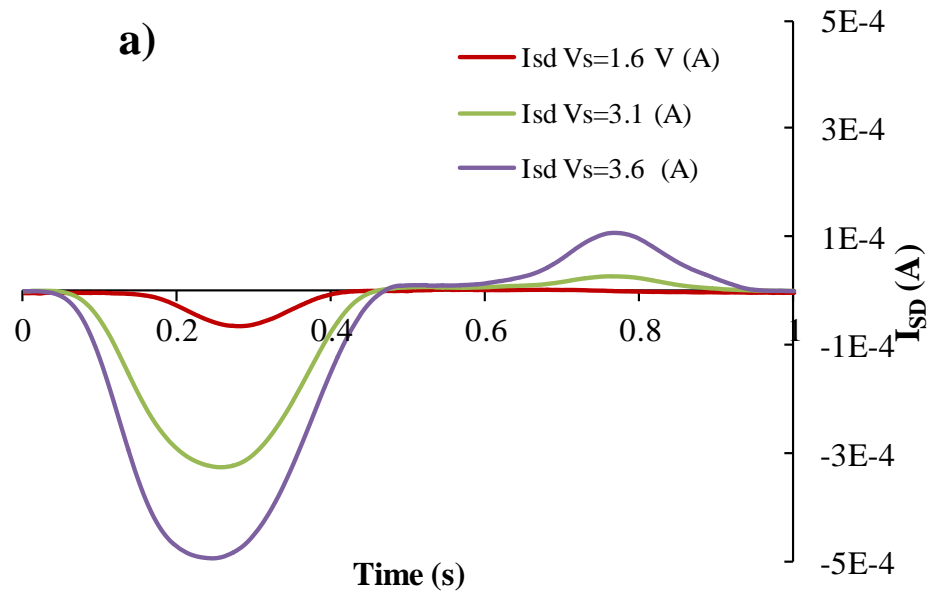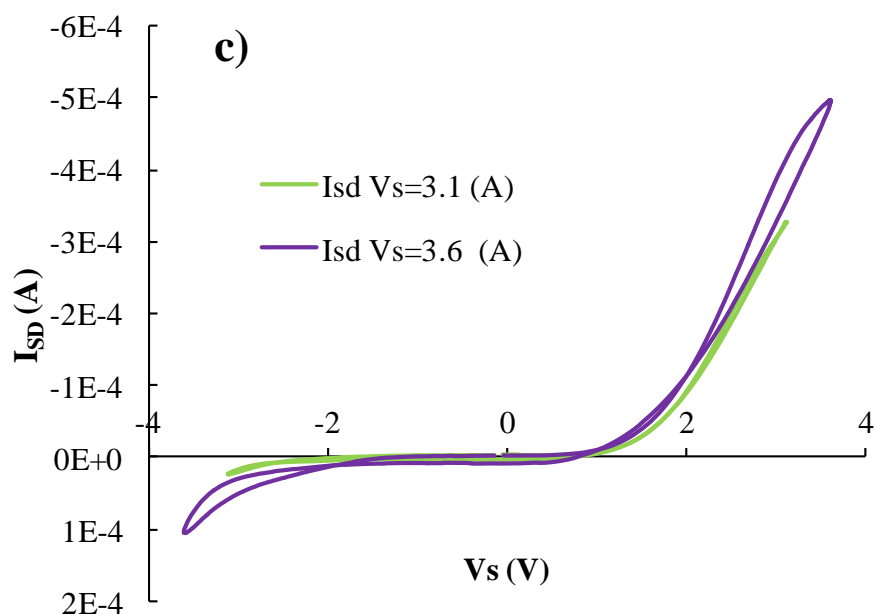
Figure 69, a measurement of I-V converter for a HMDS- ZnO *IL*- gated transistor: (a) different sinusoidal drive voltages V_S (f = 1 Hz) with amplitude ranging from 1.6 V, 3.1 V and 3.6 V and resulting saturated drain currents (I_{SD}) for each one, **b)** same saturated transfer characteristics as in Figure 69a, but shown in non- parametric form, i.e., I_D *vs. Vs*, after eliminating time for three applied voltages *Vs*=1.6, 2, 2.5 V, **c)** same saturated transfer characteristics in order to show the appearance of ambipolar behaviour for two highest applied voltages *Vs*=3.1 and 3.6 V.

Figure 69a shows the resulting saturated drain currents for ethanol- route HMDS- ZnO under sinusoidal V_S drive, when gated with *IL* at different applied voltages. For all used drive voltage amplitudes, The *IL*- gated ZnO *TFTs* turn "*on*" during the negative drive voltage half- cycle meaning that ZnO is an electron- transporting semiconductor[132]. The shape of the I_{SD} is similar to a $\sin^2$ curve, as expected using the I/V converter- based electrical characterisation scheme described in section 3.1.2. When applying a very high gate voltage amplitude (*Vs*= 3.1 V or more), Figure 69a also shows another small $\sin^2$ curve of I_{SD} in the positive drive voltage half- cycle suggesting that ZnO may also shows hole- transporting behaviour. Note that such high voltages are only accessible when gating with an IL with its exceptionally large electrochemical window. However, in principle, intrinsic inorganic semiconductors should be able to transport both holes and electrons, and ambipolar transport in "dry" ZnO *TFTs* has previously been reported[133]. Figure 69b and c shows the same saturated transfer characteristics as in Figure 69a in explicit form, after eliminating time as parameter. As seen in Figure 69c, the thresholds of electron- and hole- transporting are about V_T= 1.6 V and V_T= 2.8 V, respectively. The high threshold for holes probably comes from the mismatch of work function of Au = 5.1 eV and *ZnO* valence band about V_B = -7.7 eV, while the conduction band at C_B = -4.4 eV is practically matched

for electron injection[61] providing lower threshold. However, the ionic liquid gating can force injection even against a huge barrier between the work function of Au and *ZnO* valence band about (~ 2.6 eV).

5.1.3 Summary and conclusions

We demonstrate the first electron- transporting water- gated *TFT*, using thermally converted precursor- route *ZnO* intrinsic semiconductors with HMDS hydrophobic surface modification. Water gated HMDS- *ZnO TFTs* display low threshold and high electron mobility. So far, no *n*- type water gated organic transistors have been reported: In organic semiconductors, carrier transport is by thermally activated hopping of localised charge carriers, and localised electrons in particular are often trapped by polar trap sites[40], e.g. -OH groups. However, this does not apply to delocalised carriers in crystalline inorganic semiconductors such as *ZnO*. Also, the *ZnO* conduction band lies at 4.4 eV, well below the 'critical' *LUMO* of 3.8 eV below which -OH groups no longer trap electrons[134]. Despite the use of an electrolyte as gate medium, gate geometry is relevant for optimum performance of water- gated *TFTs*. We recommend the use of *L*- shaped electrodes that overlap the width of the *TFT* channel, and are held as close as practically possible, leaving a water gap in the order of 0.1 mm. In spite of having higher hydrophobicity in 1 LS stearic acid deposition, the HMDS- *ZnO* showed better performance in terms of the saturated I_D ($I_{D,sat}$) at high gate voltage. *IL* and its large electrochemical window help holes carrier injection to be forced against a large injection barrier and show ambipolar behavior of *ZnO*.

This promises applications of *ZnO TFTs* as transducers for interface- sensitised sensor devices. The high saturated drain currents in *ZnO TFTs* will make electric read-out of the transducer easier than for organic *TFT* sensors. For the application of interfacial sensitisers, the polar (hydrophilic) *ZnO* surface (prior to HMDS application) may be an advantage over organic semiconductor surfaces. Electron-transporting *TFT* transducers would be particularly suited for the detection of cationic waterborne species, as a positive gate voltage will lead to a cationic *EDL* at the water/semiconductor interface, where sensitiser is located. Precursor- route *ZnO* films thus constitute an attractive alternative to organic semiconductors in *TFT* transducers for the sensing of waterborne analytes.

CHAPTER 6

6.1 Organic solvent- gating TFT

The properties of the gate medium, in particular its specific capacitances, and interfacial polarity, are crucially important to the performance of *TFT*[60,135,136]. Traditionally, the gate medium has been a solid dielectric material. Recently, however, electrolytes have also been used as gate media. Under an applied gate voltage, mobile ions form an *EDL* at the semiconductor/gate-medium interface; the *EDL* has a very high specific capacitance.

Here, it is shown that some organic solvents can also act as *EDL* gate media for *TFTs*. We have tested a range of solvents to determine the physicochemical properties required for a solvent to act as an *EDL* gate medium.

6.2 Experimental details

Preparing samples: semiconductor films were prepared for electrolyte gating onto Au electrode pairs with W = 2 mm, separated by a channel with L = 20 μm; W/L = 100. Gold contacts were prepared by photolithography onto insulating SiO_2 substrates after depositing 5 nm of Cr, as an adhesion promoter. The contact geometry limits the overlap area between Au contacts and the applied solvent droplet to 0.4 mm^2, while still allowing convenient contact at distant contact pads, as described in section 1.5.4.1.

Preparing Semiconductors used for solvent-gating: as hole- transporting semiconductors, we used regioregular poly(3-hexyl)thiophene (P3HT), which has been widely used in organic *TFTs*[26,135], and poly(2,5-bis(3-tetradecylthiophen-2-yl)thieno [3,2-b]thiophene) (PBTTT); both were sourced from Ossila Itd[137]. As an electron transporting semiconductor, we used inorganic ZnO. P3HT films were prepared by spin casting at 2000 rpm from a 10 mg/ml solution in chlorobenzene,

while the PBTTT films were prepared by spin-casting a 7 mg/ml solution in 1,2-dichlorobenzene at 4000 rpm. ZnO films were prepared by thermal conversion of solution- cast zinc acetate dihydrate films, using the procedure described before[138]. ZnO films were then treated with a self- assembled hydrophobic HMDS monolayer.

Preparing Bottom- gated PBTTT transistor, we evaporated 100 nm thick Al contact by evaporation over insulating SiO_2 substrates after standard cleaning process. The Al contacts were anodised as mentioned in section 2.2.5. To self-assemble OTS over Al_2O_3, the substrates went through the process mentioned in section 2.2.4. After that the Al_2O_3 coated by OTS devices were spin- coated with a 7 mg/ml solution of PBTTT in 1,2-dichlorobenzene at 4000 rpm. The final devices were annealed under dynamic vacuum at 110 $^{\circ}$C for 1 hour.

Potential gate media used for gating: we tested the following solvents: deionised water (H_2O), methanol (H_3C-OH), isopropanol (IPA, H_3C-CHOH-CH_3), acetone (H_3C-CO-CH_3), acetonitrile (H_3C-C≡N), chloroform ($HCCl_3$), toluene (H_5C_6-CH_3), and cyclohexane (C_6H_{12}). The solvent categorise into polar aprotic, polar protic and non- polar depending on the dielectric constant values of solvent. All organic solvents were purchased from Aldrich in HPLC grade, most of the solvents contained only minute traces of water, as mentioned in Table 7. Only acetone contained up to 2% water. The solvents may also have contained trace amounts of dissolved salts, but these were not quantified. The selected solvents span a wide range of molecular dipole moments and autoprotolysis constants (Table 8). The ZnO sample was tested using all the solvents listed above, but P3HT and PBTTT are soluble in chloroform and toluene, so these were not used. Solvents were soaked into a tissue placed over the channel in order to keep the interface area fixed.

For the electrical measurements: two Tungsten (W) needles were dropped onto the substrate's contact pads using Karl Süss probeheads, so these could act as *TFT* source (S) and drain (D). As the gate contact, a third W needle was bent into an *L*-shape and dropped onto the soaked tissue, with the foot of the *L* overlapping the channel, as described before[138].

Name	Boiling Point (°C)	Traces of water (%)	Dielectric constant	Categories of solvent
Water	100	100	80	Polar protic
Chloroform	61.2	0.011	4.81	Non- polar
Methanol	64.6	0.03	33	Polar protic
Isopropanol	82.5	0.0043	18	Polar protic
Acetone	56	2	21	Polar aprotic
Acetonitrile	81.65	0.001	37.5	Polar aprotic
toluene	110	0.0039	2.38	Non- polar
cyclohexane	80.73	0.0017	2.02	Non- polar

Table 7, the list of solvent used for solvent- gated transistors including the percentage traces of water taken from solvent bottles of Sigma Aldrich and dielectric constant taken from CRC[139].

6.3   Results and Discussion
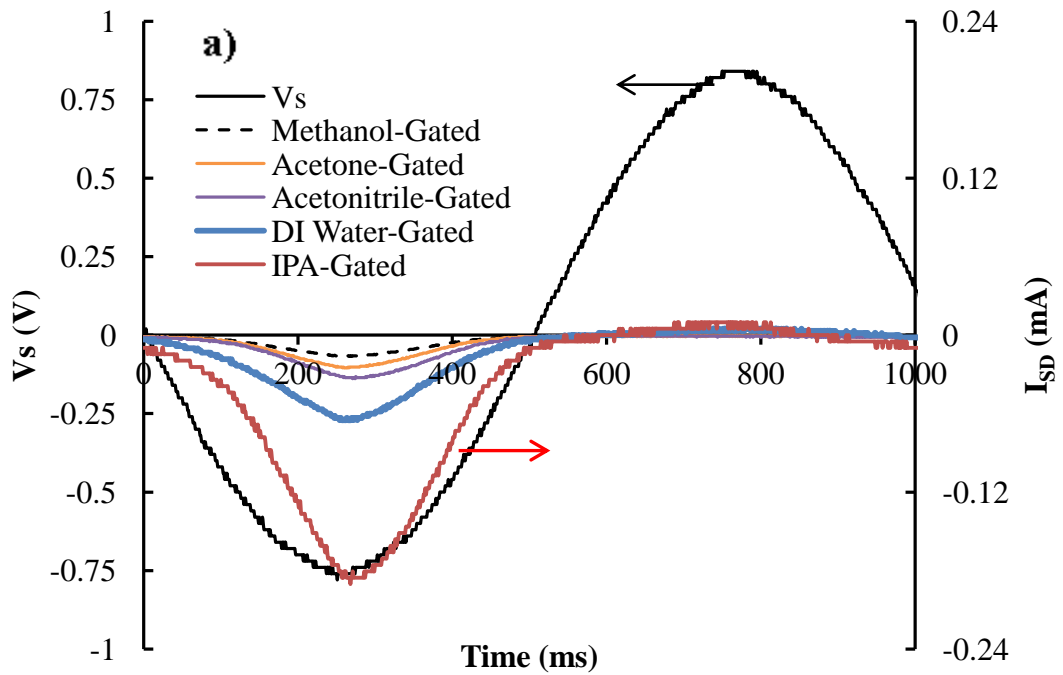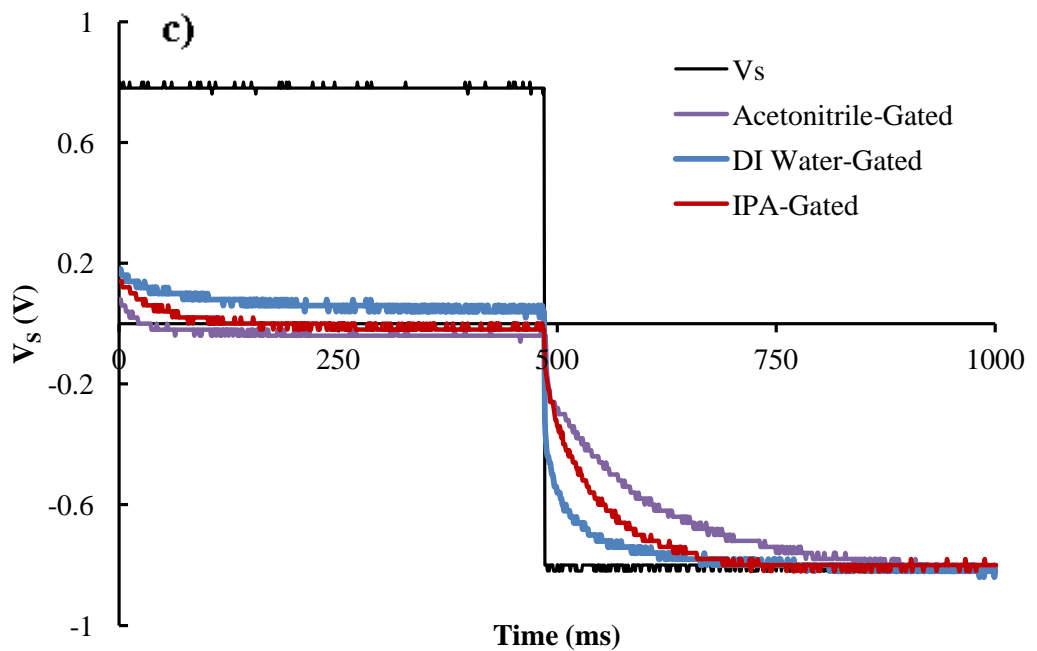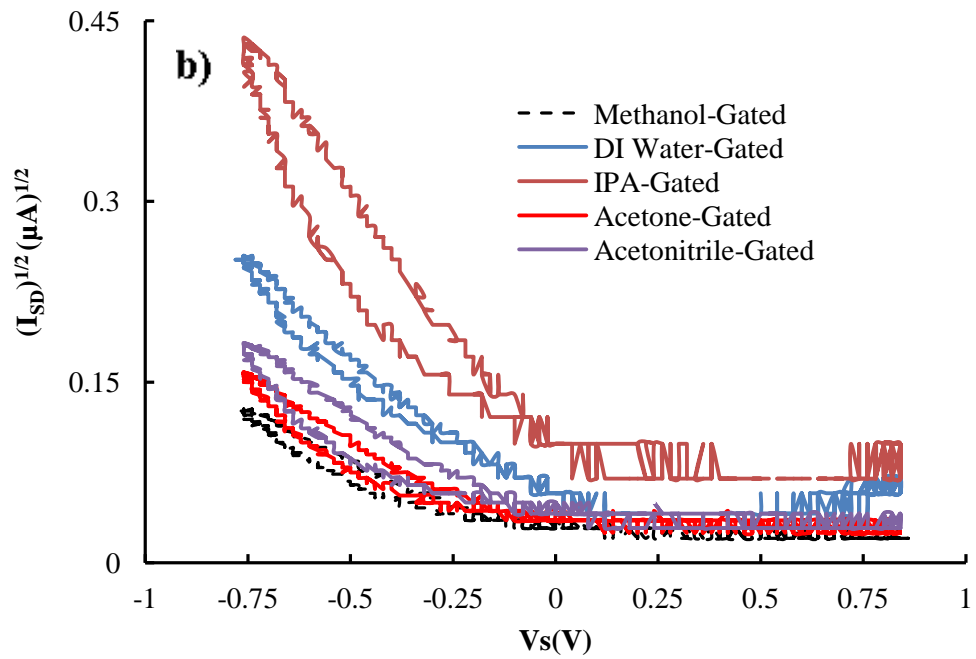
Figure 70, **a)** Sinusoidal drive voltage V_S (amplitude 0.8 V, $f = 1$ Hz), and resulting saturated drain current (I_{SD}), for ZnO TFTs gated with water, and several organic solvents. I_{SD} under water- gating is downscaled 10-fold to fit on the same scale. **b)** Same saturated transfer characteristics as in Figure 70a, but shown in the conventional form, i.e., $(I_D)^{1/2}$ *vs. V*, after eliminating time. **c)** ZnO TFTs gated with water, IPA, and acetonitrile, under a step- like voltage drive. For easy comparison of rise times, the resulting I_{SD} values are normalised to reach unity in a long- time- limit for all solvents.

Figure 70a shows the resulting saturated drain currents for ZnO films under sinusoidal V_S drive, when gated with water and various organic solvents. The water-gated ZnO *TFTs* turn "*on*" during the negative drive voltage half- cycle, which is equivalent to apply a positive gate voltage, suggesting that ZnO is an electron-transporting semiconductor[132]. The shape of the I_{SD} curve under the sinusoidal V_S drive is similar to a $\sin^2$ curve. Figure 70b shows the same saturated transfer characteristics in the conventional presentation, $(I_{SD})^{1/2}$ *vs. V*, after eliminating time from Figure 70a, as discussed[99]. The characteristics are as expected for saturated transfers (a flat line at a low current below the threshold and an approximately linear increase in $(I_{SD})^{1/2}$ with increasing gate voltage at high voltages; the observed hysteresis will be discussed below). However, since *TFTs* can be evaluated directly from their parametric form, only this form will be shown in subsequent figures. ZnO favours electron- transport over hole transport, which is in agreement with some earlier observations[60,138]. Indeed, when gated with water, a small drain current is also observed during the positive drive voltage half- cycle (this is more clearly visible prior to downscaling). This is a characteristic of hole- transport[99]. Here, we believe that weaker hole current in ZnO is the result of poor injection rather than a lack of hole mobility.

Figure 70a also shows electron drain currents when ZnO is gated with some organic solvents, however, the maximum saturated drain current is smaller than that for water- gating (the order is water > IPA > acetonitrile > methanol > acetone). For IPA, a small hole drain current can also be seen; for the other organic solvents, this is either absent, or too small to be resolved. In contrast, when gating was attempted with chloroform, toluene, or cyclohexane, no drain current was observed. The corresponding flat lines are omitted from Figure 70a.

Figure 70a also shows that the I_D peak lags slightly behind the V_S peak; we also observe some hysteresis in Figure 70b. This is consistent with a slow build- up of the *EDL*, which can alternatively be interpreted as frequency- dependent capacitance, even at $f = 1$ Hz. A slow *EDL* build- up in water is well documented[25,130] and has been described theoretically[140]. To investigate the time lag in more detail, we applied a step voltage drive, rather than a sinusoidal drive, as shown in Figure 70c (note that the drain currents in Figure 70c are normalised to reach unity in the long- time- limit). The drain currents rise to their final values approximately exponential, with time constants in the order water < IPA < acetonitrile, i.e., a gate medium that leads to a higher maximum current also gives a faster approach.
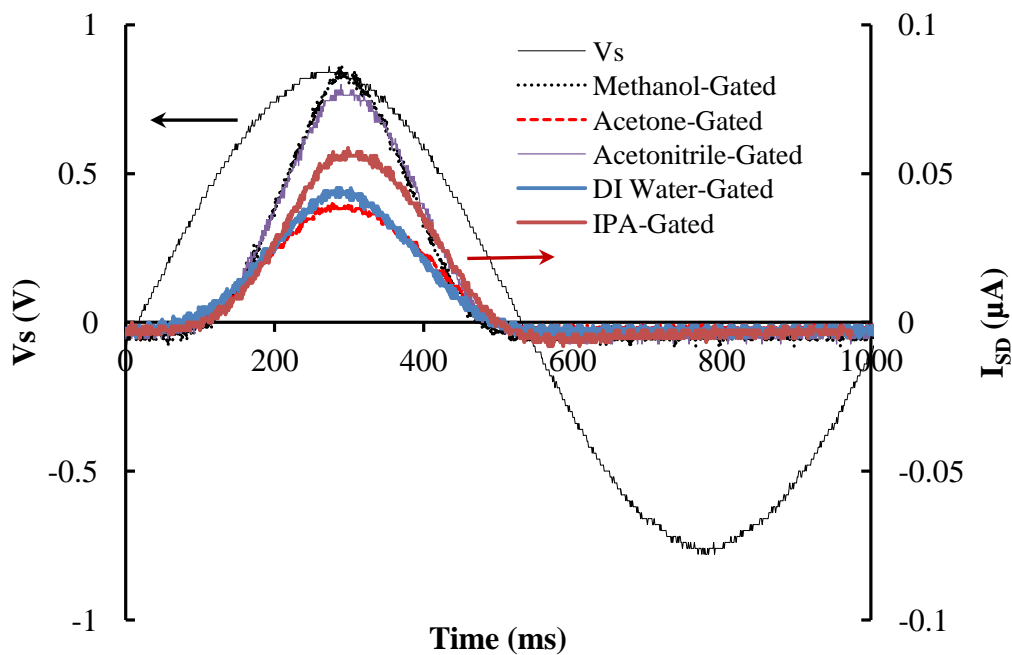
Figure 71, Sinusoidal drive voltage V_S (amplitude 0.8 V, f = 1 Hz), and the resulting saturated drain current (I_{SD}), for P3HT TFTs gated with several organic solvents. I_{SD} under water- gating is downscaled 10- fold to fit on the same scale.
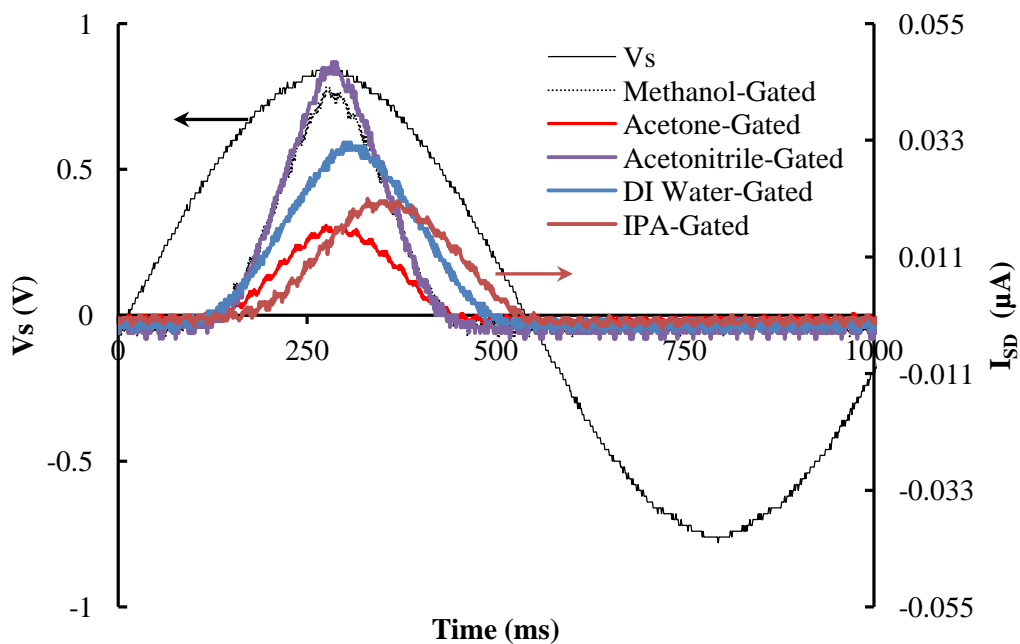
Figure 72, Sinusoidal drive voltage V_S (amplitude 0.8 V, f = 1 Hz), and resulting saturated drain current (I_{SD}), for PBTTT TFTs gated with water, and several organic solvents. I_{SD} under water- gating is downscaled 10-fold to fit on the same scale.

Figure 71 and Figure 72 show the sinusoidal drive voltage, V_S, and the resulting saturated drain currents, for TFTs using the semiconducting polymers P3HT (Figure

71) and PBTTT (Figure 72), gated with water, and other solvents. Chloroform and toluene had to be excluded because the semiconducting polymer film would dissolve in these.

These TFTs are turned "on" during the positive V_S half- cycles only, which agrees with the well- known hole- transporting properties of polythiophenes. Again, we observe a field effect not only when using water as the gate medium, but also for acetonitrile, IPA, methanol, and acetone. However, cyclohexane again fails to act as an EDL gate medium. Water again gives the highest drain currents, but the other solvents are now rank somewhat differently: acetonitrile ~ methanol > IPA > acetone. All else being equal, the hole currents in polythiophenes are lower than the electron currents in ZnO, this is explained by the higher electron mobility in ZnO[60].

	Water	Meth-anol	IPA	Acet-one	Aceto-nitrile	Chloro-form	Tolu-ene	Cyclo-hexane
pK$_a$	14	16.6	20.7	>32.5	∞	∞	∞	∞
Dipole[D]	1.85	1.7	1.66	2.88	3.92	1.04	0.36	0
H$_2$O sol. [g/L]	-	misc.	misc.	misc.	misc.	8	0.47	- 0
ZnO	Y- (Y+)	Y-	Y- (Y+)	Y-	Y-	N	N	N
V_T(V) (±0.02)	-0.1	-0.11	-0.1	-0.14	-0.15	X	X	X
P3HT	Y+	Y+	Y+	Y+	Y+	X	X	N
V_T(V) (±0.08)	0.38	0.48	0.4	0.35	0.44	X	X	X
PBTTT	Y+	Y+	Y+	Y+	Y+	X	X	N
V_T(V) (±0.05)	0.44	0.56	0.43	0.55	0.59	X	X	X
I$_{max}$ [%]	100	13.2	6.6	5.1	14.3	X	X	0

Table 8, Summary of physicochemical properties of the solvents used, and results of attempts to gate different semiconductors with different solvents. pKa = -log Ka quantifies the tendency to undergo autoprotolysis, where Ka is the chemical equilibrium constant for the autoprotolysis reaction; data are for 25 °C (Rondinini et. al.[141]). Solvents that cannot undergo autoprotolysis formally have an infinite pKa. Molecular dipole moments (in Debye) from Riddick et. al.[142]. Solubility in water in grams of solvent per litre of water; misc. indicates miscibility in any ratio. Y- / Y+: electron/hole field- effect current was observed under applied gate voltage. (Y+): small hole current. N: no field effect current observed. X: impossible to determine because of solubility or lack of transistor action. V_T is the *TFT* threshold voltage, evaluated directly from the parametric form of the saturated transfer characteristics. To account for hysteresis, V_T has been averaged between the values at rising and falling flanks.

Qualitative and quantitative results of all the experiments shown in Figure 70a, Figure 71, and Figure 72 are summarised in Table 8, together with key physicochemical properties of the solvents used. Table 8 and Figure 73 show that some (but not all) organic solvents can act as *EDL* gate media for *TFTs* in a similar way as water, solid electrolytes, and ionic liquids. The ability to act as gate medium (or not) is a property of the solvent, not of the semiconductor used in the *TFT*. If a solvent can act as a gate medium, it will gate both *n-* type and *p-* type semiconductors; if it cannot, it will gate neither. We found that only organic solvents that are fully miscible with water can act as TFT gate media. A related indicator is the solvent's dipole moment: solvents with no dipole moment or a small dipole moment (cyclohexane, toluene, and chloroform) cannot act as gate media, and also not fully miscible with water. However, a solvent does not need to undergo autoprotolysis (e.g. $2CH_3OH \rightarrow CH_3OH_2^+ + CH_3O^-$, for methanol) to act as a gate medium: Even the completely 'aprotic' acetonitrile gives working *TFTs*. Also, the ability to form carbonic acid from atmospheric carbon dioxide ($2H_2O + CO_2 \rightarrow H_2O + H_2CO_3 \rightarrow HCO_3^- + H_3O^+$) is not essential, as this is confined to water.
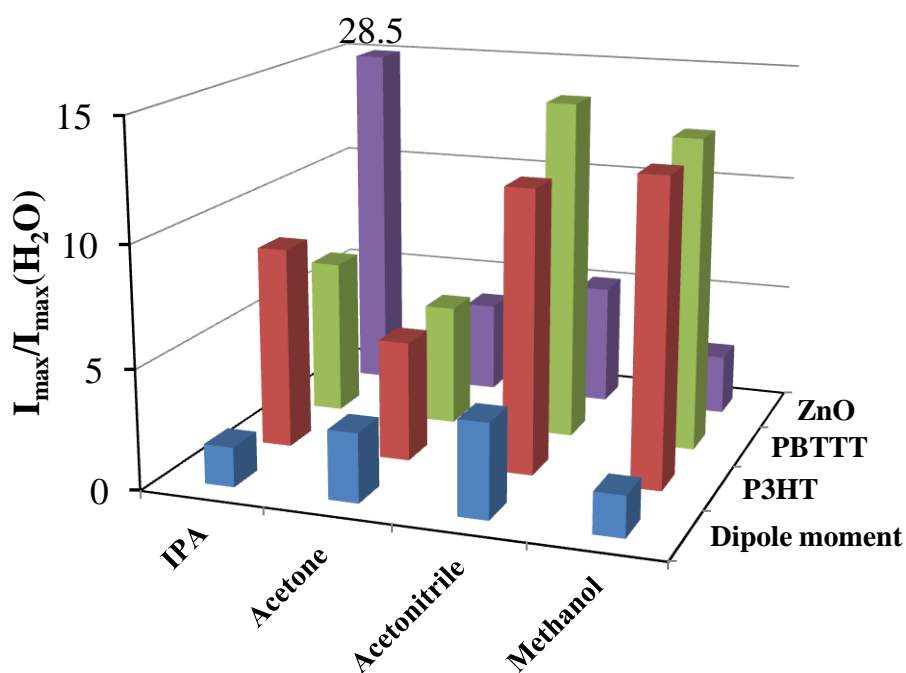
Figure 73, I_{max} gives the maximum saturated drain current during the "*on*" half- cycle of V_S as a percentage of the same semiconductor's maximum saturated drain current under water-gating.

We believe that the unintended, but inevitable, contamination of polar solvents with traces of dissolved salts supplies the ionic species required for the formation of an EDL. These contaminations will be present in solvents that are miscible with water,

but absent from less polar solvents such as chloroform, toluene, or cyclohexane. Alternatively, even in HPLC- grade solvents, minor traces of water may be present in all solvents (see the experimental section 6.2), or may be rapidly absorbed from atmospheric humidity during testing, particularly in case of water- miscible solvents. However, we consider this to be less likely, as water itself is not an ionic species, and would require dissolved ions to act as a gate medium. The contribution from autoprotolysis would be extremely low when water is present only in trace amounts. Also, the supplier quotes acetone as being the solvent with by far the highest contamination by water, but acetone gating does not give the highest drain currents.

In all cases, water gave the highest maximum current, with most drain currents under gating with other solvents being around 10% of those observed under water gating. Unlike Helmholtz's basic EDL theory[143], more complex EDL theories predict that the EDL capacitance will increase with increasing ion concentration. This is supported experimentally[143], although the quantitative dependence is highly complicated. Even in deionised water, the ion concentration resulting from autoprotolysis (and possibly carbonic acid) will be higher than the unintended impurity levels in other solvents, thus leading to a higher capacitance and higher currents. There is, however, no straightforward explanation for the different saturated drain currents obtained for gating with polar organic solvents. There is no clear correlation between the maximum current and the dipole moment, and solvents are ranked in different orders for n- type and p- type semiconductors. Different levels of unintended contaminants alone cannot explain the different current levels for different solvents. Different solvents may also be a different impacts on the carrier mobility in the semiconductor. It is well known that polar gate media lead to reduced mobility in organic semiconductors[5,135], and hydroxyl groups are known to act as charge- carrier traps[144].

Table 8 shows the observed threshold voltages, V_T. These do depend on the semiconductor, but are similar for different gate media.

To support our hypothesis that *EDL* gating by polar solvents is the result of the present of unintended traces of dissolved salts as contaminations, we have conducted a final experiment, where we deliberately added a minute flake of NaCl to an acetonitrile- soaked tissue acting as the gate medium for a PBTTT film. Figure 74 shows that the observed saturated drain current increased more than four-fold over ~ 4 mins, as the NaCl flake dissolved in the acetonitrile. The deliberate addition of salt to acetonitrile led to an increased *EDL* capacitance, and therefore a higher saturated drain

current. Note that during the *"off"* half-cycle, the observed drain current remained very low, so we can exclude both the conductivity of the salt- containing acetonitrile and electrochemical doping of PBTTT as the origin of the observed drain current increase. When we added a minute droplet of water to HPLC- grade acetonitrile as the gate medium, the observed saturated drain current decreased, possibly as a result of trapping by hydroxyle groups. These observations further support our view that traces of dissolved salts, rather than contamination with water, are the origin of the gating abilities of polar solvents.
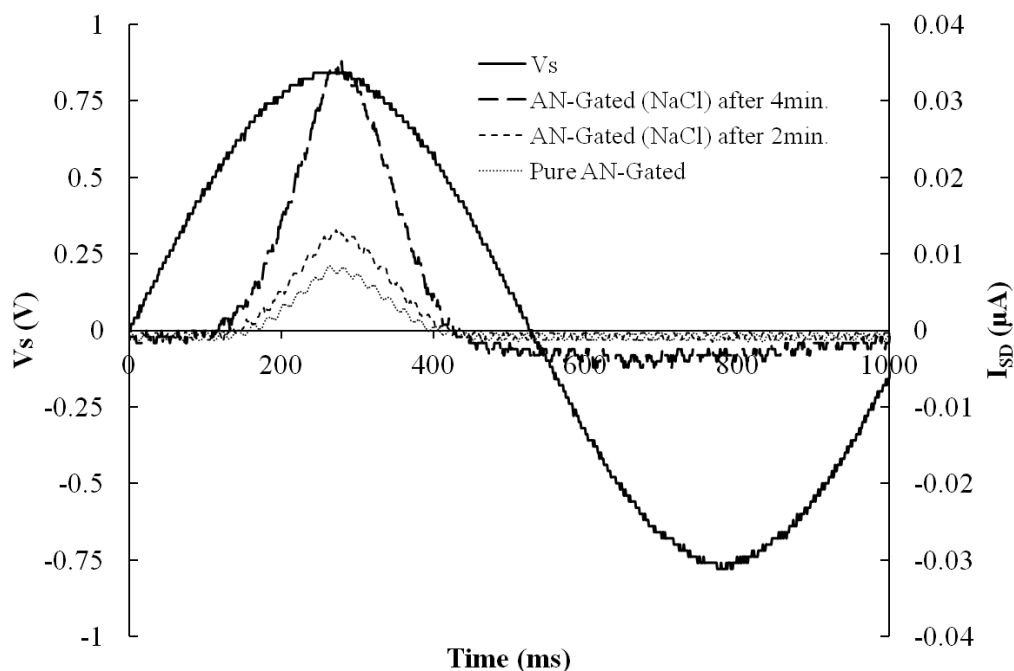
Figure 74, Sinusoidal drive voltage V_S (amplitude 0.8 V, $f = 1$ Hz), and resulting saturated drain current (I_{SD}), for PBTTT *TFTs* gated with HPLC- grade acetonitrile prior to adding a flake of NaCl, 2 mins after adding NaCl, and 4 min. after adding NaCl.

6.4 Performance between Water- gated and bottom gated transistors

Finally, we compared the electrical characteristics between water- gated PBTTT transistors and bottom- gated Al_2O_3- OTS PBTTT transistors, and a conventional PBTTT transistor with a 'dry' dielectric gate medium on the example of a bottom-gated Al_2O_3- OTS PBTTT transistor. The different architectures are illustrated in Figure 75.
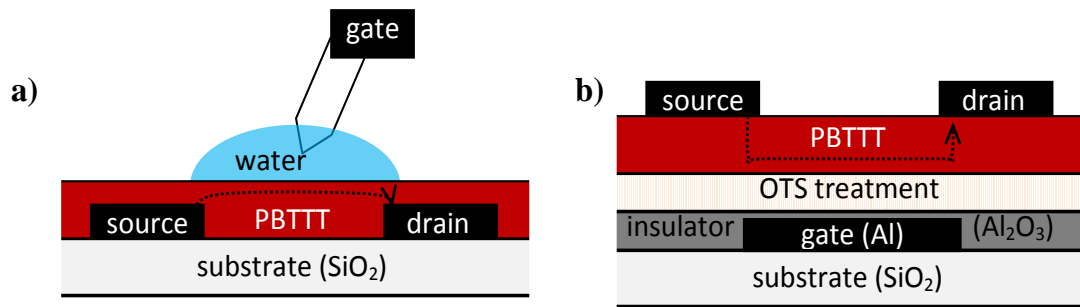
Figure 75, the graphical presentation of the overall structure for: a) water- gated PBTTT transistor and b) bottom- gated Al_2O_3- OTS PBTTT transistors.

Figure 76a) and b) show transfer characteristics for both types of PBTTT transistors. Both show the typical shape of transfer characteristics for normally "*off*" *p*- type OFETs operated with *on/off* ratio around 300. Regardless of the lower maximum applied voltage of about 0.9 V comparing to 3 V for "dry" transistors, the on- current is higher about 5.5 µA with V_T= -0.24 V, and low value of subthreshold swing about 174 mV/decade which means a faster transition from two states "on" and "off". For "dry" transistors, the transfer characteristic provides values of the on- current about 0.9 µA with V_T= -1.2 V, and The high value of subthreshold swing about 667 mV/decade. The bottom- gated transistors show lower *off*- current about 3 nA. Section 1.5.3.5 explain why an electrolyte- gated transistor in general shows higher performance that gate insulator. This is because of the concentrated high electric field is near the interfaces in electrolyte- gated transistors which, in turn, help to build up higher EDLs and cumulate more charge carriers.
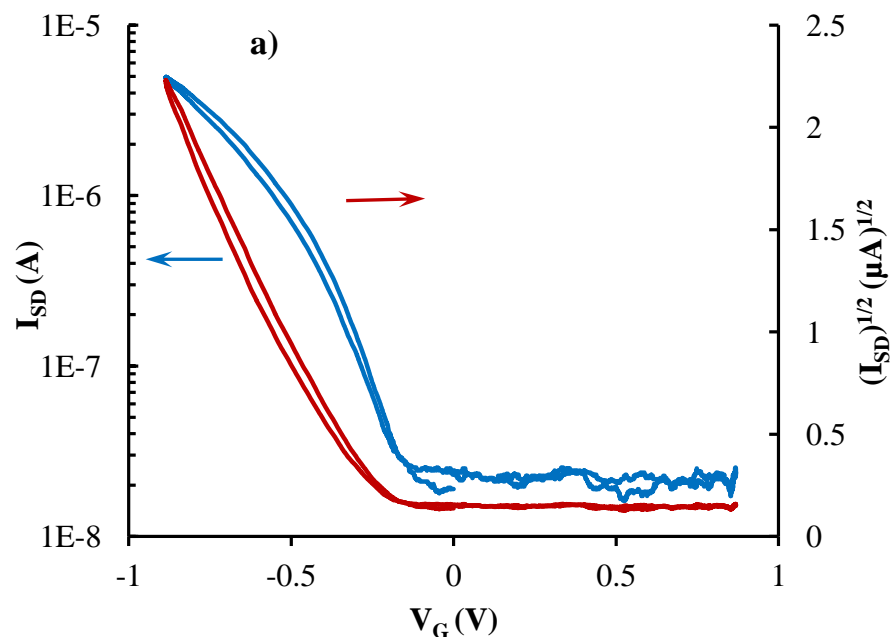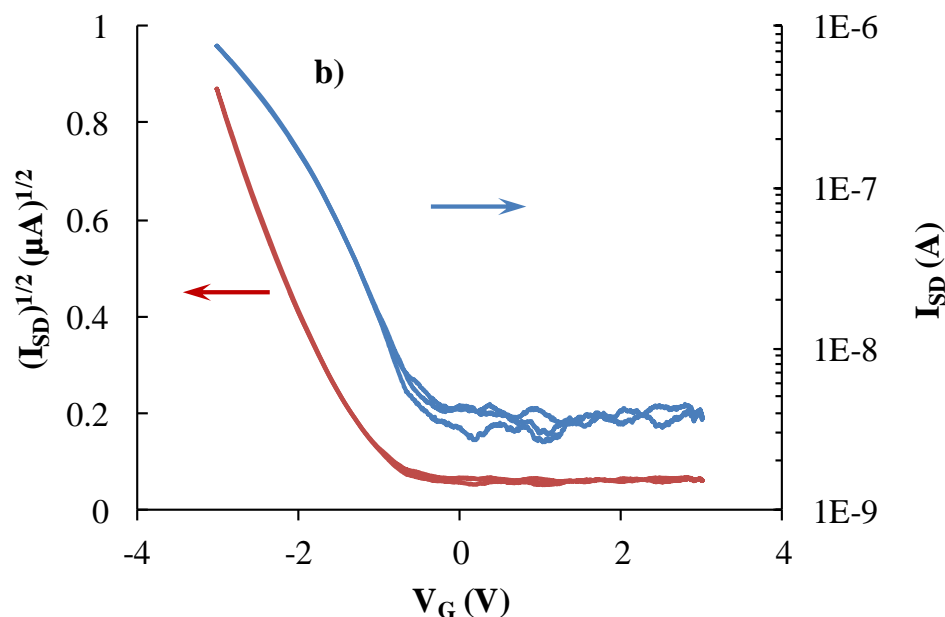
Figure 76, the saturated transfer characteristics measured by I/V converter for: a) water- gated PBTTT at R_f= 18 kΩ, f = 1 Hz and V_{SD}= 0.9 V and b) bottom gated Al_2O_3 PBTTT OTS R_f= 400 kΩ, f = 3 Hz and V_{SD}= 3 V.

6.5   Summary

It is found that organic solvents that are miscible with water (i.e., polar organic solvents) can act as EDL gate media for TFTs, in a similar way to that previously reported for solid electrolytes[127], ionic liquids[37,145], and water[25]. Solvents of low polarity, which are not miscible with water, cannot act as EDL gate media. The ability to undergo autoprotolysis or to dissolve atmospheric CO_2 is not essential for a solvent to act as a gate medium. The most likely explanation for the ability to act as an EDL gate medium is the inevitable presence of trace amounts of dissolved salts in such solvents. This is supported by the observation that the deliberate addition of salt to an organic solvent gate medium increases the observed saturated drain current, whereas the deliberate addition of water actually decreases the current.

Possible applications of our observations are in the quality control of ultra- pure organic solvents. Also, aprotic acetonitrile in particular is an attractive alternative to water as a gate medium. Acetonitrile gating avoids hydroxyl groups in the gate medium, which are known to act as charge- carrier traps[144], and offers a wider electrochemical window than water[146]. Ionic liquids are also aprotic media with large electrochemical windows[147]; however, unlike acetonitrile, they are good solvents for a wide range of organic substances, which limits their use as gate media to the most insoluble compounds[37,145].

CHAPTER 7

7.1 Electrolyte- gated nano- wire transistors

This section brings together the progress of electrolyte- gated *TFTs* of organic semiconductors with another up to date area of organic semiconductors research which is the presence of organic nano- wires (*NWs*). As discussed in section 1.6.4, *NWs* are formed as long, needle- shaped crystals that may grow when some organic semiconductors materials (namely those that crystallise with a slip- stacked crystal motif)[148] go through appropriate physicochemical treatment while in solution, for example, thermal cycles, aging or addition of non- solvent. Depending on many factors (i.e. the material itself and growth conditions), some variations on the *NW* morphology have also been reported, for instance, nano- belts with curved shapes[73], or flat- shaped as nano- fibres[149]. In order to generalize, the terms 'nano- wires' will here be used generically for all the mentioned morphologies except when discussing a particular sample. After formation of *NWs*, they may form stable suspensions in their growth medium, and can be processed into films by spin- or drop- casting, analogous to the deposition of *OSC* solutions. However, the resulting films are noticeably different in terms of morphologies from the smooth, uniform films comparing to films casted from *OSCs* solutions. Depending on *NW* density and casting conditions, films may have isolated single wires, lightly overlapping wires, or a dense multilayer *NW* 'mesh'. The literature on organic *NWs* (and related morphologies) includes many reports on *TFTs*; these have been comprehensively reviewed by Briseno *et al*[148].

The advantage of using the NW morphology is a large surface area that lead to significant sensitivity enhancement in chemi- resistor sensor devices that are utilized (PAni) Polyaniline nanofibres, compared to devices using smooth PAni films[149]. It is, therefore, tempting to employ organic NWs in electrolyte- gated *TFTs* as the active layer. However, no electrolyte- gated *NW OSC* field-effect *TFTs* have been reported previously. The work of Wanekaya *et al.*[150], despite its title, reported on an organic

electrochemical transistor (*OECT*) not a field effect transistor, and required a strongly acidic medium to operate such device. The differences between *OFETs* and *OECTs* were discussed in section 1.5.4, for more details.

Here, we show water- gated organic *NW* field- effect *TFTs* using *NWs* grown from both *p*- type, and *n*- type, *OSCs*. As *p*- type organic semiconductor, we have chosen regioregular poly(3-hexylthiophene), an *OSC* widely used for organic *TFTs*[135]. P3HT is also known for its ability to grow *NWs*[75]. As *n*- type organic semiconductor, we have selected poly(benzimidazobenzophenanthroline) (*BBL*). *BBL* can act as n- type material in organic *TFTs* with good mobility (μ_e = 0.1 $cm^2V^{-1}s^{-1}$)[71], and Briseno *et al.*[73] have reported on the growth of *BBL* 'nano- belts'. *BBL* possesses a rather deep 'lowest unoccupied molecular orbital' (*LUMO*) of – (4.0 eV)[151], which allows reasonable electron injection even from high work function metals, and may make *BBL* consistent with water- gating, despite the potential trapping of electrons by water and/or oxygen, details in section 1.2.5.

7.1.1 Experimental details

Nano- wire growth: NWs of P3HT were grown via two routes, which we will call 'CB route', and 'anisole route', respectively. For CB route, we dissolved 5 mg/ml P3HT (from Ossila) in (CB) chlorobenzene solution. The solution was initially heated to 80 °C and agitated to allow dissolution, then filtered through a 0.45 μm PTFE syringe with mounted filter. Next, at room temperature, the solution was left in the dark for several weeks or months to grow nano- wires. For Anisole route, another way of growing NWs was by using Anisole- P3HT route that were prepared via the whisker method[75]. 5 mg of rrP3HT (sourced from ADS dyes) were dissolved in 1 ml of Anisole. Then, the solution was heated to 90 °C until fully dissolved and allowed to cool to room temperature over duration of approximately 1 hr, and then left to mature for three days. This is known as the whisker method[75].

Nano- belts growth: the details of nano- belts growth was mentioned in section 2.2.7.3.

BBL thin film preparation: many groups found out methods for producing thin films of *BBL*[151]. The way used to get the thin film was by dissolving an amount of *BBL's* powder in MSA to get the range of concentration between 0.2 mg/ml to 10 mg/ml in order to prepare films of different thickness for reason that will be mentioned later. The higher concentration required heating to about (150°C) for 13.3 mg/ml to completely dissolve. Substrates were placed on spin-coater and we dispensed

about 100 µl of solution onto a spin coater rotating at 2000 rpm ('dynamic spin coating') for 60 seconds. In order to crystallize the *BBL* films, samples were gently rinsed by methanol for 30 seconds to drive out residual MSA, because it evaporates so slowly. After that, samples were immersed gently in reservoir of DI water in order to remove as much MSA as possible from samples. Unfortunately, the produced films of BBL did not adhere well to their substrates and often peeled of spontaneously in water, and most sample preparations failed. We only succeeded preparing films from solutions of 0.5 to 0.7 mg/ml *BBL* in MSA.

TFT preparation: OSC NWs and thin films were prepared onto Au electrode with W = 2 mm, separated by a L = 10 µm channel (for P3HT samples), or 20 µm channel (for BBL samples, to account for the larger size of *BBL* nano- belts, see below); W/L = 200 for P3HT; W/L = 100 for *BBL*. 100 nm thick gold contacts were prepared by photolithography onto insulating SiO_2 substrates after depositing 10 nm of Cr as adhesion layer, as seen in section 2.2.3 and 2.2.6.2. The contact geometry, sketched in Figure 77, uses 0.1 mm thin wires to connect S/D contacts to distant contact pads. This design limits overlap area between Au contacts and the water droplet applied later to ~ 0.4 mm^2, thus minimising parasitic currents across the droplet, while still allowing convenient contacting. CB P3HT *NWs* were spun at 5000 rpm onto contact substrates without prior substrate treatment. Anisole P3HT *NWs* were spun at 2000 rpm, and *BBL* nano- belts were drop- cast by repeatedly applying ≈ 2 µl droplets of nano- belt dispersion onto substrates and allowing solvent evaporation, until contacts were completely covered with nano- belts.
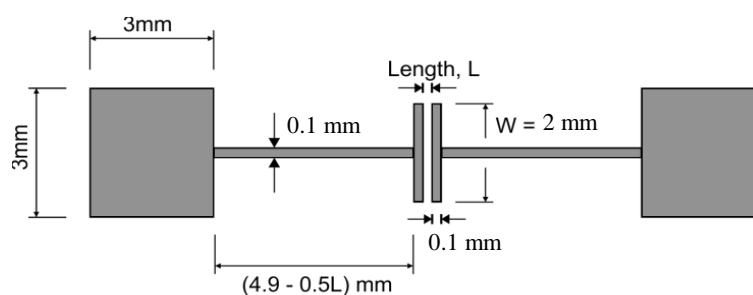
Figure 77, the contact geometry. Channels of length L = 10 or 20 µm, W = 2 mm, are linked to distant contact pads by thin (100 µm) connecting wires.

Electrolyte- gating and electrical characterisation: For electric testing, two Tungsten (W) needles were connected to the substrate's contact pads using Karl Süss probeheads, so these could act as *TFT* 'source' (S) and 'drain' (D). As gate media, we used deionised water, and acetonitrile (HPLC quality from Aldrich). For gating, a droplet of DI water or acetonitrile was applied over the channel region from a micro-

litre syringe. A third W needle was bent into *L* shape and was dropped onto the droplet with the foot of the *L* overlapping the channel, to act as 'gate' (G) contact, as suggested[138]. Transistors were driven electrically by applying a sine drive voltage $V_S(t)$ to S, connecting G to ground, and D to the virtual ground of a current/voltage (I/V) converter with a dial- in feedback resistor, R_f, as described in 3.1.2.1. Peak voltage of V_S was 0.8 V for water / 1.1 V for acetonitrile, frequency was chosen very low (1 Hz or less) to account for the slow build- up of the *EDL*[25]. The chosen setup is 'blind' to gate leakage currents. Together, $V_S(t)$ and $I_{SD}(t)$ constitute the *TFT's* saturated transfer characteristic, as described in 3.1.2. For the characterisation of subthreshold behaviour, and output characteristics, a conventional *TFT* characterisation setup with two Keithley source/measure units was used.
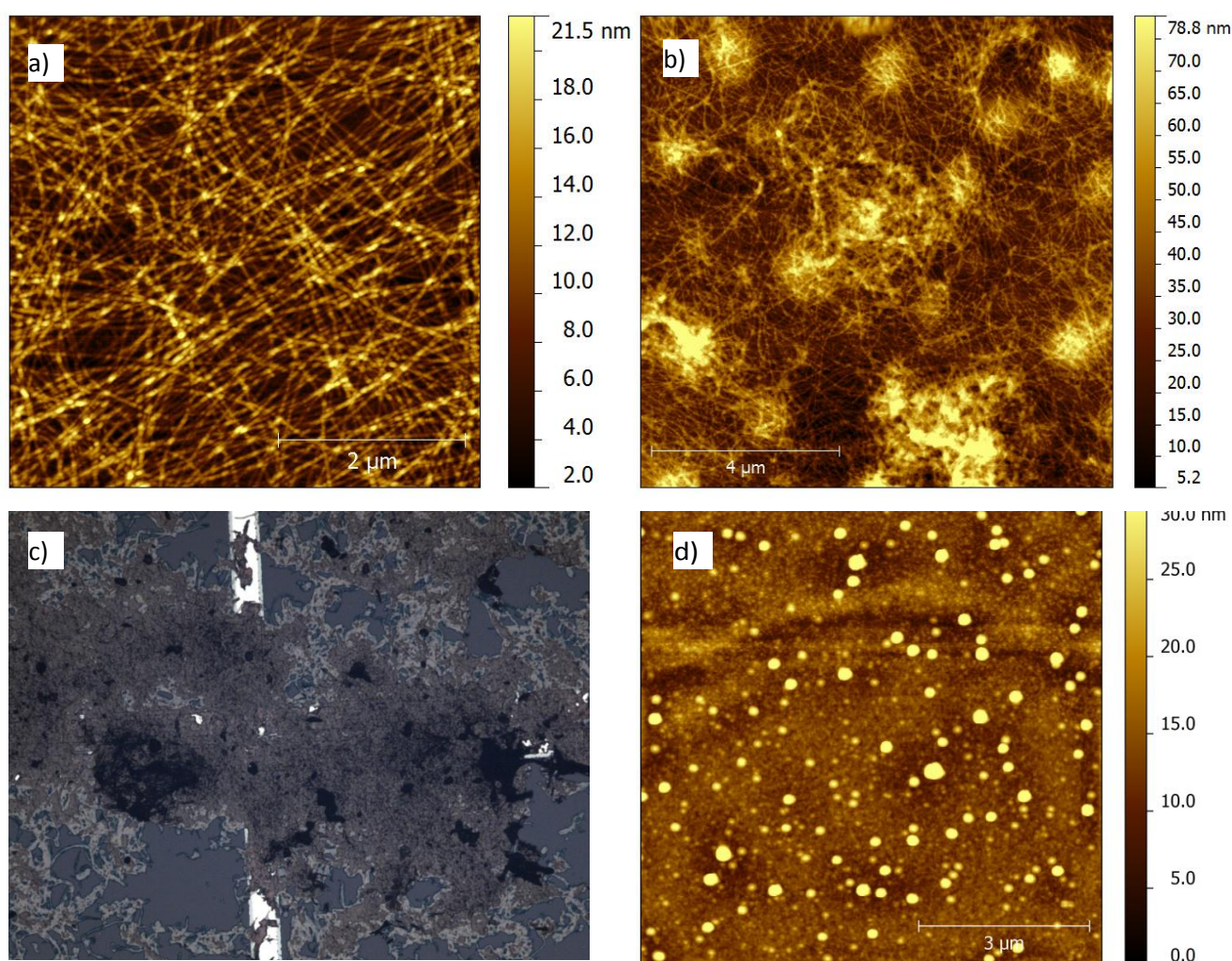
Figure 78, **a:** AFM image of CB-P3HT NWs. 5 mg/ml rrP3HT in chlorobenzene solution was matured for 5 months to allow *NW* growth, then spun at 5000 rpm onto *TFT* substrate. Image shows an area in the channel (channel length 10 μm). **b:** AFM image of Anisole- P3HT *NWs* spun onto *TFT* substrate. **c:** Optical micrograph of BBL nano- belts cast from isopropanol, covering the channel completely. Parts of the connecting wires (Figure 77) are visible; these are 100 μm wide. **d:** AFM image of the channel area of a P3HT film.

7.1.2   P3HT nano- wire *TFTs*: Results and discussion

Figure 78a shows a film cast from P3HT *NWs* grown in chlorobenzene. *NWs* are rather rigid, typically a few μm long, and they do lightly overlap. Figure 78b shows 'Anisole- P3HT' *NWs*, which display a rather different morphology: Several *NWs* radiate out from a central 'seed', *NWs* are longer than CB- P3HT *NWs*, and curved. Different *NW* growth protocols thus lead to different morphologies. Figure 78c shows the optical microscope of *BBL* nano- belts cast from isopropanol. Figure 78d shows thin film of P3HT dissolved in chlorobenzene.
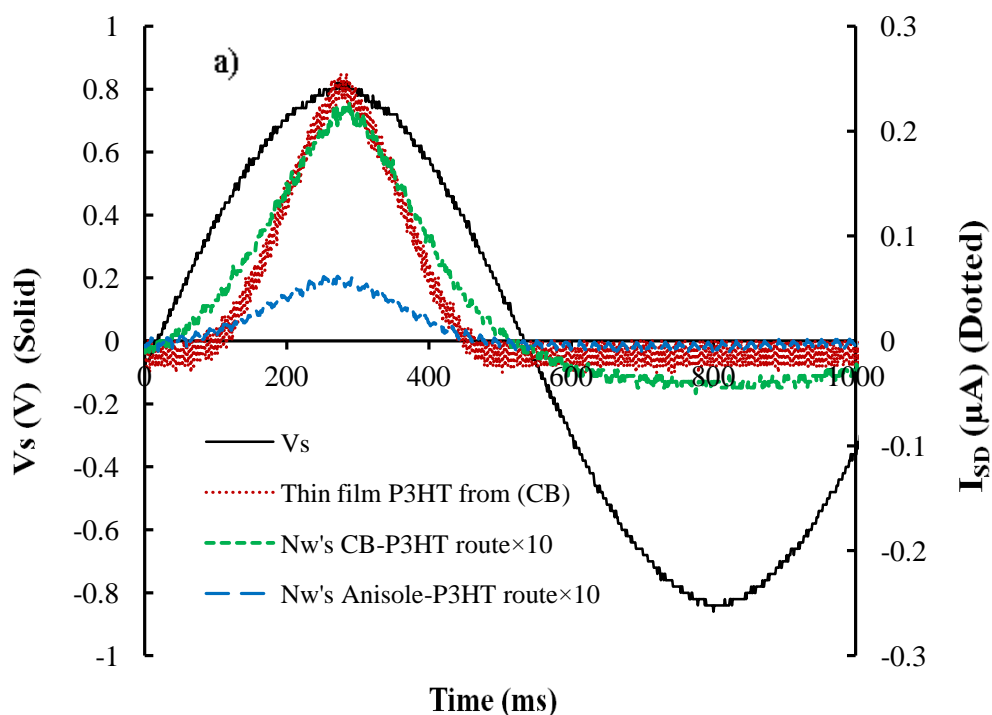
Figure 79, **a.)** Sine drive voltage, $V_S(t)$, and resulting *TFT* source- drain current $I_{SD}(t)$, for water- gated CB- P3HT *NW*, and Anisole- P3HT *NW*, films (as shown in Figure 78a,b,d). P3HT film is also shown, note I_{SD} for both *NW TFTs* is magnified tenfold. **b.)** Saturated transfer characteristics for CB- *NW*, and Anisole- *NW* films, in the form $I_{SD}^{1/2}$ *vs.* V_S; derived from Figure 79a by eliminating time. Threshold, V_T, is read as described in section 3.1.2.5.

In Figure 79a, we show the saturated transfer characteristics parametric in time for CB- P3HT, and Anisole- P3HT, when gated with DI- water, and driven from the source. For comparison, we also include the characteristics of a conventional P3HT film under otherwise the same conditions. Figure 79a shows that both CB- P3HT and Anisole- P3HT *NW* films display low threshold voltage *TFT* characteristics, with a clearly distinct '*on*'- cycle for positive V_S / '*off*' cycle for negative V_S, as it is typical for *p*- type organic transistors driven from the source contact[99]. The low current in the '*off*' cycle shows that very little parasitic current flows across the gate droplet (rather than the semiconductor), thanks to the small overlap- area between contacts and water droplet. The saturated drain current is somewhat higher for CB- P3HT *NWs* than for Anisole- P3HT; however, both are significantly lower compared to conventional P3HT films under water gating (note the scaling used in Figure 79a, the *NW* device currents are shown 10x amplified). We note that the current observed for the conventional P3HT film agrees within 25% with the value reported previously by Kergoat *et al*[25] after the different channel geometry is taken into account.

The low currents observed for water- gated organic NW TFTs agree with similar observations on 'dry' organic NW TFTs, which despite of the high carrier mobility

148

along the axis of individual NWs typically display rather low source- drain currents, the examples shown in the review by Briseno *et. al.*[148]. This is due to the often incomplete filling of the channel width (W) with NWs (e.g. Figure 78a), and the contact problems between bottom contacts and NWs, which are evident in the NW TFT output characteristics shown in[148]. Nevertheless, Figure 79a shows that organic NW films can be gated within the electrochemical window of water to realise electrolyte- gated organic NW TFTs. In fact, the threshold voltage (V_T) is lower for NW TFTs than for conventional P3HT films, as can be seen more clearly from the $(I_{SD})^{1/2}$ *vs.* V_S plots shown in Fig. 3b. This gives $V_T = (0.38 \pm 0.02)$ V for conventional P3HT film, $V_T = (0.27 \pm 0.02)$ V for Anisole- P3HT, and (0.22 ± 0.02) V for CB-P3HT. Note that attempts to calculate a carrier mobility for NW TFTs are ill- advised due to the unknown channel fill- factor.

7.1.3   P3HT nano- wire TFTs as sensors

The results presented in section 7.1.2 show that the *NW* morphology is therefore accessible in principle for water- gated *p*- type organic *TFT* sensor devices, to exploit the large surface area of *NWs* for sensitivity enhancement[149]. As an example to demonstrate this, we have gated both, P3HT NWs, and conventionally cast P3HT films, with dilute solutions of octylamine. An amine has been chosen as example because amines occur as a result of protein breakdown in foodstuffs, for example meat and fish[152]. Amine sensors are therefore of great interest for detecting food spoilage. We used real time measurements to record the responses of devices fabricated as explained in section 3.1.2.7. Hague *et al.* demonstrated previously that the exposure of octylamine vapour reduces the conductivity of pentacene as a *p*- type organic semiconductor, because charge carriers get trapped by analytes of octylamine vapour[132]. Both Figure 80 and Figure 81 show that the on- currents' responses of P3HT *TFTs* and conventionally cast thin films after applying ≈ 2 µl droplets of different concentration of octylamine dissolved in *DI*- water in the range 0.5 ppm to 28 ppm, respectively. However, comparison of Figure 80 and Figure 81 shows that the *NW* morphology enhances the sensitivity of P3HT *TFTs* to dissolved amine, as the response to any given octylamine concentration is higher for the NW morphology (at small concentration 0.5 ppm). The recovery after applying DI- water at the end of experiment indicated to the slower recovery of *NW* morphology and to the faster recovery for conventionally cast thin films.
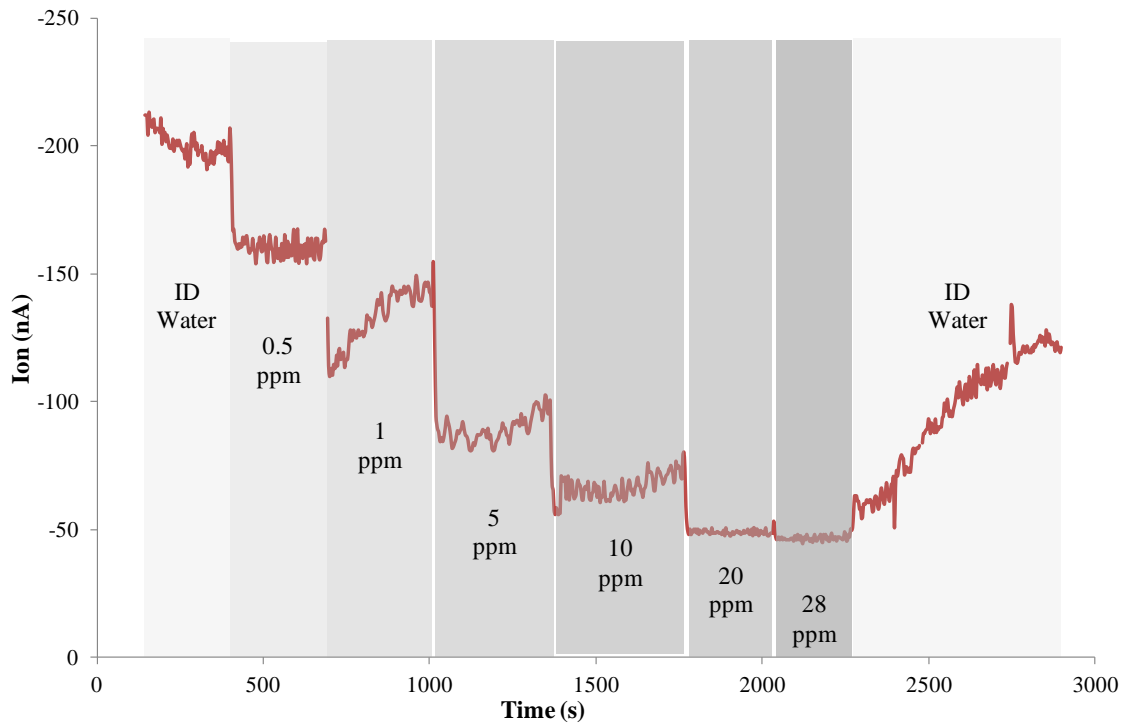
Figure 80, the recorded responses of *NW'S* CB- P3HT TFT after applying range of concentration from 0.5 ppm to 28 ppm of octylamine.
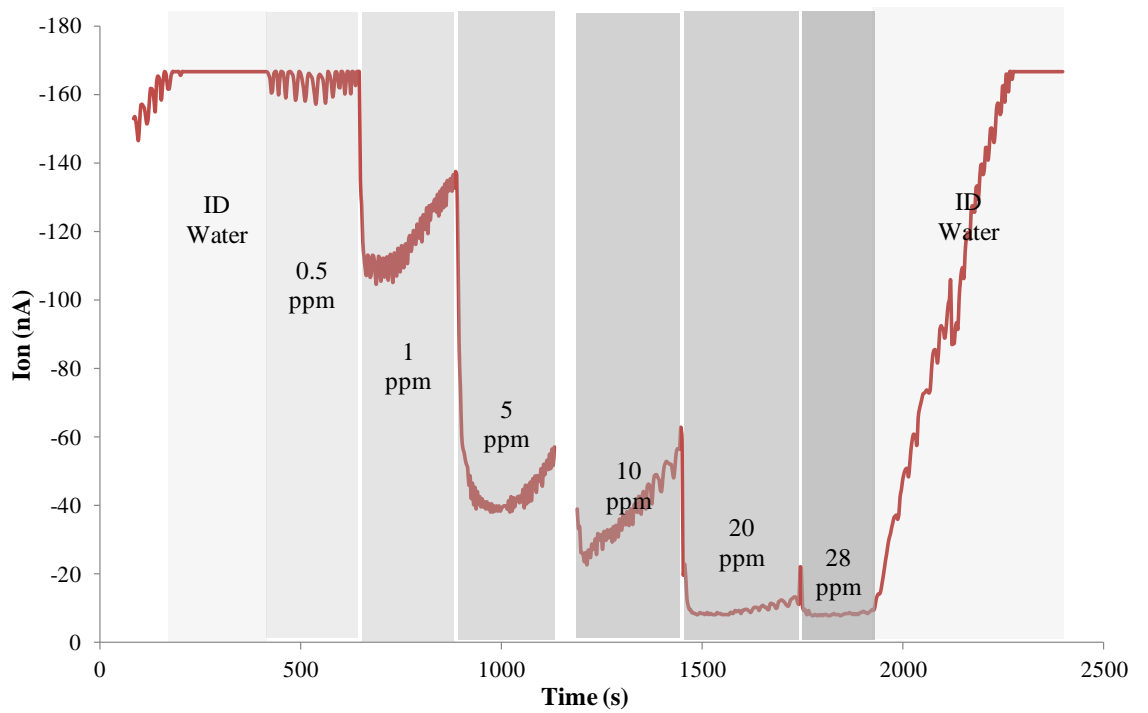
Figure 81, the recorded responses of thin film CB- P3HT TFT after applying range of concentration from 0.5 ppm to 28 ppm of octylamine.

7.1.4 BBL nano- belt TFTs: Results and discussion

Figure 78c shows the morphology of *BBL* nano- belts grown, purified, and processed along the somewhat more intricate procedure described in the experimental section. *BBL* grows into flat ribbons ('belts'), rather than one- dimensional wires like P3HT, and ribbons are larger than *NWs*; these are hence adequately imaged by optical microscopy, rather than AFM. We did not observe any systematic morphological differences between the different solvents (methanol, ethanol, isopropanol) used to displace MSA.

We have also attempted water- gating of *n*- type *NWs*. The option to use n-type, as well as *p*- type, *TFTs*, is generally desirable for organic electronics, as it allows to mimic 'CMOS' type devices like complementary inverters[153]. In the context of sensor technology, dry *n*- type *OSC TFTs* have been shown to be more sensitive to some odours than *p*- type *TFTs*[99], and *n*- type electrolyte- gated *TFTs* are turned on by a cationic (rather than anionic) *EDL*, hence n- type *OSCs* have an advantage over *p*- types for the sensing of waterborne cations. Initially, however, we had no success with water- gating *BBL* nano- belts, presumably due to electron trapping by -OH groups, despite the low *LUMO*. Therefore, we have used acetonitrile, as an alternative to water, as gate medium for *BBL* nano- belts. Acetonitrile (H_3C-$C{\equiv}N$) is aprotic (free of -OH groups), yet highly polar. It is widely used in electrochemistry for its aprotic character, wide electrochemical window and ability to dissolve salts[146]. Figure 82a shows the saturated transfer characteristics of acetonitrile (HPLC grade)- gated *BBL* nanobelt *TFTs*. Note the maximum drive voltage can be selected somewhat higher than for water gating due to the bigger electrochemical window of acetonitrile.

We find clearly distinct '*on*'- cycle for negative V_S / '*off*' cycle for positive V_S, as it is typical for *n*- type organic transistors driven from the source contact[99]. These characteristics remained stable for 5 to 6 minutes. Thresholds can be evaluated similarly as for P3HT in Figure 79b, giving $V_T = (0.22 \pm 0.02)$ V.
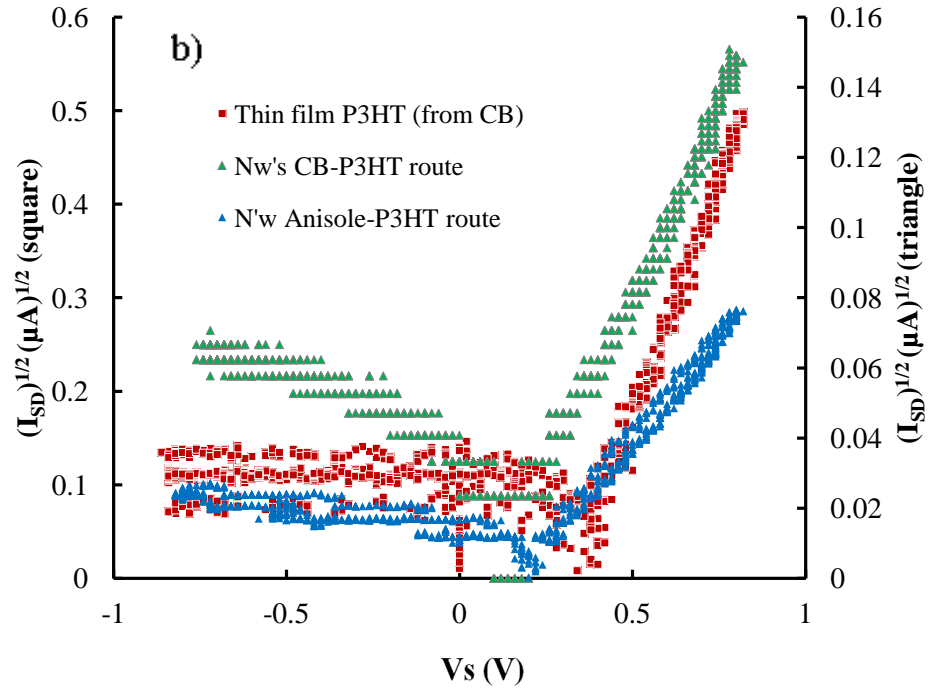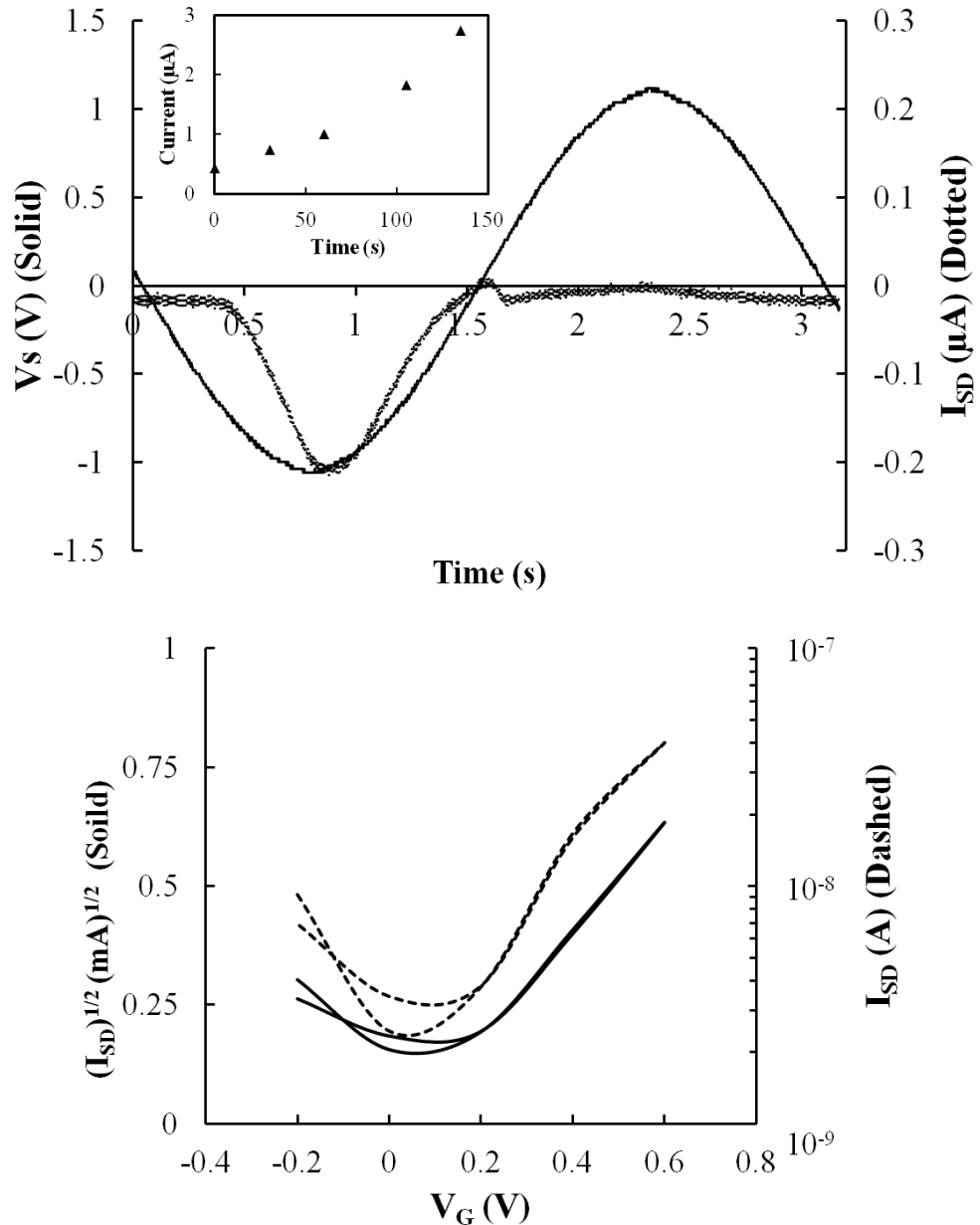
Figure 82, **a.)** Sine drive voltage, $V_S(t)$, and resulting *TFT* source- drain current $I_{SD}(t)$, for acetonitrile- gated *BBL NWs*, calculated from V_{OUT} of the I/V converter by $V_{OUT} = -10\ R_f I_{SD}$. **Inset:** *TFT 'on'* current at maximum drive voltage, $I_{SD}(V_S = 1.1\ V)$, for acetonitrile- gated *BBL TFT* over time, while a minute flake of NaCl dissolves in the gate droplet. **b.)** Saturated transfer characteristics in the form $I_{SD}^{1/2}$, and $\log I_{SD}$, *vs* V_G, measured by a conventional setup.

From Figure 82b, an inverse subthreshold slope was calculated about 285 mV/dec for HPLC- grade acetonitrile gating. The highest accessible saturated drain currents (limited by the electrochemical window of acetonitrile) range from ~ (200...400) nA for different samples, larger than for water- gated P3HT *NWs*, but similar to the maximum drain current observed for dry- gated BBL nano- belt *TFTs* (limited by the dielectric breakdown of the dry gate insulator) with similar nano- belt morphology, and device geometry (~ 360 nA)[73]. However, here we achieve this current with a gate voltage of only 1.1 V , while Briseno *et al*[73] required 80 V to reach maximum current.

This confirms that electrolyte- gated *n*- type *OSC NW TFTs* are viable, as long as a suitable (i.e., aprotic) gate medium is used. Due to the high *EDL* capacitance, maximum current is reached at much lower voltage than for a 'dry' gate insulator. Also, unlike for P3HT, saturated drain currents in *BBL* nano- belt *TFTs* are similar to those found for solution- cast *BBL* film transistors of similar geometry (~ 300 nA)[151]. This indicates near- complete filling of the channel with nano- belts, which is not the case for P3HT nanowires, as seen in Figure 78.

In fact, when the HPLC acetonitrile gate droplet is allowed to evaporate, I_{SD} at first somewhat increases, probably because trace salts become more concentrated (as the gate droplet dries up completely, the transistor eventually fails). We have therefore attempted to enhance maximum current in acetonitrile- gated *BBL* nano- belt *TFTs* by deliberately adding salt to acetonitrile. The inset to Figure 82a shows the '*on*' current I_{SD}(1.1 V) of the same *BBL* nano- belt *TFT* over time, while a minute flake of NaCl dissolves in the gate medium. As the salt slowly dissolves, I_{SD} increases more than 5- fold, eventually reaching almost 3 µA.
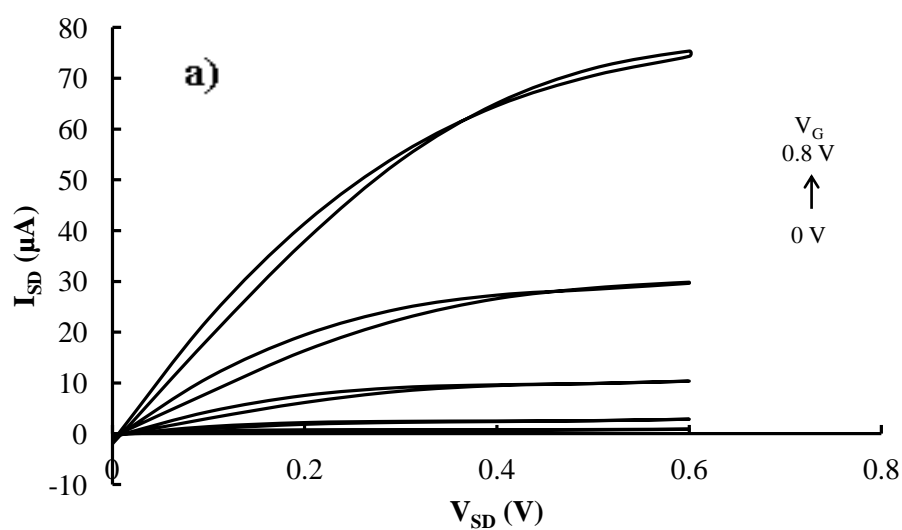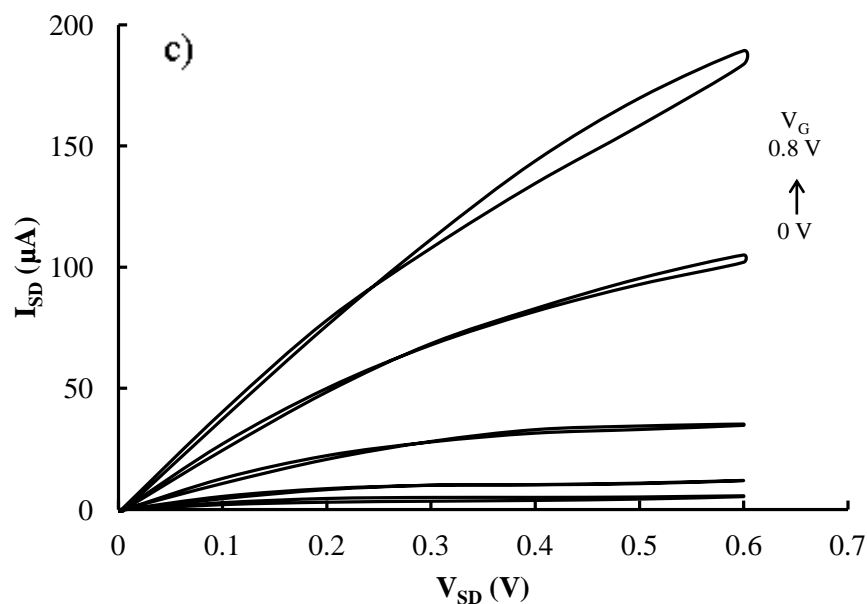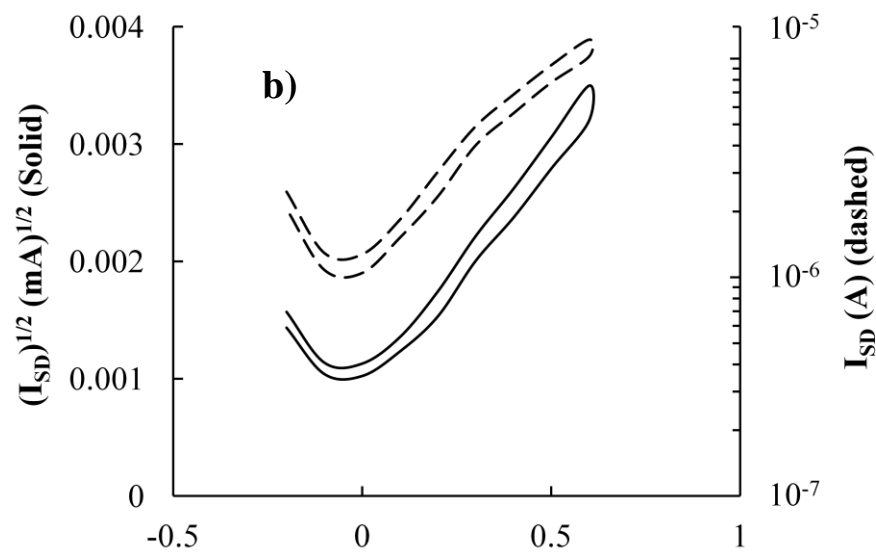
Figure 83, Output (**a**)- and transfer at (V_{SD}=0.8V) (**b**) characteristics of BBL nanobelt film gated with water after acetonitrile dried up, immediately after applying the water gate droplet. **c.)** 2 min. after applying the droplet. Note the droplet has not evaporated. Output characteristics are shown for increasing and decreasing V_{SD}.

When we again attempted to gate a BBL nano- belt film with water, after it had first been gated with acetonitrile that was then allowed to dry up, we recognised a remarkable finding: After such prior 'conditioning', water gating now succeeded and led to TFTs with unusually high saturated drain current. Figure 83a shows the near-ideal output characteristics of such devices, displaying a saturated drain current of more than 70 µA at less than 1 V, which increases further over a few minutes (Figure

83c) to almost 200 µA, an almost 3 order- of- magnitude increase over the saturated drain current observed for the same film under prior acetonitrile- gating. Figure 83b shows the transfer characteristics of *BBL* nano- belt film at V_{SD}=0.8 V gated with water after acetonitrile dried up. When data from Figure 83a are evaluated with the standard saturated drain current equation for a *TFT* (assuming completely filled channel), and assuming a gate capacitance of (C_i = 3 µF/cm^2)[25], we find electron mobility μ_e= 1.4 cm^{2}V^{-1}s^{-1}, higher than reported previously for solution- cast *BBL* films (μ_e = 0.1 cm^{2}V^{-1}s^{-1})[151], or dry- gated *BBL* nano- belt *TFTs* (μ_e < 10^{-2} cm^{2}V^{-1}s^{-1})[73]. Table 9 shows all data for samples of *BBL TFTs*. The reason for slowing down the frequency is to have as high building up of *EDL* as possible to archive the higher value of I_{SD}.

Sample No.	Applied voltage (V)	R_f (MΩ)	Calc. I_{SD} (µA)	Freq. (Hz)	Washing medium NW/Film	V_{Th} (V)
0	1.2	3.20	0.375	1.00	Ethanol	-0.83
1	1.2	8.20	0.146	1.00	Ethanol	-0.51
2	1.2	3.40	0.353	0.40	Ethanol	-0.55
4	1.2	9.70	0.124	0.40	Ethanol	-0.68
5	1.2	1.70	0.706	0.30	Isopropanol	-0.53
6	1.2	2.10	0.57	0.30	Isopropanol	-0.51
7	1.2	4.00	0.30	0.30	Isopropanol	-0.64
8	1.2	4.00	0.30	0.30	Isopropanol	-0.62
11	1	1.82	0.55	0.30	Methanol	-0.42
0	1.1	0.90	0.122	0.30	Isopropanol	-0.45
2	1.1	2.30	0.48	0.30	Ethanol	-0.37
3	1.1	5.30	0.21	0.30	Ethanol	-0.52
0	1.1	1.60	0.688	0.30	Isopropanol	-0.28
2	1.1	6.55	0.168	0.30	Ethanol	0.32

0	0.86	9.00	0.10	0.30	Isopropanol	-0.35
1	1.1	0.22	0.52	0.30	Isopropanol	-0.53
2	1.1	2.20	0.50	0.30	Isopropanol	-0.38
5	1	0.15	6.67	1.00	Film	-0.47
6	1	0.10	10.0	0.30	Film	-0.35
7	1	0.07	14.3	0.30	Film	-0.30

Table 9, the data with transistor parameters from I-V converter (sine- wave) for Acetonitrile- gated *BBL* devices.

At longer times, *TFT* properties deteriorate. Current remains high, but output characteristics become largely independent of gate voltage. The device behaves similar to a resistor, rather than a transistor. When the gate droplet is left to dry up completely, and then is replaced with fresh water, the characteristics shown in Figure 83a can not be recovered.

We believe the acetonitrile conditioning may leave a very thin acetonitrile layer on the surface of *BBL* nanobelts that later shields them from direct contact with water, and thus the -OH groups detrimental to electron transport- until the protective layer eventually dissolves into the water droplet. However, we cannot offer a full explanation for the remarkably high drain currents observed.

7.1.5 **Summary**

We conclude that both *p-* type, and *n-* type, organic *NW* films can be gated with the *EDL* that forms at the interface between *NWs*, and an electrolyte gate medium. As *p-* type *NWs*, we have grown *NWs* from P3HT solutions via two different routes, using different solvents (CB and Anisole) as growth media, and thermal cycling, or simply long- term maturing. Different growth media resulted in *NWs* with different morphologies. Films of both morphologies can be gated with water without prior conditioning, resulting in *TFTs* with very low threshold; even lower than for conventionally cast P3HT films. The resulting saturated drain currents are lower than for conventional P3HT films; however, this is similar to the observations in 'dry' *NW* transistors[148]. Reduced drain currents are probably due to the partial filling of the transistor channel, and injection problems at the metal/*NW* contacts. We propose water- gated *NW TFTs* for use in sensors for waterborne analytes, as the high surface area of *NWs* promises higher sensitivity than conventional organic semiconductor

films. As *n-* type *NWs*, we have grown 'nano- belts' from the *n-* type organic semiconductor, poly(benzimidazobenzophenanthroline) (*BBL*) by a solvent/non-solvent mixing route with later displacement of the solvent in favour of a non- solvent as dispersion medium. When gating of such films with water was attempted, we initially did not observe a resulting drain current. However, *BBL* nano- belts can be gated with an aprotic gate medium (acetonitrile), to give *n-* type *EDL* gated organic field effect nano- belt *TFTs*. Drain current was similar to that observed in dry- gated *BBL* nano- belt *TFTs*, and dry- gated *TFTs* using conventionally cast *BBL* films. However, this was achieved at substantially lower gate voltage, and could be further enhanced by adding salt to the gate medium. Remarkably, *BBL NW* films can also be gated by water (a protic gate medium) after first conditioning them with acetonitrile. Such *TFTs* display very high drain currents; however this remarkable behaviour is transient on a timescale of minutes. While we have no detailed explanation of this behaviour, we believe it may be related to a thin protective acetonitrile film on the nano- belt surface that remains from the prior conditioning. We propose to explore more permanent protective films.

CHAPTER 8

Conclusions and future work

In this thesis, the concept of electrolyte- gated thin films of solution- processed semiconductors was investigated. We used both organic and inorganic semiconductors, and a variety of different electrolytes as electric double layer (*EDL*) gate media. *p-* and *n-* type thin- film transistors (*TFTs*) were fabricated and tested–for their compatibility and performance with different *EDL* gate media to build a scientific foundation for their future applications. Furthermore, suggestions to improve the functionality of electrolyte- gated thin film transistors to be a promising transducer for sensors were offered. In fact, the typically low threshold voltages (below 1 V) of electrolyte- gated thin film transistors, which results from the high capacitance of EDL gate media, is a key asset of such devices, as ordinary batteries can therefore power such transistors.

The key observations and results reported in this thesis are summarized as follows:

1. Depositing layers of calixarenes over the surface of semiconductors using Langmuir trough shows a positive impact on the performance of semiconductors in electrolyte- gated TFTs by suppressing unwanted electrochemical doping often competes with field effect.

2. Electron- transporting water gated TFTs were demonstrated. Previously, reports on water- gated organic *TFTs* had used *p-* type semiconductors only, probably due to the problem of electron trapping at –OH groups in organic semiconductors. Here, we sidestepped this problem by using precursor- route zinc- oxide (ZnO) as a semiconductor. Performance of such films as *n-* type *TFTs* relied in suitable hydrophobic surface modifications.

3. We have shown that in addition to water- based electrolytes, ionic liquids, and solid electrolytes, some organic solvents may act as *EDL* gate media. The

ability for *EDL* gating is a property of the solvent, not the semiconductor. The criterion for a solvent to act as *EDL* medium is its ability to dissolve salts.

4. Both *p*- type and *n*- type organic nano- wires (*NW*) films were gated by water. On the example of P3HT as semiconductor, resulting *TFTs* show lower drain currents, but also lower thresholds compared to conventional films.

5. Water gated organic *NW TFTs* were more sensitive to an analyte dissolved in water than *TFTs* made from a cast thin film of the same material.

6. Using an ionic liquid (*IL*) as *EDL* gate medium for a thin film of ZnO shows ambipolar behaviour at high applied voltages. Such voltages are uniquely accessible to *ILs*, due to their exceptionally large electrochemical window.

For future work, the next step will be to introduce sensitizers into water- gated *TFTs* for the detection of waterborne analytes, for example biomedically relevant molecules, or specific metal cations. A typical sensitizer family for the latter would be calixarenes the work reported in this thesis is a platform on which such efforts can be built.

Another suggestion towards future development of these devices is to deposit newly synthesized material similar to calixarene but including in its lower rim polymer with polyelectrolyte chains, which are called 'brush'. These materials can be deposited over thin- film transistors (ZnO or PBTTT) from the Langmuir trough. This 'calix-brush' has an ability to expand and collapse in response to different pH values, and many studies have recorded this behavior using ellipsometry. Hopefully, our thin-film transistors can record this behavior by changing threshold because the expanding and collapsing brush changes the surface potential of the transistor's channel.

Appendices

9.1   Published papers and attended conferences

1-   Delia Puzzovio, **Abdullah Al Naim**, Lee Hague, Mary Deasy, James Ward, Tim Richardson, Martin Grell, "Technology Platform for Sampling Water with Electrolyte-Gated Organic Transistors Sensitised with Langmuir-Deposited Calixarene Surface Layers," Journal of Surfaces and Interfaces of Materials (2012). doi:**10.1166/jsim.2012.1007**

2-   **Abdullah F. Al Naim** and Martin Grell, "Electron transporting water-gated thin film transistors," Applied Physics Letters **101** (14), 141603-141604 (2012).

3-   **Abdullah F. Al Naim** and Martin Grell, "Organic solvents as gate media for thin-film transistors," Journal of Applied Physics **112** (11), 114502-114505 (2012).

4-   **Abdullah F. Al Naim**, Adam Hobson, Richard T. Grant, Antonis Dragoneas, Mark Hampton, Chris Dunscombe, Tim Richardson, J. Emyr Macdonald, and Martin Grell, "Water-gated organic nanowire transistors," Organic Electronics **14** (4), 1057-1063 (2013).

5-   **Abdullah F. Al Naim** and Martin Grell, "Progress in electrolyte- gated thin film transistors", poster presented in *SID* held in Imperial Collage, London, UK. (Sep. 2012)

6-   **Abdullah F. Al Naim** and Martin Grell, "Progress in electrolyte- gated thin film transistors", poster presented in *NPL* held in Surrey, London, UK. (Dec. 2012)

7-   Antonis Dragoneas, **Abdullah F. Al Naim**, Adam Hobson, Tim Richardson, Martin Grell, Mark Hampton, J. Emyr Macdonald, "Polythiophene nanowires thin-film devices", poster presented in *MRS Fall Meeting & Exhibit* held in Boston, MA, USA. (Nov. 2012)

References

1   Marcus Ahles, Roland Schmechel, and Heinz von Seggern, "< equation> n</equation>-type organic field-effect transistor based on interface-doped pentacene," Applied Physics Letters **85** (19), 4499-4501 (2004).

2   Oana D. Jurchescu, Jacob Baas, and Thomas T. M. Palstra, "Effect of impurities on the mobility of single crystal pentacene," Applied Physics Letters **84** (16), 3061-3063 (2004);   Wilhelm Warta and Norbert Karl, "Hot holes in naphthalene: High, electric-field-dependent mobilities," Physical Review B **32** (2), 1172 (1985).

3   G. Horowitz, *Semiconducting Polymers: Chemistry, Physics and Engineering*. (Wiley-VCH Verlag GmbH & Co. KGaA, 2007).

4   H. Bässler, "Charge Transport in Disordered Organic Photoconductors a Monte Carlo Simulation Study," physica status solidi (b) **175** (1), 15-56 (1993).

5   J. Veres, S. D. Ogier, S. W. Leeming, D. C. Cupertino, and S. Mohialdin Khaffaf, "Low-k Insulators as the Choice of Dielectrics in Organic Field-Effect Transistors," Advanced Functional Materials **13** (3), 199-204 (2003).

6   Michael Redecker, Donal D. C. Bradley, M. Inbasekaran, W. W. Wu, and E. P. Woo, "High Mobility Hole Transport Fluorene-Triarylamine Copolymers," Advanced Materials **11** (3), 241-246 (1999).

7   M. Redecker, D. D. C. Bradley, M. Inbasekaran, and E. P. Woo, "Mobility enhancement through homogeneous nematic alignment of a liquid-crystalline polyfluorene," Applied Physics Letters **74** (10), 1400-1402 (1999);   M. Redecker, D. D. C. Bradley, M. Jandke, and P. Strohriegl, "Electron transport in starburst phenylquinoxalines," Applied Physics Letters **75** (1), 109-111 (1999).

8   R. Schmechel and H. von Seggern, "Electronic Traps in Organic Transport Layers", in *Physics of Organic Semiconductors* (Wiley-VCH Verlag GmbH & Co. KGaA, 2006), pp. 271-303.

9   Lay-Lay Chua, Jana Zaumseil, Jui-Fen Chang, Eric C. W. Ou, Peter K. H. Ho, Henning Sirringhaus, and Richard H. Friend, "General observation of n-type field-effect behaviour in organic semiconductors," Nature **434** (7030), 194-199 (2005).

10   Thomas D Anthopoulos, Sepas Setayesh, Edsger Smits, Michael Cölle, Eugenio Cantatore, Bert de Boer, Paul WM Blom, and Dago M de Leeuw, "Air-Stable Complementary-like Circuits Based on Organic Ambipolar Transistors," Advanced Materials **18** (14), 1900-1904 (2006).

11   EJ Meijer, DM De Leeuw, S Setayesh, E Van Veenendaal, B-H Huisman, PWM Blom, JC Hummelen, U Scherf, and TM Klapwijk, "Solution-processed ambipolar organic field-effect transistors and inverters," Nature Materials **2** (10), 678-682 (2003).

12   Ananth Dodabalapur, HE Katz, L Torsi, and RC Haddon, "Organic heterostructure field-effect transistors," Science **269** (5230), 1560-1562 (1995).

13   H. T. Nicolai, M. Kuik, G. A. H. Wetzelaer, B. de Boer, C. Campbell, C. Risko, J. L. Brédas, and P. W. M. Blom, "Unification of trap-limited electron transport in semiconducting polymers," Nat Mater **11** (10), 882-887 (2012).

14   A.B. Bhattacharyya, *Compact MOSFET Models for VLSI Design*. (Wiley, 2009).

15   S.M. Sze, *Semiconductor devices, physics and technology*. (Wiley, 2001).

16   P. Drude, "Zur Elektronentheorie der Metalle," Annalen der Physik **306** (3), 566-613 (1900).

17   M. A. Green, *Solar cells : operating principles, technology, and system applications / Martin A. Green*. (Prentice-Hall, Englewood Cliffs, N.J, 1982).

18   A. Goetzberger, J. Knobloch, and B. Voss, *Crystalline Silicon Solar Cells*. (Wiley, 1998).

19   Michael C. Petty, *Molecular Electronics*. (2007).

20   Hua Bai and Gaoquan Shi, "Gas Sensors Based on Conducting Polymers," Sensors **7** (3), 267-307 (2007); Luisa Torsi and Ananth Dodabalapur, "Organic Thin-Film Transistors as Plastic Analytical Sensors," Analytical Chemistry **77** (19), 380 A-387 A (2005);   David C Wedge, Arindam Das, René Dost, Jeff Kettle, Marie-Beatrice Madec, John J Morrison, Martin Grell, Douglas B Kell, Tim H Richardson, and Stephen Yeates, "Real-time vapour sensing using an OFET-based electronic nose and genetic programming," Sensors and Actuators B: Chemical **143** (1), 365-372 (2009).

21   Takao Someya, Ananth Dodabalapur, Alan Gelperin, Howard E. Katz, and Zhenan Bao, "Integration and Response of Organic Electronics with Aqueous Microfluidics," Langmuir **18** (13), 5299-5302 (2002).

22   Mark E. Roberts, Stefan C. B. Mannsfeld, Núria Queraltó, Colin Reese, Jason Locklin, Wolfgang Knoll, and Zhenan Bao, "Water-stable organic transistors and their application in chemical and biological sensors," Proceedings of the National Academy of Sciences **105** (34), 12134-12139 (2008).

23   Hideki Shirakawa, Edwin J Louis, Alan G MacDiarmid, Chwan K Chiang, and Alan J Heeger, "Synthesis of electrically conducting organic polymers: halogen derivatives of polyacetylene,(CH) x," Journal of the Chemical Society, Chemical Communications (16), 578-580 (1977).

24   Jeffrey T Mabeck and George G Malliaras, "Chemical and biological sensors based on organic thin-film transistors," Analytical and bioanalytical chemistry **384** (2), 343-353 (2006);   Hadayat Ullah Khan, Mark E Roberts, Wolfgang Knoll, and Zhenan Bao, "Pentacene based organic thin film transistors as the transducer for biochemical sensing in aqueous media," Chemistry of Materials **23** (7), 1946-1953 (2011);   Oren Knopfmacher, Mallory L Hammock, Anthony L Appleton, Gregor Schwartz, Jianguo Mei, Ting Lei, Jian Pei, and Zhenan Bao, "Highly stable organic polymer field-effect transistor sensor for selective detection in the marine environment," Nature communications **5** (2014).

25   Loig Kergoat, Lars Herlogsson, Daniele Braga, Benoit Piro, Minh-Chau Pham, Xavier Crispin, Magnus Berggren, and Gilles Horowitz, "A Water-Gate Organic Field-Effect Transistor," Advanced Materials **22** (23), 2565-2569 (2010).

26   Loig Kergoat, Nicolas Battaglini, Luciano Miozzo, Benoit Piro, Minh-Chau Pham, Abderrahim Yassar, and Gilles Horowitz, "Use of poly(3-hexylthiophene)/poly(methyl methacrylate) (P3HT/PMMA) blends to improve the performance of water-gated organic field-effect transistors," Organic Electronics **12** (7), 1253-1257 (2011).

27   Paul K Weimer, "The TFT a new thin-film transistor," Proceedings of the IRE **50** (6), 1462-1469 (1962).

28   A Tsumura, H Koezuka, and T Ando, "Macromolecular electronic device: Field-effect transistor with a polythiophene thin film," Applied Physics Letters **49** (18), 1210-1212 (1986).

29   C Clarisse, MT Riou, M Gauneau, and M Le Contellec, "Field-effect transistor with diphthalocyanine thin film," Electronics Letters **24** (11), 674-675 (1988).

30   Henry S White, Gregg P Kittlesen, and Mark S Wrighton, "Chemical derivatization of an array of three gold microelectrodes with polypyrrole: fabrication of a molecule-based transistor," Journal of the American Chemical Society **106** (18), 5375-5377 (1984).

31   Oskar Heil, UK (1935).

32   Fang-Chung Chen, Yung-Sheng Lin, Tung-Hsien Chen, and Li-Jen Kung, "Efficient hole-injection in highly transparent organic thin-film transistors," Electrochemical and solid-state letters **10** (6), H186-H188 (2007).

33   N. E. McTigue, Symons, J. M., "The water dictionary: A comprehensive reference of water terminology", (American Water Works Association, Denver, Colo, 2010).

34   Y. He S. H. Yalkowski, P. Jain, *Handbook of Aqueous Solubility Data (2nd ed.)*. (CRC Press, 2010).

35   Kosuke Izutsu, *Electrochemistry in nonaqueous solutions*. (John Wiley & Sons, 2009).

36   Rika Hagiwara, Kazuhiko Matsumoto, Yoji Nakamori, Tetsuya Tsuda, Yasuhiko Ito, Hajime Matsumoto, and Kunitaka Momota, "Physicochemical properties of 1, 3-dialkylimidazolium fluorohydrogenate room-temperature molten salts," Journal of the electrochemical society **150** (12), D195-D199 (2003).

37   S. Ono, S. Seki, R. Hirahara, Y. Tominari, and J. Takeya, "High-mobility, low-power, and fast-switching organic field-effect transistors with ionic liquids," Applied Physics Letters **92** (10), 103313-103313 (2008).

38   Sung W. Lee, Hyun J. Lee, Ji H. Choi, Won G. Koh, Jae M. Myoung, Jae H. Hur, Jong J. Park, Jeong H. Cho, and Unyong Jeong, "Periodic Array of Polyelectrolyte-Gated Organic Transistors from Electrospun Poly(3-hexylthiophene) Nanofibers," Nano Letters **10** (1), 347-351 (2009).

39   Antonio Facchetti, M-H Yoon, and Tobin J Marks, "Gate dielectrics for organic field-effect transistors: new opportunities for organic electronics," Advanced Materials **17** (14), 1705-1725 (2005).

40   Lay-Lay Chua, Jana Zaumseil, Jui-Fen Chang, Eric C-W Ou, Peter K-H Ho, Henning Sirringhaus, and Richard H Friend, "General observation of n-type field-effect behaviour in organic semiconductors," Nature **434** (7030), 194-199 (2005).

41   Se Hyun Kim, Kihyon Hong, Wei Xie, Keun Hyung Lee, Sipei Zhang, Timothy P. Lodge, and C. Daniel Frisbie, "Electrolyte-Gated Transistors for Organic and Printed Electronics," Advanced Materials, n/a-n/a (2012).

42   A. Maliakal, *in Organic Field-Effect Transistor*. (CRC Press, Boca Raton, FL, 2007), Z. Bao and J. Locklin ed.

43   S. Nakamura K. Ueno, H. Shimotani, A. Ohtomo, N. Kimura, T. Nojima, H. Aoki, Y. Iwasa, and M. Kawasaki, "Electric-field-induced superconductivity in an insulator," Nature Materials **7**, 855 - 858 (2008); J. T. Ye, S. Inoue, K. Kobayashi, Y. Kasahara, H. T. Yuan, H. Shimotani, and Y. Iwasa, "Liquid-gated interface superconductivity on an atomically flat film," Nat Mater **9** (2), 125-128 (2010).

44   Mahiar Hamedi, Lars Herlogsson, Xavier Crispin, Rebeca Marcilla, Magnus Berggren, and Olle Inganäs, "Fiber-Embedded Electrolyte-Gated Field-Effect Transistors for e-Textiles," Advanced Materials **21** (5), 573-577 (2009).

45   Hainan Wang and Laurent Pilon, "Intrinsic limitations of impedance measurements in determining electric double layer capacitances," Electrochimica Acta **63** (0), 55-63 (2012).

46   Lars Herlogsson, Yong-Young Noh, Ni Zhao, Xavier Crispin, Henning Sirringhaus, and Magnus Berggren, "Downscaling of Organic Field-Effect Transistors with a Polyelectrolyte Gate Insulator," Advanced Materials **20** (24), 4708-4713 (2008).

47   Matthew J Panzer and C Daniel Frisbie, "High Carrier Density and Metallic Conductivity in Poly (3-hexylthiophene) Achieved by Electrostatic Charge Injection," Advanced Functional Materials **16** (8), 1051-1056 (2006).

48   Olle Inganas, "Hybrid electronics and electrochemistry with conjugated polymers," Chemical Society Reviews **39** (7), 2633-2642 (2010).

49   V. Böhmer Eds Z. Asfari, J.M. Harrowfield, J. Vicens, Kluwer, *Calixarenes 2001*. (Academic Publishers, Dordrecht, The Netherlands, 2001).

50   Mark E. Roberts, Anatoliy N. Sokolov, and Zhenan Bao, "Material and device considerations for organic thin-film transistor sensors," Journal of Materials Chemistry **19** (21), 3351 (2009).

51   J. Takeya, K. Yamada, K. Hara, K. Shigeto, K. Tsukagoshi, S. Ikehata, and Y. Aoyagi, "High-density electrostatic carrier doping in organic single-crystal transistors with polymer gel electrolyte," Applied Physics Letters **88** (11), 112102-112103 (2006).

52   Elias Said, Oscar Larsson, Magnus Berggren, and Xavier Crispin, "Effects of the Ionic Currents in Electrolyte-gated Organic Field-Effect Transistors," Advanced Functional Materials **18** (21), 3529-3536 (2008).

53   Annica Crispin, Xavier Crispin, Mats Fahlman, Magnus Berggren, and William R. Salaneck, "Transition between energy level alignment regimes at a low band gap polymer-electrode interfaces," Applied Physics Letters **89** (21), 213503-213503 (2006).

54   Z. Bao and J.J. Locklin, *Organic Field-Effect Transistors*. (CRC Press, Taylor & Francis, 2007).

55   A. Che Mofor, A. El-Shaer, A. Bakin, A. Waag, H. Ahlers, U. Siegner, S. Sievers, M. Albrecht, W. Schoch, N. Izyumskaya, V. Avrutin, S. Sorokin, S. Ivanov, and J. Stoimenos, "Magnetic property investigations on Mn-doped ZnO Layers on sapphire," Applied Physics Letters **87** (6), - (2005).

56   H. T. Wang, B. S. Kang, F. Ren, L. C. Tien, P. W. Sadik, D. P. Norton, S. J. Pearton, and Jenshan Lin, "Hydrogen-selective sensing at room temperature with ZnO nanorods," Applied Physics Letters **86** (24), - (2005); L. C. Tien, P. W. Sadik, D. P. Norton, L. F. Voss, S. J. Pearton, H. T. Wang, B. S. Kang, F. Ren, J. Jun, and J. Lin, "Hydrogen sensing at room temperature with Pt-coated ZnO thin films and nanorods," Applied Physics Letters **87** (22), - (2005).

57   Yong Qin, Xudong Wang, and Zhong Lin Wang, "Microfibre-nanowire hybrid structure for energy scavenging," Nature **451** (7180), 809-813 (2008).

58   Z. H. Wang, D. Y. Geng, Z. Han, and Z. D. Zhang, "Characterization and optical properties of ZnO nanoparticles obtained by oxidation of Zn nanoparticles," Materials Letters **63** (29), 2533-2535 (2009).

59   Parmod Sagar, Manoj Kumar, and R. M. Mehra, "Influence of hydrogen incorporation in sol-gel derived aluminum doped ZnO thin films," Thin Solid Films **489** (1–2), 94-98 (2005); Weifeng Liu, Guotong Du, Yanfeng Sun, Yibin Xu, Tianpeng Yang, Xinsheng Wang, Yuchun Chang, and Fabin Qiu, "Al-doped ZnO thin films deposited by reactive frequency magnetron sputtering: H2-induced property changes," Thin Solid Films **515** (5), 3057-3060 (2007).

60   Beng S Ong, Chensha Li, Yuning Li, Yiliang Wu, and Rafik Loutfy, "Stable, solution-processed, high-mobility ZnO thin-film transistors," Journal of the American Chemical Society **129** (10), 2750-2751 (2007).

61   Michael H Huang, Samuel Mao, Henning Feick, Haoquan Yan, Yiying Wu, Hannes Kind, Eicke Weber, Richard Russo, and Peidong Yang, "Room-temperature ultraviolet nanowire nanolasers," Science **292** (5523), 1897-1899 (2001).

62   Kenji Nomura, Hiromichi Ohta, Kazushige Ueda, Toshio Kamiya, Masahiro Hirano, and Hideo Hosono, "Thin-Film Transistor Fabricated in Single-Crystalline Transparent Oxide Semiconductor," Science **300** (5623), 1269-1272 (2003); P. F. Carcia, R. S. McLean, M. H. Reilly, and Jr G. Nunes, "Transparent

ZnO thin-film transistor fabricated by rf magnetron sputtering," Applied Physics Letters **82** (7), 1117-1119 (2003).

63   P. F. Carcia, R. S. McLean, and M. H. Reilly, "High-performance ZnO thin-film transistors on gate dielectrics grown by atomic layer deposition," Applied Physics Letters **88** (12), 123509-123503 (2006).

64   Si Yun Park, Beom Joon Kim, Kyongjun Kim, Moon Sung Kang, Keon-Hee Lim, Tae Il Lee, Jae M. Myoung, Hong Koo Baik, Jeong Ho Cho, and Youn Sang Kim, "Low-Temperature, Solution-Processed and Alkali Metal Doped ZnO for High-Performance Thin-Film Transistors," Advanced Materials **24** (6), 834-838 (2012).

65   Jonathan Rivnay, Leslie H Jimison, John E Northrup, Michael F Toney, Rodrigo Noriega, Shaofeng Lu, Tobin J Marks, Antonio Facchetti, and Alberto Salleo, "Large modulation of carrier transport by grain-boundary molecular packing and microstructure in organic thin films," Nature Materials **8** (12), 952-958 (2009).

66   Brooks A. Jones, Michael J. Ahrens, Myung-Han Yoon, Antonio Facchetti, Tobin J. Marks, and Michael R. Wasielewski, "High-Mobility Air-Stable n-Type Semiconductors with Processing Versatility: Dicyanoperylene-3,4:9,10-bis(dicarboximides)," Angewandte Chemie International Edition **43** (46), 6363-6366 (2004).

67   Richard D. McCullough and Renae D. Lowe, "Enhanced electrical conductivity in regioselectively synthesized poly(3-alkylthiophenes)," Journal of the Chemical Society, Chemical Communications (1), 70-72 (1992).

68   Iain McCulloch, Martin Heeney, Clare Bailey, Kristijonas Genevicius, Iain MacDonald, Maxim Shkunov, David Sparrowe, Steve Tierney, Robert Wagner, and Weimin Zhang, "Liquid-crystalline semiconducting polymers with high charge-carrier mobility," Nature Materials **5** (4), 328-333 (2006).

69   RA Street, JE Northrup, and A Salleo, "Transport in polycrystalline polymer thin-film transistors," Physical Review B **71** (16), 165202 (2005).

70   Samson A. Jenekhe and Paul O. Johnson, "Complexation-mediated solubilization and processing of rigid-chain and ladder polymers in aprotic organic solvents," Macromolecules **23** (20), 4419-4429 (1990).

71   Alejandro L Briseno, Felix Sunjoo Kim, Amit Babel, Younan Xia, and Samson A Jenekhe, "n-Channel polymer thin film transistors with long-term air-stability and durability and their use in complementary inverters," Journal of Materials Chemistry **21** (41), 16461-16466 (2011).

72   Hakan Usta, Chad Risko, Zhiming Wang, Hui Huang, Murat K Deliomeroglu, Aleksandr Zhukhovitskiy, Antonio Facchetti, and Tobin J Marks, "Design, synthesis, and characterization of ladder-type molecules and polymers. Air-stable, solution-processable n-channel and ambipolar semiconductors for thin-film transistors via experiment and theory," Journal of the American Chemical Society **131** (15), 5586-5608 (2009).

73   Alejandro L Briseno, Stefan CB Mannsfeld, Patrick J Shamberger, Fumio S Ohuchi, Zhenan Bao, Samson A Jenekhe, and Younan Xia, "Self-assembly, molecular packing, and electron transport in n-type polymer semiconductor nanobelts," Chemistry of Materials **20** (14), 4712-4719 (2008).

74   FE Arnold and RL Van Deusen, "Preparation and Properties of High Molecular Weight, Soluble Oxobenz [de] imidazobenzimidazoisoquinoline Ladder Polymer," Macromolecules **2** (5), 497-502 (1969).

75   Kyo Jin Ihn, Jeff Moulton, and Paul Smith, "Whiskers of poly (3-alkylthiophene) s," Journal of Polymer Science Part B: Polymer Physics **31** (6), 735-742 (1993).

76   Nataliya Kiriy, Evelin Jähne, Hans-Juergen Adler, Mareike Schneider, Anton Kiriy, Ganna Gorodyska, Sergiy Minko, Dieter Jehnichen, Paul Simon, and Andrey A Fokin, "One-dimensional aggregation of regioregular polyalkylthiophenes," Nano Letters **3** (6), 707-712 (2003).

77   Wibren D Oosterbaan, Veerle Vrindts, Solenn Berson, Stéphane Guillerez, Olivier Douhéret, Bart Ruttens, Jan D'Haen, Peter Adriaensens, Jean Manca, and Laurence Lutsen, "Efficient formation, isolation and characterization of poly (3-alkylthiophene) nanofibres: probing order as a function of side-chain length," Journal of Materials Chemistry **19** (30), 5424-5435 (2009).

78   Solenn Berson, Rémi De Bettignies, Séverine Bailly, and Stéphane Guillerez, "Poly (3-hexylthiophene) Fibers for Photovoltaic Applications," Advanced Functional Materials **17** (8), 1377-1384 (2007).

79   Jong Soo Kim, Ji Hwang Lee, Jong Hwan Park, Chiyeoung Shim, Myungsun Sim, and Kilwon Cho, "High-Efficiency Organic Solar Cells Based on Preformed Poly (3-hexylthiophene) Nanowires," Advanced Functional Materials **21** (3), 480-486 (2011).

80   Hiroaki Yonemura, Koichi Yuno, Yuuichi Yamamoto, Sunao Yamada, Yoshihisa Fujiwara, and Yoshifumi Tanimoto, "Orientation of nanowires consisting of poly (3-hexylthiophene) using strong magnetic field," Synthetic Metals **159** (9), 955-960 (2009).

81   Jeffrey A Merlo and C Daniel Frisbie, "Field effect transport and trapping in regioregular polythiophene nanofibers," The Journal of Physical Chemistry B **108** (50), 19169-19179 (2004).

82   C.D. . . J.F. Stoddart. (ed.) : . Gutsche, *Calixarenes Revisited*. (The Royal Society of Chemistry

Cambridge, UK, 1998).

83   Bernadette S Creaven, Denis F Donlon, and John McGinley, "Coordination chemistry of calix [4] arene derivatives with lower rim functionalisation and their applications," Coordination Chemistry Reviews **253** (7), 893-962 (2009).

84   Aodhmar M Cadogan, Dermot Diamond, Malcolm R Smyth, Mary Deasy, M Anthony McKervey, and Stephen J Harris, "Sodium-selective polymeric membrane electrodes based on calix [4] arene ionophores," Analyst **114** (12), 1551-1554 (1989); M AnthonyáMcKervey, "Calixarene-based sensing agents," Chemical Society Reviews **25** (1), 15-24 (1996); Jian-Quan Lu, Dai-Wen Pang, Xian-Shun Zeng, and Xi-Wen He, "A new solid-state silver ion-selective electrode based on a novel tweezer-type calixarene derivative," Journal of Electroanalytical Chemistry **568**, 37-43 (2004).

85   Lizhu Zhang, Jiangli Fan, and Xiaojun Peng, "X-ray crystallographic and photophysical properties of rhodamine-based chemosensor for Fe^{3+}," Spectrochimica Acta Part A: Molecular and Biomolecular Spectroscopy **73** (2), 398-402 (2009).

86   R Mlika, H Ben Ouada, N Jaffrezic-Renault, I Dumazet, R Lamartine, M Gamoudi, and G Guillaud, "Study of ion-selective evaporated calixarene film used as a sensitive layer on ISFET sensors," Sensors and Actuators B: Chemical **47** (1), 43-47 (1998); Yutaka Tsujimura, Masaaki Yokoyama, and Keiichi Kimura, "Oligosiloxane-modified calix [4] arene ionophores for silicone-rubber-membrane sodium ion-sensitive field-effect transistors," Electroanalysis **5** (9-10), 803-807 (1993).

87   R Mlika, I Dumazet, H Ben Ouada, N Jaffrezic-Renault, R Lamartine, M Gamoudi, and G Guillaud, "Cu^{2+}-ISFET type microsensors based on thermally evaporated *p*-*tert*-butylcalix [9 and 11] arene thin films," Sensors and Actuators B: Chemical **62** (1), 8-12 (2000).

88   RH Tredgold, "The physics of Langmuir-Blodgett films," Reports on Progress in Physics **50** (12), 1609 (1987).

89   H.Y. Erbil, *Surface Chemistry of Solid and Liquid Interfaces*. (Wiley, 2006).

90   Michael C Petty, *Langmuir-Blodgett films: an introduction*. (Cambridge University Press, 1996).

91   KV Shaitan and PP Pustoshilov, "Molecular Dynamics of a Stearic Acid Monolayer," BIOPHYSICS-PERGAMON THEN MAIK NAUKA-C/C OF BIOFIZIKA **44** (3), 429-434 (1999).

92   Robert C. Osthoff and Simon W. Kantor, "Organosilazane Compounds", in *Inorganic Syntheses* (John Wiley & Sons, Inc., 2007), pp. 55-64.

93   Leszek Artur Majewski, Raoul Schroeder, and Martin Grell, "Flexible high capacitance gate insulators for organic field effect transistors," Journal of Physics D: Applied Physics **37** (1), 21 (2004).

94   René Dost, Arindam Das, and Martin Grell, "A novel characterization scheme for organic field-effect transistors," Journal of Physics D: Applied Physics **40** (12), 3563 (2007).

95   Hagen Klauk, "Organic thin-film transistors," Chemical Society Reviews **39** (7), 2643-2666 (2010).

96   Faridah L. Supian, Tim H. Richardson, Mary Deasy, Fintan Kelleher, James P. Ward, and Vickie McKee, "Interaction between Langmuir and Langmuir–Blodgett Films of Two Calix[4]arenes with Aqueous Copper and Lithium Ions," Langmuir **26** (13), 10906-10912 (2010).

97   Loïg Kergoat, Lars Herlogsson, Benoit Piro, Minh Chau Pham, Gilles Horowitz, Xavier Crispin, and Magnus Berggren, "Tuning the threshold voltage in electrolyte-gated organic field-effect transistors," Proceedings of the National Academy of Sciences **109** (22), 8394-8399 (2012).

98   S. Young Park, Mikyung Park, and Hong H. Lee, "Cooperative polymer gate dielectrics in organic thin-film transistors," Applied Physics Letters **85** (12), 2283-2285 (2004).

99   L. Hague, D. Puzzovio, A. Dragoneas, and M. Grell, "Simplified Real-Time Organic Transistor Characterisation Schemes for Sensing Applications," Sci Adv Mater **3** (6), 907-911 (2011).

100   Ute Zschieschang, R Thomas Weitz, Klaus Kern, and Hagen Klauk, "Bias stress effect in low-voltage organic thin-film transistors," Applied Physics A **95** (1), 139-145 (2009).

101   Ari Laiho, Lars Herlogsson, Robert Forchheimer, Xavier Crispin, and Magnus Berggren, "Controlling the dimensionality of charge transport in organic thin-film transistors," Proceedings of the National Academy of Sciences (2011).

102   T. S. Chow, "Wetting of rough surfaces," Journal of Physics: Condensed Matter **10** (27), L445 (1998).

103   H. G. Tompkins, J. H. Baker, S. Smith, and D. Convey, presented at the Electronic-Enhanced Optics, Optical Sensing in Semiconductor Manufacturing, Electro-Optics in Space, Broadband Optical Networks, 2000. Digest of the LEOS Summer Topical Meetings, 2000 (unpublished).

104   N. Clark, *Scanning Probe microscopy; Imaging surfaces using STM and AFM*. (Material Research Center (MRC), 2009).

105   A. Raman, *Atomic Force Microscopy (AFM)*. (Purdue University, 2005).

106   Bruker AFM Probes, (Camarillo).

107   J.C. Vickerman and I. Gilmore, *Surface Analysis: The Principal Techniques*. (John Wiley & Sons, 2009).

108   Mark E. Roberts, Anatoliy N. Sokolov, and Zhenan Bao, "Material and device considerations for organic thin-film transistor sensors," Journal of Materials Chemistry **19** (21), 3351-3363 (2009).

109   Vandna Arora, Har Mohindra Chawla, and Suneel Pratap Singh, "Calixarenes as sensor materials for recognition and separation of metal ions," Arkivoc **2**, 172-200 (2007);   R. Ludwig and N. T. K. Dzung, "Calixarene-based molecules for cation recognition," Sensors **2** (10), 397-416 (2002).

110   LA Majewski, JW Kingsley, C Balocco, and AM Song, "Influence of processing conditions on the stability of poly (3-hexylthiophene)-based field-effect transistors," Applied Physics Letters **88** (22), 222108 (2006).

111   FL Supian, TH RIcHARDSoN, M DeASy, F KeLLeHeR, JP Ward, and V McKee, "A Surface Potential Study of Ion-Uptake by 5, 11, 17, 23-Tetra-Tert-Butyl-25, 27-Diethoxycarbonyl Methyleneoxy-26, 28, Dihydroxycalix [4] Arene and 5, 17-(3-Nitrobenzylideneamino)-11,   23-Di-Tert-Butyl-25,   27-Diethoxycarbonyl Methyleneoxy-26, 28-Dihydroxycalix [4] Arene Langmuir Blodgett (LB) Monolayers," Sains Malaysiana **39** (3), 423-433 (2010).

112   Serafina Cotrone, Marianna Ambrico, Henrik Toss, M. Daniela Angione, Maria Magliulo, Antonia Mallardi, Magnus Berggren, Gerardo Palazzo, Gilles Horowitz, Teresa Ligonzo, and Luisa Torsi, "Phospholipid film in electrolyte-gated organic field-effect transistors," Organic Electronics **13** (4), 638-644 (2012).

113   He Yan, Zhihua Chen, Yan Zheng, Christopher Newman, Jordan R. Quinn, Florian Dotz, Marcel Kastler, and Antonio Facchetti, "A high-mobility electron-transporting polymer for printed transistors," Nature **457** (7230), 679-686 (2009).

114   Loig Kergoat, Benoît Piro, Magnus Berggren, Minh-Chau Pham, Abderrahim Yassar, and Gilles Horowitz, "DNA detection with a water-gated organic field-effect transistor," Organic Electronics **13** (1), 1-6 (2012).

115   Abdullah Al Naim Delia Puzzovio, Lee Hague, Mary Deasy, James Ward, Tim Richardson, Martin Grell, "Technology Platform for Sampling Water with Electrolyte-Gated Organic Transistors Sensitised with Langmuir-Deposited Calixarene Surface Layers," Journal of Surfaces and Interfaces of Materials (2012).

116   Elvira MC Fortunato, Pedro MC Barquinha, ACMBG Pimentel, Alexandra MF Gonçalves, António JS Marques, Luís MN Pereira, and Rodrigo FP Martins, "Fully Transparent ZnO Thin-Film Transistor Produced at Room Temperature," Advanced Materials **17** (5), 590-594 (2005).

117   Myung-Gil Kim, Mercouri G Kanatzidis, Antonio Facchetti, and Tobin J Marks, "Low-temperature fabrication of high-performance metal oxide thin-film electronics via combustion processing," Nature Materials **10** (5), 382-388 (2011).

118   Young Hwan Hwang, Seok-Jun Seo, Jun-Hyuck Jeon, and Byeong-Soo Bae, "Ultraviolet photo-annealing process for low temperature processed sol-gel zinc tin oxide thin film transistors," Electrochemical and solid-state letters **15** (4), H91-H93 (2012).

119   Pradipta K Nayak, MN Hedhili, Dongkyu Cha, and HN Alshareef, "High performance solution-deposited amorphous indium gallium zinc oxide thin film transistors by oxygen plasma treatment," Applied Physics Letters **100** (20), 202106 (2012).

120   Si Yun Park, Beom Joon Kim, Kyongjun Kim, Moon Sung Kang, Keon-Hee Lim, Tae Il Lee, Jae M Myoung, Hong Koo Baik, Jeong Ho Cho, and Youn Sang Kim, "Low-Temperature, Solution-Processed and Alkali Metal Doped ZnO for

High-Performance Thin-Film Transistors," Advanced Materials **24** (6), 834-838 (2012).

121   Akira Kawai and Junko Kawakami, "Characterization of SiO2 Surface Treated by HMDS Vapor and O2 Plasma with AFM Tip," Journal of Photopolymer Science and Technology **16** (5), 665-668 (2003).

122   Changming Jin, JD Luttmer, Douglas M Smith, and Teresa A Ramos, "Nanoporous silica as an ultralow-k dielectric," MRS Bulletin **22** (10), 39-42 (1997).

123   M. Spijkman, E. C. P. Smits, J. F. M. Cillessen, F. Biscarini, P. W. M. Blom, and D. M. de Leeuw, "Beyond the Nernst-limit with dual-gate ZnO ion-sensitive field-effect transistors," Applied Physics Letters **98** (4), - (2011).

124   Susanne Oertel, Michael PM Jank, Erik Teuber, Anton J Bauer, and Lothar Frey, "High-mobility metal-oxide thin-film transistors by spray deposition of environmentally friendly precursors," Thin Solid Films (2013).

125   K Grundke, C Werner, K Pöschel, and H-J Jacobasch, "Characterization of adsorbed protein layers by low-rate dynamic liquid–fluid contact angle measurements using axisymmetric drop shape analysis (part II)," Colloids and Surfaces A: Physicochemical and Engineering Aspects **156** (1), 19-31 (1999).

126   C Murray, C Flannery, I Streiter, SE Schulz, MR Baklanov, KP Mogilnikov, C Himcinschi, M Friedrich, DRT Zahn, and T Gessner, "Comparison of Techniques to Characterise the Density, Porosity and Elastic Modulus of Porous low-< i> k</i> SiO< sub> 2</sub> Xerogel Films," Microelectronic Engineering **60** (1), 133-141 (2002).

127   Elias Said, Xavier Crispin, Lars Herlogsson, Sami Elhag, Nathaniel D Robinson, and Magnus Berggren, "Polymer field-effect transistor gated via a poly (styrenesulfonic acid) thin film," Applied Physics Letters **89** (14), 143507 (2006).

128   M. Spijkman, E. C. P. Smits, J. F. M. Cillessen, F. Biscarini, P. W. M. Blom, and D. M. de Leeuw, "Beyond the Nernst-limit with dual-gate ZnO ion-sensitive field-effect transistors," Applied Physics Letters **98** (4), 043502-043503 (2011).

129   Leszek Artur Majewski, Raoul Schroeder, and Martin Grell, "One volt organic transistor," Advanced Materials **17** (2), 192-196 (2005).

130   Robert J. Klein, Shihai Zhang, Shichen Dou, Brad H. Jones, Ralph H. Colby, and James Runt, "Modeling electrode polarization in dielectric spectroscopy: Ion mobility and mobile ion concentration of single-ion polymer electrolytes," The Journal of Chemical Physics **124** (14), 144903-144908 (2006).

131   Di Wei and Ari Ivaska, "Applications of ionic liquids in electrochemical sensors," Analytica chimica acta **607** (2), 126-135 (2008).

132   Lee Hague, Delia Puzzovio, Tim H Richardson, and Martin Grell, "Discovery of a New Odour Sensing Mechanism Using an n-Type Organic Transistor," Sensor Letters **9** (5), 1692-1696 (2011).

133   Chun-Yuen Wong, Lo-Ming Lai, Siu-Ling Leung, V. A. L. Roy, and Edwin Yue-Bun Pun, "Ambipolar charge transport and electroluminescence properties of ZnO nanorods," Applied Physics Letters **93** (2), 023502 (2008).

134   Brooks A Jones, Antonio Facchetti, Michael R Wasielewski, and Tobin J Marks, "Effects of Arylene Diimide Thin Film Growth Conditions on n-Channel OFET Performance," Advanced Functional Materials **18** (8), 1329-1339 (2008).

135   Gilles Horowitz, "Organic Field-Effect Transistors," Advanced Materials **10** (5), 365-377 (1998); Christos D Dimitrakopoulos and Patrick RL Malenfant, "Organic thin film transistors for large area electronics," Advanced Materials **14** (2), 99-117 (2002).

136   Seok-Jun Seo, Chaun Gi Choi, Young Hwan Hwang, and Byeong-Soo Bae, "High performance solution-processed amorphous zinc tin oxide thin film transistor," Journal of Physics D: Applied Physics **42** (3), 035106 (2009).

137   Ltd Ossila, "http://www.ossila.com/", (Kroto Innovation Centre, Broad Lane, Sheffield S3 7HQ, 2009-2011).

138   Abdullah F. Al Naim and Martin Grell, "Electron transporting water-gated thin film transistors," Applied Physics Letters **101** (14), 141603-141604 (2012).

139   David R. Lide, *CRC handbook of chemistry and physics : a ready-reference book of chemical and physical data*. (CRC, Boca Raton, Fla. ; London, 2009), 90th ed.

140   J Ross Macdonald, "Theory of ac space-charge polarization effects in photoconductors, semiconductors, and electrolytes," Physical Review **92** (1), 4 (1953).

141   S Rondinini, P Longhi, PR Mussini, and T Mussini, "AUTOPROTOLYSIS CONSTANTS IN NONAQUEOUS SOLVENTS AND AQUEOUS ORGANIC SOLVENT," Pure & Appl. Chem. **59** (12) (1987).

142   John A Riddick, William B Bunger, and Theodore K Sakano, "Organic solvents: physical properties and methods of purification", (John Wiley and Sons, New York, NY, New York, 1986).

143   E Kirowa-Eisner E Gileadi, J Penciner *Interfacial Chemistry: An Experimental Approach*. (Addison-Wesley, USA 1975).

144   Brooks A. Jones, Antonio Facchetti, Michael R. Wasielewski, and Tobin J. Marks, "Tuning Orbital Energetics in Arylene Diimide Semiconductors. Materials Design for Ambient Stability of n-Type Charge Transport," Journal of the American Chemical Society **129** (49), 15259-15278 (2007); Wen-Ya Lee, Joon Hak Oh, Sabin-Lucian Suraru, Wen-Chang Chen, Frank Würthner, and Zhenan Bao, "High-Mobility Air-Stable Solution-Shear-Processed n-Channel Organic Transistors Based on Core-Chlorinated Naphthalene Diimides," Advanced Functional Materials **21** (21), 4173-4181 (2011).

145   T. Uemura, M. Yamagishi, S. Ono, and J. Takeya, "Low-voltage operation of n-type organic field-effect transistors with ionic liquid," Applied Physics Letters **95** (10), - (2009).

146   A.J. Bard and L.R. Faulkner, *Electrochemical methods: fundamentals and applications*. (Wiley, USA, 2001), 2nd ed.

147   LE Barrosse-Antle, AM Bond, RG Compton, AMO Mahony, EI Rogers, and DS Silvester, "FOCUS REVIEWS," Chem. Asian J **5**, 202-230 (2010); Rika Hagiwara and Yasuhiko Ito, "Room temperature ionic liquids of alkylimidazolium cations and fluoroanions," Journal of Fluorine Chemistry **105** (2), 221-227 (2000).

148   Alejandro L Briseno, Stefan CB Mannsfeld, Samson A Jenekhe, Zhenan Bao, and Younan Xia, "Introducing organic nanowire transistors," Materials Today **11** (4), 38-47 (2008).

149   Jiaxing Huang, Shabnam Virji, Bruce H Weiller, and Richard B Kaner, "Polyaniline nanofibers: facile synthesis and chemical sensors," Journal of the American Chemical Society **125** (2), 314-315 (2003).

150   Adam K Wanekaya, Mangesh A Bangar, Minhee Yun, Wilfred Chen, Nosang V Myung, and Ashok Mulchandani, "Field-effect transistors based on single nanowires of conducting polymers," The Journal of Physical Chemistry C **111** (13), 5218-5221 (2007).

151   Amit Babel and Samson A. Jenekhe, "High Electron Mobility in Ladder Polymer Field-Effect Transistors," Journal of the American Chemical Society **125** (45), 13656-13657 (2003).

152   MH Santos, "Biogenic amines: their importance in foods," International journal of food microbiology **29** (2), 213-231 (1996).

153   Hakan Usta, Antonio Facchetti, and Tobin J Marks, "n-Channel semiconductor materials design for organic complementary circuits," Accounts of Chemical Research **44** (7), 501-510 (2011).